An analytical framework for the structural stability analysis of damageable structures and its application to delaminated composites

vorgelegt von
Anton Köllner, M.Eng. (Hons)
geb. in Leipzig

von der Fakultät V – Verkehrs- und Maschinensysteme
der Technischen Universität Berlin
zur Erlangung des akademischen Grades

Doktor der Ingenieurwissenschaften
- Dr.-Ing. -

genehmigte Dissertation

Promotionsausschuss:

Vorsitzender:	Prof. Dr.-Ing. Utz von Wagner
Gutachterin:	Prof. Dr. Christina Völlmecke
Gutachter:	Prof. Dr. M. Ahmer Wadee
Gutachter:	Prof. Dr. rer. nat. Wolfgang H. Müller

Tag der wissenschaftlichen Aussprache: 24.08.2017

Berlin 2017

Technische Universität Berlin
Faculty V
Mechanical Engineering and Transport Systems
Institute of Mechanics
Stability and Failure of Functionally Optimized
Structures Group
Sekr. MS 2
Einsteinufer 5
D-10587 Berlin

Doctoral committee:

Chairman: Prof. Dr.-Ing. Utz von Wagner
Technische Universität Berlin
Institute of Mechanics
Chair of Mechatronics and Machine Dynamics Group
Sekr. MS 2, Einsteinufer 5
D-10587 Berlin

Examiner: Prof. Dr. Christina Völlmecke
Technische Universität Berlin
Institute of Mechanics
Chair of Stability and Failure of Functionally Optimized
Structures Group
Sekr. MS 2, Einsteinufer 5
D-10587 Berlin

Examiner: Prof. Dr. M. Ahmer Wadee
Imperial College London
Faculty of Engineering
Department of Civil and Environmental Engineering
Professor of Non-linear Mechanics
421 Skempton Building, South Kensington Campus
London SW7 2AZ, UK

Examiner: Prof. Dr. rer. nat. Wolfgang H. Müller
Technische Universität Berlin
Institute of Mechanics
Chair of Continuum Mechanics and Material Theory Group
Sekr. MS 2, Einsteinufer 5
D-10587 Berlin

Abstract

In the current work, a novel analytical framework is developed which extends the general elastic stability theory to certain non-conservative deformation processes for which an extended total potential energy can be derived. The extended total potential energy constitutes the governing functional for the non-conservative deformation processes. The mechanical systems considered are described by a set of generalized coordinates. The framework enables the semi-analytical modelling of structural stability phenomena while considering material damage and its propagation. With the aid of the analytical framework, the problems of delaminated multi-layered composite struts and plates subjected to compressive in-plane loading are investigated. The modelling approaches developed constitute highly efficient engineering tools which require tremendously less computational cost than standard finite element simulations. Qualitatively and quantitatively substantial and conclusive results are obtained where the post-buckling behaviour deviates up to 5% and the growth characteristics up to 12% from the respective finite element simulations.

Kurzfasssung

In der vorliegenden Arbeit wird ein analytischer Formalismus entwickelt, welcher die allgemeine elastische Stabilitätstheorie dahingehend erweitert, dass nicht-konservative Deformationsprozesse, die die Herleitung eines erweiterten Gesamtpotentials ermöglichen, berücksichtigt werden können. Das erweiterte Gesamtpotential ist ein Funktional zur Beschreibung der nicht-konservativen Prozesse. Die in der Arbeit untersuchten mechanischen Systeme werden mit generalisierten Koordinaten beschrieben. Der entwickelte Formalismus ermöglicht die Analyse strukturstabilitätsrelevanter Phänomene unter Beachtung von Materialschäden und deren Ausbreitung. Mit Hilfe dieses Formalismus werden delaminierte Kompositmehrschichtverbundstützen und -platten unter axialer ebener Druckbelastung untersucht. Die Modellierungsansätze sind hocheffizient, so dass verglichen mit gewöhnlichen Finite-Elemente-Simulationen signifikant weniger Rechenaufwand benötigt wird. Das Ergebnis sind qualitativ und quantitativ schlüssige und aussagekräftige Resultate, die im Vergleich zu Finite-Elemente-Simulationen Abweichungen von bis zu 5% hinsichtlich des postkritischen Verhaltens und von bis zu 12% bezüglich der Schadenscharakteristiken aufweisen.

Acknowledgements

I would like to express my gratitude to my supervisor Prof. Dr. Christina Völlmecke for giving me the opportunity to perform research in this fascinating field of engineering. I am particularly grateful for her ongoing encouraging supervision and the many fruitful scientific discussions, which have been highly beneficial to this work.

I would like to extend my gratitude to Prof. Dr. M. Ahmer Wadee for his enriching feedback and the profound discussions at the Engineering Mechanics Institute conferences 2016 and 2017.

A special thanks goes to Prof. Dr. rer. nat. Wolfgang H. Müller for his scientific advice during the initial period of this work. Furthermore, I would like to emphasize the highly valuable expertise gained by assisting university courses of Prof. Dr. Christina Völlmecke and Prof. Dr. rer. nat. Wolfgang H. Müller which has strongly contributed to my scientific advancement.

It is of utmost importance to mention the exceptional working atmosphere at the chairs of Prof. Dr. Christina Völlmecke and Prof. Dr. rer. nat. Wolfgang H. Müller which is strongly related with the mutual support and the helpful attitude of all my colleagues. This constitutes the foundation of a prospering scientific environment.

Additionally, I would like to thank my colleague Dr.-Ing. Rolf Jungnickel for enriching discussions about and beyond the subject of the current work as well as his support in building up the finite element simulations used for verification purposes within the work. Furthermore, I would like to mention the exceptional support received by my colleagues Arion Juritza and Guido Harneit regarding any hardware and software issues during the making of this work.

Contents

List of Figures

List of Tables

1 Introduction

Structures which are part of lightweight constructions fulfil, amongst other items, the following criteria: slenderness and functional optimization. A special group of lightweight structures complying with the above-mentioned criteria are layered composites such as struts, plates and shells, which are focused upon in this work. The criterion *slenderness* applies, if a certain ratio between effective length and gyration radius is fulfilled. Slender structures, once loaded under axial compression, are specifically prone to *buckling*, *i.e.* the loss of stability forcing a system to leave its current equilibrium path.

The buckling and post-buckling behaviour of composite struts and plates describes a main area of ongoing structural stability research. However, particularly the use of composites requires the consideration of material damage and failure. The layered construction and the heterogeneity give rise to various damage mechanisms and hence inelastic deformations, which might have an influence on the stability behaviour. Therefore, the possibility of inelastic deformations has to be considered in a structural stability analysis.

The necessity to include material failure into the stability analysis of structures becomes apparent when considering the well-known problem of a delaminated multi-layered composite strut under compressive loading as shown in Fig. 1.1. The post-buckling behaviour, as predicted by assuming a conservative process, might be significantly altered if damage growth is considered. Thus, instead of a stable post-buckling response, the structure could fail under unstable delamination growth.

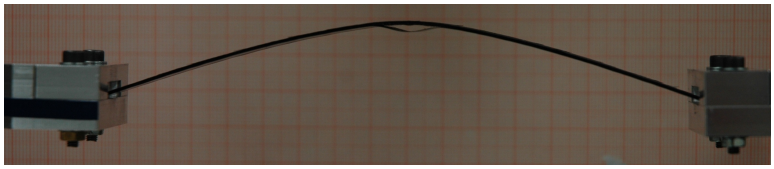

Fig. 1.1: Simply-supported composite strut with a through-the-width delamination.

In the monograph [94], Thompson and Hunt propose a highly regarded and well established general elastic stability theory. However, the theory of Thompson and Hunt and ensuing textbooks related to elastic structural stability, *e.g.* see [4, 33, 95], focus on conservative, *i.e.* non-dissipative, processes which limits the

applicability. Thus, it stands to reason to turn towards a structural stability analysis of structures prone to buckling and damage propagation by deriving an extension of the theory described in [94].

This is achieved in the current work by extending the energy formulation while keeping the benefits from the formalism of THOMPSON and HUNT. As a result, an analytical framework is presented in which structural stability analysis and damage propagation are combined into a single formulation allowing the modelling of stability phenomena of certain inelastic deformation processes. The framework is applied to the problem of delaminated composites loaded under axial compression. Deformation paths and their stability are readily modelled for entire loading processes comprising elastic and inelastic deformation.

Before presenting the analytical framework and its application, the fundamentals used to derive the framework are described within the introductory chapter. First, main aspects of the general elastic stability theory of THOMPSON and HUNT are reviewed. Then, the concept of deriving strain energy-like potentials following SCHAPERY is presented. The introduction closes with the research objective and an outline of the thesis.

1.1 Fundamentals of the general elastic stability theory of Thompson and Hunt

In the well-established textbooks [94, 95], THOMPSON and HUNT propose a general non-linear mathematical theory of elastic stability of conservative[1] mechanical systems described by a *finite* set of generalized coordinates. A LAGRANGIAN energy formulation, *i.e.*

$$\mathcal{L}(\dot{q}_i, q_i) = K(\dot{q}_i, q_i) - V(q_i), \tag{1.1.1}$$

is employed in which q_i are the generalized coordinates describing the spatial configuration of the system, with $i = 1, 2, ..., I$. In Eq. (1.1.1), the kinetic energy is denoted by K and the total potential energy of the system by V.[2] A dot implies differentiation with respect to time. Since both monographs of THOMPSON and HUNT [94, 95] as well as the present work are concerned with statical equilibrium, the kinetic energy function is of no further interest for the subsequent text.

The mechanical system is in a statical equilibrium state if the first variation of

[1] Gyroscopic systems which also conserve energy are not considered in [94, 95] and in the current work.

[2] V is referred to as the *total* potential energy to underline that it comprises both *inner* potential and *outer* potential. The inner potential is the deformation energy of the system and the applied forces can be derived from the outer potential.

the total potential energy vanishes, *i.e.* the total potential energy is stationary with respect to the generalized coordinates. This can be easily proved by the calculus of variation yielding the balance of linear (or angular) momentum and *vice versa* [66]. In the matter of the discrete coordinate approach, the condition for equilibrium can be written as

$$\frac{\partial V}{\partial q_i} \equiv V_i = 0. \tag{1.1.2}$$

Eq. (1.1.2) is formulated in [94] as one of two fundamental axioms for the general elastic stability theory and reads as follows.

Axiom 1: *A stationary value of the total potential energy with respect to the generalized coordinates is necessary and sufficient for the equilibrium of the system.*

Regarding the stability of an equilibrium state, THOMPSON and HUNT formulate a second axiom.

Axiom 2: *A complete relative minimum of the total potential energy with respect to the generalized coordinates is necessary and sufficient for the stability of an equilibrium state.*

The second axiom can be visualized by the so-called rolling ball analogy shown in Fig. 1.2 in which, for demonstration and illustration purposes, total potential energy profiles for three distinct two-degree of freedom systems are illustrated.

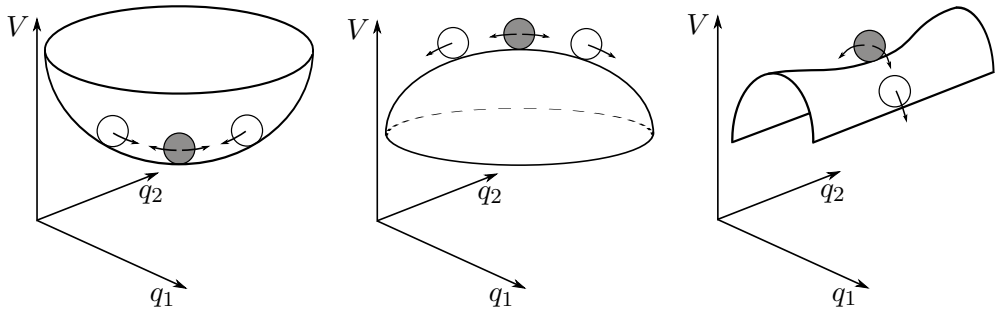

(a) **(b)** **(c)**

Fig. 1.2: Rolling ball analogy; **(a)** local minimum (stable), **(b)** local maximum (unstable), and **(c)** saddle point (unstable).

For each profile in Fig. 1.2, the grey-shaded ball rests at the point where the total potential energy is stationary, thus at an equilibrium state. Following the second axiom, the behaviour of the total potential energy in the neighbourhood

of the respective equilibrium states determines whether the equilibrium state is stable or unstable. The profile of the total potential energy shown in Fig. 1.2a describes a complete local minimum which indicates a *stable* equilibrium state. Small perturbations of the equilibrium state illustrated by perturbing the grey-shaded ball do not cause the system to leave ultimately its equilibrium state; the system will remain in the vicinity of the equilibrium state for all time.[3] The profiles in Fig. 1.2b and Fig. 1.2c exhibit a local maximum and a saddle point respectively, so that following Axiom 2 the equilibrium state is *unstable*. Small perturbations force the system to leave ultimately its current equilibrium state.

This concept can be readily mathematically implemented by studying higher order derivatives of the total potential energy. Unless the system is in a critical state, *i.e.* a change in stability occurs as for a bifurcation point or a limit point, the second order derivatives of the total potential energy at an equilibrium state (q_i^{E}), thus

$$\left.\frac{\partial^2 V}{\partial q_i \partial q_j}\right|_{q_i^{\mathrm{E}}} \equiv V_{ij}^{\mathrm{E}}, \tag{1.1.3}$$

determine whether the equilibrium state is stable or unstable. Positive-definiteness of the matrix V_{ij}^{E} indicates stable equilibrium and negative-definiteness unstable equilibrium. At a critical state, the matrix V_{ij}^{E} becomes singular, thus the stability cannot be determined by the second derivatives. To study the stability of critical states, higher order derivatives need to be evaluated.

Next, with the aid of an equilibrium path, main aspects of the total potential energy formalism are reviewed. Fig. 1.3 shows an equilibrium path of a one-degree of freedom system in terms of prescribed load against generalized coordinate. The prescribed load is denoted by the *loading parameter* λ which may be understood as any basic parameter whose influence is aimed to be studied [94]. An obvious choice for a loading parameter are prescribed forces or prescribed displacements. However, an elastic modulus or a characteristic length may also be used [94].

Fig. 1.3 also shows the corresponding contours of the total potential energy for certain values of the prescribed load (λ^{I}, λ^{II}, λ^{III}). On the equilibrium path the total potential energy must be stationary which is fulfilled for λ^{I} and λ^{II}. Regarding λ^{III}, no local equilibrium state exists for the q_1 examined in Fig. 1.3 as the total potential energy does not exhibit a stationary point.

[3] This follows an intuitive illustrative concept. A general definition of stability is given by Lyapunov, see for instance [54, 60]. Briefly summarized, a deformation state $q_i^{\mathrm{E}}(t)$ is stable when the variations $\delta q_i(t)$ satisfy $|\delta q_i(t)| < \epsilon$ for $t > t_0$ if $|\delta q_i(t_0)| < \eta(\epsilon)$ holds at the initial time t_0 where ϵ and $\eta(\epsilon)$ are arbitrary small positive numbers [60].

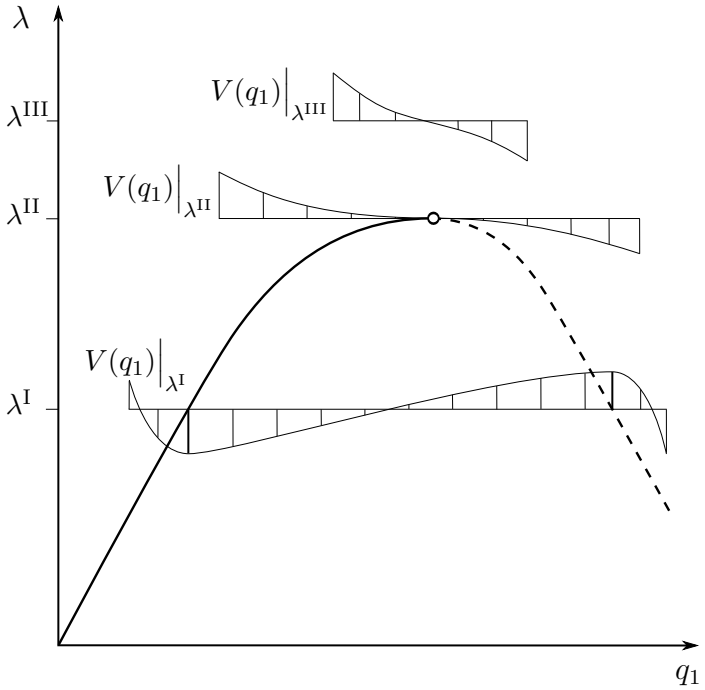

Fig. 1.3: Equilibrium path of a one-degree of freedom system with corresponding total potential energy contours; adopted from [94].

Next, the stability of the system under certain prescribed magnitudes of load may be analysed. Stable equilibrium is indicated in Fig. 1.3 by a solid line and unstable equilibrium by a dashed line. A complete local minimum of the total potential energy is given for the solid line as can be exemplarily seen at λ^{I}. The stability of the equilibrium path changes at λ^{II} highlighted by the symbol "$\circ$" in Fig. 1.3. This deformation state describes a critical equilibrium state referred to as a *limit point* or a saddle-node bifurcation. At the limit point, the total potential energy has a horizontal point of inflexion. Studying higher order derivatives of the total potential energy yields that such a critical equilibrium state is *unstable*. On the subsequent unstable equilibrium path (dashed line) the total potential energy exhibits a local maximum for the respective prescribed loads. This is illustrated in Fig. 1.3 for the prescribed load λ^{I}. Other phenomena comprising the loss of stability of a fundamental equilibrium path are stable and unstable symmetric and asymmetric bifurcation points. Such phenomena are discussed in detail in [94, 95] and relevant aspects for the buckling and post-buckling behaviour of composite struts and plates are summarized in Chapters 3 and 4.

Thompson and Hunt consider the dependency on the respective prescribed load input by defining the total potential energy, such that

$$V = V(q_i, \lambda), \tag{1.1.4}$$

in which λ denotes the *loading parameter*. Assuming a load input in the form of a prescribed conservative force P, the total potential energy can be written as

$$V = V(q_i, P) = W(q_i) - P\mathcal{E}(q_i). \tag{1.1.5}$$

where W describes the strain energy of the system and the second term on the right hand side in Eq. (1.1.5) is the work done by the applied forces. The conjugate displacement to the prescribed force P is denoted by $\mathcal{E}$.

Despite using a discrete coordinate approach, the formalism may also be efficiently applied to non-linear elastic continua by employing continuous mode-forms as in Rayleigh–Ritz analyses. Therefore, the response of the mechanical system is, in general, approximated by a finite modal analysis [94]. Thus, continuous mechanical systems may be described and analysed by means of the discrete coordinate approach employing generalized coordinates. Within the current work, such continuous mode-forms are used for modelling the buckling and post-buckling behaviour of delaminated composite struts and plates.

1.2 Work potentials following Schapery

The theory for deriving so-called *work potentials* or *strain energy-like potentials* was proposed by Schapery [55, 82, 83]. A work potential is to be understood as a constitutive potential characterizing the mechanical behaviour of a given structure with growing damage. The subsequent review of the theory strongly follows the work of Schapery in [82, 83].

As pointed out by Schapery, deformation processes comprising inelastic behaviour are—in general—path dependent, *i.e.* the total work of deformation does not obey a potential. However, there exist certain deformation processes, such as micro and macro-cracking in composites [55, 82] and ceramics [83], as well as metal-like inelasticity (plastic slip) [80, 83], which exhibit path independence for at least limited deformation paths. For such processes, a potential formulation may be derived.

As an introductory example, consider an elastic material with a certain state of damage defined by a set of damage parameters D_k with $k = 1, 2, ..., K$. For a constant state of damage, the strain energy density w is a constitutive potential, thus

$$S_{ij} = \left.\frac{\partial w(E_{ij}, D_k)}{\partial E_{ij}}\right|_{D_k}, \tag{1.2.1}$$

where S_{ij} and E_{ij} are the components of the Second Piola–Kirchhoff stress

tensor and the Green–Lagrange strain tensor respectively considering geometrically non-linear behaviour.[4] Since isothermal processes are considered, the strain energy density w is the Helmholtz free energy density which is a well-known thermodynamic potential of the stresses. The derivation of the strain energy density from the *first* and *second law of thermodynamics* is described in Appendix A.

Next, assume that the damage parameters D_k change with time[5] as a result of straining. In order to characterize the effective constitutive behaviour the relationships governing these changes must be determined. If these changes are known, then the parameters D_k may be expressed in terms of the instantaneous strains E_{ij}, *i.e.* $D_k(E_{ij})$. Following Schapery [82], if the damage parameters are found as functions of the strains, a *strain energy-like* potential $\hat{w}$ may be found from which the constitutive equations can be derived by differentiation, *i.e.*

$$S_{ij} = \frac{\partial \hat{w}(E_{ij}, D_k(E_{ij}))}{\partial E_{ij}}, \tag{1.2.2}$$

where $\hat{w}$ is a constitutive potential which depends on the instantaneous strains only but accounts for changing damage.

1.2.1 Illustrative one-dimensional example

To provide an illustration for the existence of work potentials, a simple example, as given in [82], is reviewed. Therefore, a one-dimensional deformation path, shown in Fig. 1.4, is considered. In contrast to the general theory that follows, this example does not require the consideration of thermodynamic principles and thus should just be regarded for illustration purposes.

In Fig. 1.4, the stress–strain curve (σ *vs.* ε) consists of a loading and an unloading path. The material—supposed to be undamaged in its initial state—is monotonically strained up to a certain maximum strain ε_m associated with growing damage within the specimen. Subsequently, the specimen is unloaded. Elastic behaviour and constant damage is assumed during unloading. Hence, the stress during unloading σ_u is a function of the instantaneous strain ε and the maximum strain occurring during loading ε_m, thus

$$\sigma_\mathrm{u} = f(\varepsilon, \varepsilon_\mathrm{m}). \tag{1.2.3}$$

[4] For geometrically linear behaviour S_{ij} would be the Cauchy stress tensor σ_{ij} and E_{ij} the infinitesimal strain tensor ε_{ij}.

[5] Herein, time is not strictly understood as the *natural time*. Regarding quasi-static processes, time may be any scalar parameter defining the change of the response of the system from one loading step to another.

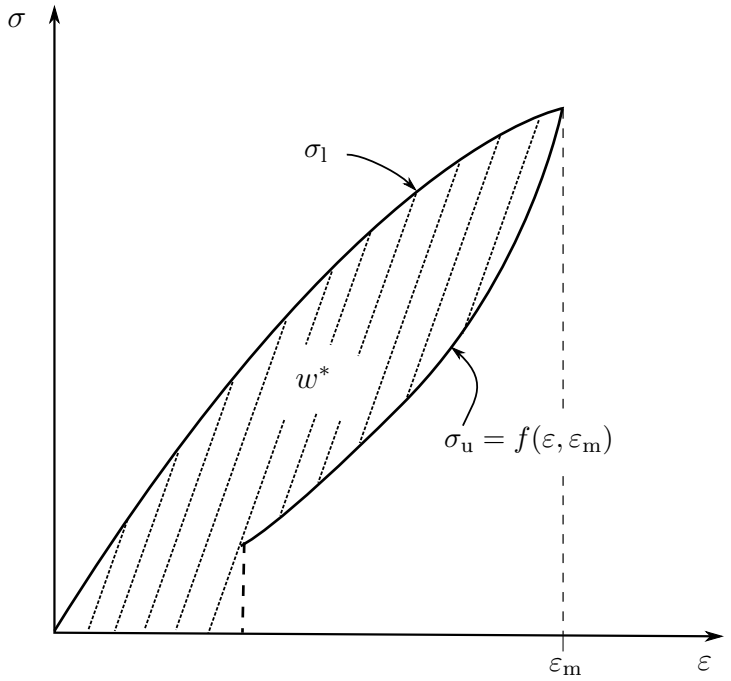

Fig. 1.4: Uniaxial stress–strain curve of an elastic material with increasing damage during loading and constant damage during unloading; adopted from [82].

Regarding the strain energy density w, the maximum strain serves as a measure of the amount and effect of damage, *i.e.* defines the respective current state of damage, thus $D_k = D_1 = \varepsilon_\mathrm{m}$ and $w = w(\varepsilon, \varepsilon_\mathrm{m})$. The unloading path is characterized by the constant damage parameter ε_m. However, during loading damage changes with time—from one loading step to another—as a result of straining. In order to derive a constitutive potential as shown in Eq. (1.2.2), the damage parameter ε_m needs to be expressed in the terms of $\varepsilon_\mathrm{m}(\varepsilon)$.

As can be seen in Fig. 1.4, the loading stress σ_l is also the upper end of an unloading curve (unloading stress σ_u). Hence, the loading stress can also be expressed with the function f considering that on the loading curve the maximum strain is the current strain, *i.e.*:

$$\sigma_\mathrm{l} = f(\varepsilon, \varepsilon_\mathrm{m} = \varepsilon). \tag{1.2.4}$$

The mechanical work density during loading w_l and unloading w_u can be determined using Eqs. (1.2.3) and (1.2.4) by integrating the function f over the respective strain path, thus

$$w_\mathrm{l} = \int_0^\varepsilon f(\tilde{\varepsilon}, \tilde{\varepsilon})\,\mathrm{d}\tilde{\varepsilon} \qquad \text{and} \qquad w_\mathrm{u} = w_\mathrm{l}(\varepsilon = \varepsilon_\mathrm{m}) + \int_{\varepsilon_\mathrm{m}}^\varepsilon f(\tilde{\varepsilon}, \varepsilon_\mathrm{m})\,\mathrm{d}\tilde{\varepsilon}. \tag{1.2.5}$$

It should be noted that as damage increases during loading (accounts for inelas-

ticity) the mechanical work w_l is not equal to the strain energy density.

Following Eq. (1.2.5), a function w^* can be defined which equals w_l during loading and w_u during unloading. Hence, the constitutive equation describing the one-dimensional behaviour of an elastic material with growing damage may be expressed as

$$\sigma = \frac{\partial w^*}{\partial \varepsilon}, \tag{1.2.6}$$

where w^* is the *work potential* or *strain energy-like potential* and the net work to the material at any stage of loading or unloading.

1.2.2 General theory

Following Schapery [83], in order to establish a general condition for deriving a work potential, the systems investigated are described in terms of generalized forces A_m and generalized displacements α_m with $m = 1, 2, ..., M$.[6] The generalized displacements are treated as being independent herein, however, systems which are exposed to independent generalized forces or independent generalized forces and displacements may also be considered.

It is assumed that a strain energy function $W = W(\alpha_m, \xi_k)$ exists,[7] for all processes of interest, such that

$$A_m = \left.\frac{\partial W}{\partial \alpha_m}\right|_{\xi_k}, \tag{1.2.7}$$

where ξ_k $(k = 1, 2, ..., K)$ are the only thermodynamic state variables besides α_m needed to account for changes in the strain energy [83]. The parameters ξ_k completely describe the given state of damage in a structure and comprise the damage parameters D_k of the introductory example; however, they also allow for a more general interpretation regarding changes in structure such as geometry of individual micro and macro-cracks or statistical averages, void volume, degree of molecular entanglements, crosslinking or crystallinity [83]. The parameters ξ_k are commonly referred to as *internal state variables* following Rice [80]. Schapery proposes the terminology *structural parameters*. However, in order to distinguish the terminology from the general structural stability analysis ξ_k is referred to *damage parameters* in the subsequent text.

[6] The notation is changed in comparison with [83] to provide a clear distinction between the generalized displacements and generalized coordinates.

[7] *Cf.* Appendix A.

First, consider the work done during an *actual*[8] deformation process which can be written as

$$W_{\text{tot}} = \int A_m \, \mathrm{d}\alpha_m, \tag{1.2.8}$$

where W_{tot} describes the total work of deformation. In contrast to the strain energy, Eq. (1.2.8) describes the work done when changes in structure occur.

Evaluating the total derivative of the strain energy yields

$$\mathrm{d}W = \left.\frac{\partial W}{\partial \alpha_m}\right|_{\xi_k} \mathrm{d}\alpha_m + \left.\frac{\partial W}{\partial \xi_k}\right|_{\alpha_m} \mathrm{d}\xi_k, \tag{1.2.9}$$

where the first partial derivative gives the generalized forces A_m (*cf.* Eq. (1.2.7)) and the second derivative may be expressed by a set of parameters f_k, such that

$$f_k = -\left.\frac{\partial W}{\partial \xi_k}\right|_{\alpha_m} \tag{1.2.10}$$

describes the change of the strain energy with respect to the kth damage parameter. The parameters f_k may be understood as thermodynamic forces[9] available for producing a change in structure [80, 83]. Thus, Eq. (1.2.9) can be rewritten in the form of

$$\mathrm{d}W = A_m \, \mathrm{d}\alpha_m - f_k \, \mathrm{d}\xi_k. \tag{1.2.11}$$

Note that if no change in damage occurs ($\mathrm{d}\xi_k = 0$), the expected relation $\mathrm{d}W = \mathrm{d}W_{\text{tot}}$ is obtained. Rearranging Eq. (1.2.11) and integrating from an arbitrary state $\left(\alpha_m^{(1)}, \xi_k^{(1)}\right)$ at time t_1 along the *actual* path to the current state (α_m, ξ_k) yields

$$\Delta W_{\text{tot}} = W - W^{(1)} + \int_1 f_k \, \mathrm{d}\xi_k. \tag{1.2.12}$$

Here, it should be noted that any changes in structure need to satisfy the *second law of thermodynamics* [65], *i.e* only those changes in ξ_k are possible which correspond with a non-negative entropy production rate Σ. This reads, in terms

[8] An *actual* deformation process is understood as one in which the damage parameters ξ_k vary in time in accordance with the appropriate constitutive equations governing their changes [83].

[9] The change in energy associated with a change in damage is often referred to as *force* which is adopted in the present work.

of the processes considered,

$$f_k \dot{\xi}_k = T\Sigma \geq 0, \tag{1.2.13}$$

where T is the temperature. Thus, Eq. (1.2.12) may be rewritten, so that

$$\Delta W_{\mathrm{tot}} = W - W^{(1)} + \int_{t_1}^{t} T\Sigma \, \mathrm{d}t, \tag{1.2.14}$$

from which it is shown that the latter term in Eq. (1.2.12) is never negative.

It should be stressed that f_k is a function of the independent generalized displacements and the damage parameters, *i.e.* $f_k = f_k(\alpha_m, \xi_k)$. Thus, the total work of deformation, as stated in Eqs. (1.2.12) and (1.2.14), cannot be expressed in the form of a work potential yet.

The requirement so that the total work of deformation may be expressed in the form of a work potential is reviewed next. This is based on the assumption that whenever $\dot{\xi}_m \neq 0$, *i.e.* a change in structure occurs (regarding quasi-static processes from one loading step to another), the condition

$$f_k = \frac{\partial W_{\mathrm{d}}}{\partial \xi_k} \tag{1.2.15}$$

holds, in which W_{d} may be referred to as *work of structural change*. On the contrary, it is assumed that if Eq. (1.2.15) is not satisfied for any given ξ_k, then $\dot{\xi}_k = 0$.[10] It is further assumed that the work of structural change is a function depending on the damage parameters only, *i.e.* $W_{\mathrm{d}} = W_{\mathrm{d}}(\xi_k)$. Thus, W_{d} is a state function. If Eq. (1.2.15) holds, then the total work in Eq. (1.2.12) is also a state function. Substituting Eq. (1.2.15) into Eq. (1.2.12) and taking $W = 0$ and $W_{\mathrm{d}} = 0$ for a chosen reference state (previously denoted with $^{(1)}$), the total work can be expressed as,

$$W_{\mathrm{tot}} = W + W_{\mathrm{d}}. \tag{1.2.16}$$

In the view that f_k is the thermodynamic force available for producing changes in the corresponding damage parameters, the quantity $\partial W_{\mathrm{d}}/\partial \xi_k$ may be regarded as the force required for these changes. Further it is assumed that all active, *i.e.* non-constant, damage parameters ξ_a $(1 \leq a \leq k)$ may be derived from Eq. (1.2.15) as functions of time-varying or constant α_m assuming that Eq. (1.2.15) provides

[10] This describes a theoretical condition to construct the work potential theory formulated by Schapery. It should be treated with care once applied to deformation processes. It should not be assumed *a priori* that this condition is fulfilled. The study of the behaviour of the parameters f_k during the respective deformation processes determines whether a work potential may be derived or not.

a unique solution, differentiable in α_m, at least if processes are suitably limited [83]. As a consequence, Eq. (1.2.15) may be considered as an *evolution law* for the damage parameters and it constitutes the *sufficient condition* for deriving a work potential. By substituting $\xi_a(\alpha_m)$ into Eq. (1.2.16) the total work of deformation is a function of the independent generalized displacements only, such that

$$A_m = \frac{\partial W_{\mathrm{tot}}}{\partial \alpha_m}, \tag{1.2.17}$$

in which W_{tot} describes a true constitutive potential of the generalized forces.

Next, it is also shown that if Eq. (1.2.15) holds, the total work of deformation is stationary with respect to the active damage parameters. Therefore, the total work W_{tot} (Eq. (1.2.16)) is differentiated with respect to the active damage parameters,[11]

$$\frac{\partial W_{\mathrm{tot}}}{\partial \xi_a} = \frac{\partial W}{\partial \xi_a} + \frac{\partial W_{\mathrm{d}}}{\partial \xi_a} = 0, \tag{1.2.18}$$

where Eqs. (1.2.10) and (1.2.15) have been used. Eq. (1.2.18) shows that if Eq. (1.2.15) holds, the total work of deformation is stationary with respect to the damage parameters. Subsequently, the stability of the deformation state regarding a change in structure is investigated for any given state of loading (prescribed α_m), *i.e.* introducing small changes $\delta\xi_a$ to W_{tot}. Writing W_{tot} as a TAYLOR series yields

$$W_{\mathrm{tot}}(\xi_a + \delta\xi_a) = W_{\mathrm{tot}}(\xi_a) + \underbrace{\frac{\partial W_{\mathrm{tot}}}{\partial \xi_a}}_{=0} \delta\xi_a + \frac{1}{2}\frac{\partial^2 W_{\mathrm{tot}}}{\partial \xi_a \partial \xi_r}\delta\xi_a\,\delta\xi_r + \mathcal{O}(3). \tag{1.2.19}$$

Rewriting Eq. (1.2.19) leads to

$$\Delta W_{\mathrm{tot}} = \frac{1}{2}\frac{\partial^2 W_{\mathrm{tot}}}{\partial \xi_a \partial \xi_r}\delta\xi_a\,\delta\xi_r + \mathcal{O}(3) = \frac{1}{2}\underbrace{\left(\frac{\partial^2 W}{\partial \xi_a \partial \xi_r} + \frac{\partial^2 W_{\mathrm{d}}}{\partial \xi_a \partial \xi_r}\right)}_{H_{ar}}\delta\xi_a\,\delta\xi_r + \mathcal{O}(3), \tag{1.2.20}$$

in which H_{ar} determines whether the deformation state is *stable* or *unstable* with respect to a change in damage. A stable state is given if the matrix H_{ar} (evaluated at the reference state) is positive-definite, thus the total work exhibits a local minimum. Otherwise, it is unstable.

[11] Note that the damage parameters are not expressed in terms of the generalized displacements for evaluating stationarity and stability.

1.3 Research objective

The advantages associated with employing the theory of Thompson and Hunt for structural stability analyses are manifold. Its discrete approach implementing generalized coordinates enables exploratory studies of yet not fully understood mechanical systems and deformation mechanisms in such a way that specific phenomena may be added separately to a model description. This provides the possibility to either focus on certain phenomena assumed to have a major influence on a structure's response or to develop geometric models of increasing accuracy regarding the "real-world" deformation behaviour. This in turn enables the restriction to a specific finite—in many cases small—amount of generalized coordinates required to capture most phenomena of interest.

As an outcome, most applications of the theory of Thompson and Hunt provide highly efficient models for structural mechanics problems. Such freedom regarding the development of appropriate model descriptions applies for purely discrete systems, *e.g.* see [29, 31, 100, 101, 103, 113], and systems in which continuous mode-forms are implemented, *e.g.* see [6, 7, 19, 20, 30, 31, 32, 99, 102].

The current work aims at removing a major limitation of the theory of Thompson and Hunt—its restriction to conservative deformation processes. In many structural applications, specifically since the increasing use of composite materials, the stability behaviour is strongly affected by material defects and damage propagation. Deformation processes associated with structural and material instability are nowadays entirely investigated by means of purely numerical studies such as finite element simulations, *e.g.* [26, 27, 58, 68, 69, 92]. Regarding such applications, to the authors knowledge, analytical or semi-analytical models do not exist.

The analytical framework developed in the current work fills this gap. Stability phenomena considering damage growth are modelled by a set of generalized coordinates only. Therefore, the theory of Thompson and Hunt and features of the theory for deriving work potentials are merged which allows to analyse the structural stability, the damage propagation and the stability of the damage propagation efficiently.

With the aid of the framework, delaminated plated composite structures subjected to in-plane compressive loads are investigated in the present work. Deformation paths beyond the elastic limit are modelled. Thus, the framework enables the analysis of the structural stability behaviour of such structures once damage growth is initiated in a highly efficient manner. This adds valuable insight regarding the structural stability and the damage growth behaviour of delaminated composite structures.

1.4 Outline of the thesis

The main body of the thesis starts in Chapter 2 in which the analytical framework developed to model the structural stability behaviour of damageable structures is presented. The fundamentals to this framework have been introduced in Sections 1.1 and 1.2.

The framework distinguishes whether a deformation process is purely elastic (reversible) or contains inelastic deformations (irreversible). Hence, the first two parts of Chapter 2 are concerned with reversible and irreversible processes respectively. So long as the system exhibits elastic behaviour, *i.e.* all damage parameters remain constant, the theory of Thompson and Hunt is employed. The governing functional is the total potential energy Π.[12] The variational principle, $\delta\Pi = 0$, is used to obtain the deformation paths in the conservative (non-dissipative) range.

For the irreversible processes, a novel governing functional Π^*—the *extended total potential energy*—is derived. Therefore, first, the derivation of the damage parameters as functions of the generalized coordinates and the load parameters is elucidated. The *extended total potential energy* is a functional of the generalized coordinates only. The deformation path during the non-conservative process is obtained by a variational principle $\delta\Pi^* = 0$. The damage propagation is determined by inserting the deformation path obtained in the functions derived for the respective damage parameters.

In the third part of Chapter 2, a structural stability analysis formalism which considers damage propagation is presented. The formalism provides a summary of the analytical framework and delineates the modelling steps required to determine the structural stability behaviour of damageable structures.

Chapter 3 presents the first application example of the analytical framework. The non-linear buckling behaviour of delaminated composite struts is investigated. The chapter commences with an overview of characteristic buckling phenomena of struts and the current state of research regarding the buckling and damage behaviour of delaminated struts loaded under in-plane compression. It becomes obvious that there is a lack of analytical or semi-analytical modelling capable of describing post-buckling responses beyond the state where delamination growth is initiated which is thus far solely modelled by finite element simulations.

In the second part of Chapter 3, the geometric model used to describe the buckling behaviour of the composite strut is presented. The non-linear buckling response and the damage propagation of multi-layered struts are modelled by four generalized coordinates only. Continuous mode-forms as part of a Rayleigh–Ritz

[12] In the upcoming chapters, it will be strictly distinguished between the total potential energy functional Π and the total potential energy function V (*cf.* Section 2.1).

formulation are implemented. Characteristic buckling responses for non-growing delaminations are presented and analysed. Results obtained for the reversible buckling behaviour are compared with findings provided within the literature. Results considering delamination growth are compared with finite element simulations using the commercial software package Abaqus [93]. The study provides detailed insight into the non-linear buckling phenomena of delaminated composites without the restriction of non-growing delaminations. The chapter closes with a critical discussion about the results obtained and the model implementation.

Chapter 4 deals with another type of delaminated composite structures. Whereas the delaminated composite strut is mainly analysed to describe and obtain fundamental aspects of delamination buckling and buckling-driven delamination propagation, the composite plate with an embedded delamination illustrates an example closer to "real-world" applications. First, characteristic buckling phenomena of plates and pre-existing studies regarding the deformation behaviour of composite plates with an embedded delamination loaded under in-plane compression are reviewed. Second, the geometric model is presented. The description of the system with a set of generalized coordinates contains several obstacles which are reviewed. The amount of generalized coordinates required to model the buckling responses efficiently is determined. As performed in Chapter 3, a Rayleigh–Ritz formulation is applied approximating the displacement field.

Non-linear buckling responses for a fully clamped composite plate with an embedded elliptical delamination are presented and discussed. The derivation of the damage parameter in terms of the generalized coordinates and the load parameter is presented. Results for the conservative and non-conservative range are compared with finite element simulations using Abaqus. A critical discussion regarding the assumptions made and the delamination growth characteristics enabled by the model description closes Chapter 4.

Chapter 5 is concerned with a general discussion regarding the analytical framework and its application to the problems studied in Chapters 3 and 4. The general applicability of the framework is reviewed by means of theoretical considerations and the insight obtained from both application examples. Furthermore, requirements regarding appropriate model descriptions are discussed in detail.

The thesis closes with Chapter 6. It summarizes main aspects of the analytical framework and the two application examples from which conclusions are drawn with respect to the novelty and significance of the work as well as the applicability of the framework. Further work regarding the analytical framework and future application examples is outlined.

2 An analytical framework for the structural stability analysis of damageable structures

Within this chapter, an analytical framework for the structural stability analysis of mechanical systems prone to instability and damage propagation is developed. Mechanical systems which can be described by I generalized coordinates q_i, M loading parameters λ_m and K damage parameters (internal state variables) ξ_k are considered. The loading parameters are in the form of prescribed forces A_m or prescribed displacements α_m. It is assumed that the systems contain an arbitrary pre-existing state of damage which can be defined by the K damage parameters. The framework subdivides the deformation processes to be investigated into two parts:

- deformations in which all damage parameters remain constant (conservative process) and
- deformations in which at least one damage parameter evolves from a loading step to another (non-conservative process),

whereby it is not required that both types of deformation occur during a process. In the present work, the terminology conservative and non-conservative is strictly related to elastic, thus reversible, deformations and inelastic, thus irreversible, deformations respectively.

With the aid of the deformation paths shown in Fig. 2.1, the separation into reversible and irreversible deformation processes, as well as the uncertainty regarding the deformation behaviour in the inelastic region, is visualized. For illustration purposes, a system subjected to a single prescribed load A is considered. Initially, the deformation path is reversible but not necessarily linear. At the deformation state described by (α^0, A^0), inelastic deformation is caused. The dotted line in Figs. 2.1a and 2.1b indicates the system's response if purely elastic deformations were present (omitting damage growth). The dashed lines illustrate possible actual deformation paths considering inelastic deformations. Thus, in Figs. 2.1a and 2.1b, the area beneath the prescribed load *vs.* displacement curve (actual deformation

paths) describes the total work of deformation. Up to the deformation state (α^0, A^0) indicated by the symbol "$\circ$" the total work of deformation is equal to the strain energy. Thus, the symbol "$\circ$" illustrates the deformation state where the conventional elastic stability theory loses its validity.

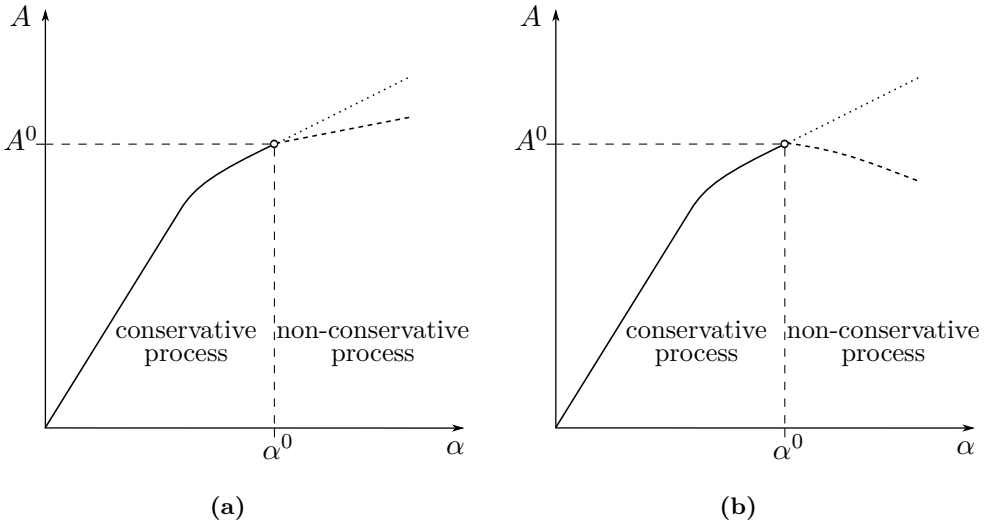

Fig. 2.1: Equilibrium paths for processes with a reversible (solid lines) and an irreversible part (dashed lines); **(a)** stable response in the inelastic region; **(b)** unstable response in the inelastic region; hypothetical reversible paths are indicated by dotted lines.

The stability of the equilibrium states during inelastic deformation can be examined from Figs. 2.1a and 2.1b. Whereas the deformation path in Fig. 2.1a is stable beyond the state where damage growth occurs, the path shown in Fig. 2.1b is unstable. In Fig. 2.1b, the deformation state at (α^0, A^0) describes a limit point from where the equilibrium loses its stability which has been elucidated in Section 1.1.

As discussed in the introductory chapter, quasi-static deformation processes are investigated throughout this work. Such a process is to be understood as a sequence of statical equilibrium states characterized by monotonically varying magnitudes of the prescribed loading parameter(s), such as the applied forces A_m. In general, the deformation path and its stability are determined with respect to changes in the physical quantities of interest from one loading step to another, *i.e.* in rate form. The governing functional depends on the velocity field (*e.g.* see [24, 74]), whereby *velocity* is understood as the change of the deformation state with respect to a monotonically varying loading parameter or a characteristic geometric parameter [24].

On the other hand, so long as purely elastic deformations occur, the same deformation path can be obtained by evaluating distinct prescribed magnitudes of the

loading parameter which are independent from each other, *i.e.* they do not follow a specific loading regime. Regarding the stability of statical equilibrium states and the deformation path itself, there is also no need to differentiate between a sequence of statical equilibrium states and statical equilibrium states corresponding to sets of independent magnitudes of the loading parameter. This is easily understood by recalling that the work of deformation is strictly path independent during elastic deformation. Thus, a perturbed process remains on the actual deformation path which is also obtained by a set of distinct magnitudes of load input. As a consequence, it is not necessary to describe the deformation process in rate form. Thus, in the elastic range, the deformation path corresponding to consecutive but independent magnitudes of loading constitutes the response of the system during a quasi-static process.[1]

This does not necessarily hold when inelastic deformations are present since the total work of deformation is, in general, path dependent. Hence, the change from one loading step to another becomes relevant, *i.e.* the rate form of the physical quantities of interest, and therefore distinct independent magnitudes of load input do not adequately describe the deformation behaviour. However, as described in Section 1.2, if the processes investigated are, at least in a limited sense, path independent, then the total work of deformation obeys a potential. Therefore, a description of such deformation processes in rate form is also not necessary.

Concluding the introductory thoughts, emphasis is placed on distinguishing between deformations with constant (reversible processes) and changing damage parameters (irreversible processes) as this is how the framework is set forth in the following.[2]

2.1 Reversible processes

For purely elastic deformations, the framework follows the total potential energy formalism of Thompson and Hunt described in [94]. The possibility of multiple independent load parameters is taken into account which is not specifically considered in [94] but which does not affect the theory to determine equilibrium states and their stability as described in Section 1.1. However, it plays a role in defining critical states such as limit and bifurcation points for which Huseyin [33] provides detailed explanation.

[1] Ref. [94] applies both possibilities in order to derive post-critical deformation paths for quasi-static deformation processes in the elastic range. First, distinct, for instance critical, deformation states are determined and subsequently the deformation path is derived by evaluating the response of the system for a change in the loading parameter, for instance with the aid of a Taylor series.

[2] Main aspects of the analytical framework developed in the current chapter are also described in the work [48] of the author.

In the following chapters, changes in the notation in comparison with Section 1.1 are implemented. This is done to draw attention specifically to the upcoming applications in which deformable continuum bodies are studied. Thus, the total potential energy is a functional Π of the displacement field $u_i = \{u, v, w\}^{\mathrm{T}}$ (in terms of a CARTESIAN coordinate system), thus

$$\Pi(u_i) = \int_V F\left(x_i, u_i, \frac{\partial u_i}{\partial x_j}\right) \mathrm{d}V, \tag{2.1.1}$$

where F can be regarded as the total potential energy density. If the boundary is subjected to prescribed displacements, F is the strain energy density w. For illustrative purposes, in terms of linear elastic behaviour and the assumption of infinitesimal strains,[3] Eq. (2.1.1) can be rewritten such that

$$\Pi(u_i) = \int_V \frac{1}{2}\sigma_{ij}\varepsilon_{ji}\,\mathrm{d}V - \int_{\partial V_{\mathrm{t}}} t_i u_i\,\mathrm{d}A \tag{2.1.2}$$

where σ_{ij} are the CAUCHY stresses, ε_{ij} the infinitesimal strains and t_i the surface tractions. The first part of Eq. (2.1.2) is the strain energy and the second part describes the work done by the surface tractions.[4]

By employing the discrete coordinate approach in the form of a finite set of continuous mode-forms, for instance as in a RAYLEIGH–RITZ formulation, the displacement field u_i is, in general, approximated and expressed in terms of the generalized coordinates q_i and the respective mode or shape functions depending on the spatial coordinates x_k, thus $u_j \approx \hat{u}_j(x_k, q_i)$. However, as the continuous mode or shape functions are fixed, *i.e.* the magnitude of the displacement depends on the generalized coordinates only, the approximated displacement field is generally expressed as $\hat{u}_j = \hat{u}_j(q_i)$. Therefore, the total potential energy can be written in terms of the generalized coordinates rather than the displacement field, *i.e.*:

$$\Pi(q_i) = \int_V w\left(q_i\right)\,\mathrm{d}V - \int_{\partial V_{\mathrm{t}}} t_j \hat{u}_j(q_i)\,\mathrm{d}A, \tag{2.1.3}$$

where Π may still be regarded as the total potential energy functional and therefore the notation for continuous descriptions is adopted henceforth. It should be noted that in Eq. (2.1.3), w denotes the strain energy density and the displacement field u_j in the work done by the surface tractions is replaced by $\hat{u}_j$.

[3] Eq. (2.1.2) can be readily rewritten in terms of geometrically non-linear behaviour using the reference configuration as well as the SECOND PIOLA–KIRCHHOFF stresses S_{ij} and the GREEN–LAGRANGE strains E_{ij} instead of σ_{ij} and ε_{ij} respectively.

[4] Since body forces are not considered in the current work, the work done by the body forces is omitted in the total potential energy Π in Eq. (2.1.2).

On the other hand, the specific characterization of the respective loading parameter is adopted from [94], such that $\Pi = \Pi(q_i, \lambda)$. However, the dependence of the functional on the generalized coordinates only remains unaffected.

The notation V will be used in the subsequent passage to refer to a thermodynamic state function characterizing an isothermal reversible process in terms of a force measure A_m. This function is referred to as the total potential energy function which is a potential of the conjugate displacements to the prescribed forces. The total potential energy function can be directly deduced from the well-known thermodynamic state functions,

$$\phi = \phi(\varepsilon_{ij}, T) \quad \text{and} \quad \psi = \psi(\sigma_{ij}, T), \tag{2.1.4}$$

where ϕ is the specific HELMHOLTZ free energy and ψ is the specific GIBBS free energy. In Eq. (2.1.4), ε_{ij} and σ_{ij} describe a strain and stress measure respectively. For the isothermal processes considered within this work, the GIBBS free energy and the HELMHOLTZ free energy are the total potential energy function V and the strain energy function W_{rev} respectively (*cf.* Appendix A).

In the current work, the systems are examined in terms of generalized displacements (α_m) and generalized forces (A_m) which replace the strain and stress measure in Eq. (2.1.4) respectively. Thus, the total potential energy is a function of the generalized forces, *i.e.* $V = V(A_m)$ which can be readily derived from the strain energy $W_{\text{rev}} = W_{\text{rev}}(\alpha_m)$ using the LEGENDRE transformation [63],

$$\begin{aligned}
\mathrm{d}W_{\text{rev}} = &\quad \frac{\partial W_{\text{rev}}}{\partial \alpha_m}\,\mathrm{d}\alpha_m \quad \text{with} \quad \frac{\partial W_{\text{rev}}}{\partial \alpha_m} = A_m \quad \text{follows,} \\
= &\quad \mathrm{d}(A_m \alpha_m) \quad - \alpha_m\,\mathrm{d}A_m, \\
\mathrm{d}(\underbrace{W_{\text{rev}} - A_m \alpha_m}_{V}) = &\quad -\alpha_m\,\mathrm{d}A_m, \\
\mathrm{d}V = &\quad \frac{\partial V}{\partial A_m}\,\mathrm{d}A_m \quad \Longrightarrow V = V(A_m).
\end{aligned} \tag{2.1.5}$$

The functions V and W_{rev} are used in Section 2.2.1 to derive other thermodynamic state functions which allow the description of irreversible deformation processes in terms of the prescribed loading parameters only.

2.1.1 Total potential energy principle

The total potential energy (Π) of a mechanical system described by I generalized coordinates q_i, and adopting the notation given in Section 2.1, reads

$$\Pi(q_i, A_m) = W(q_i) - A_m \alpha_m(q_i), \tag{2.1.6}$$

with W being the strain energy, $i = 1, 2, ..., I$ and $m = 1, 2, ..., M$. The prescribed loads (A_m) and their conjugate displacements (α_m) describe the work done by the external forces. If not explicitly stated otherwise, the summation convention is employed in which a repeated index is to be summed over its range. The prescribed loads A_m and the conjugate displacements α_m may also be understood as independent generalized forces and generalized displacements respectively. Applying the well-known variational principle [76],

$$\delta\Pi = \frac{\partial \Pi}{\partial q_i}\delta q_i = 0 \implies \frac{\partial \Pi}{\partial q_i} = 0, \tag{2.1.7}$$

yields the equilibrium solutions, *i.e.* the deformation paths $A_m(q_i)$.[5]

In Eq. (2.1.6), the current state of damage may be considered by a set of damage parameters ξ_k. However, the assumption that all damage parameters do not change must hold. Thus, the total potential energy given in Eq. (2.1.6) may be expressed as

$$\Pi(q_i, A_m, \xi_k) = W(q_i, \xi_k) - A_m \alpha_m(q_i, \xi_k), \quad \text{for} \quad \xi_k = \text{const.}, \tag{2.1.8}$$

in which the dependency with respect to the current state of damage is accounted for and treated as a prescribed constant input not dissimilar to the treatment of imperfections in [94]. However, only the deformation behaviour under a given constant state of damage may be modelled.

2.1.2 Thermodynamic forces

Equilibrium states along the deformation path obtained from Eq. (2.1.7) in terms of $q_i(A_m)$ can be examined with regards to the available forces for producing a change in the structure, referred to as the thermodynamic forces f_k. These forces are the conjugate parameters to the damage parameters ξ_k which have to be considered when the thermodynamic state of structures possessing a certain state of damage is characterized. Thus, the total potential energy function can be expressed as

$$V = V(A_m, \xi_k) \quad \text{for} \quad \xi_k = \text{const.} \tag{2.1.9}$$

Differentiating Eq. (2.1.9) with respect to the kth damage parameter yields the thermodynamic force,

[5] Eq. (2.1.7) provides the solution in terms of $q_i(A_m)$ which, however, is commonly expressed in terms of $A_m(q_i)$ [4, 94, 95].

$$f_k = -\frac{\partial V}{\partial \xi_k}, \tag{2.1.10}$$

available for producing a change in the kth damage parameter. So long as the thermodynamic force is smaller than a certain threshold, no change in structure occurs and the total potential energy principle can be applied.

By considering the conjugate parameters f_k and ξ_k, the system is taken through a sequence of so-called constrained equilibrium states in which the damage parameters are locked but the conjugate forces do not necessarily vanish [63]. This also applies later on when irreversible processes are considered in which the damage parameters evolve from one loading step to another. However, for each loading step the system remains in a constrained equilibrium, if an equilibrium exists.

2.2 Irreversible processes

The analytical framework for modelling inelastic deformations is based on the derivation of an extended total potential energy functional $\Pi^*(q_i)$. This allows the description of the response of the system by a set of generalized coordinates only, without the limitation of a non-evolving state of damage (ξ_k are not assumed constant any more).

First, the deformation state must be determined where the thermodynamic force reaches the threshold required for producing a change in structure which is denoted by the parameters g_k. A change in structure occurs if, at least for one damage parameter, the following condition is fulfilled:

$$f_k \geq g_k. \tag{2.2.1}$$

At this deformation state, the total potential energy principle described in Section 2.1.1 loses its validity.

Before an extended total potential energy functional in terms of $\Pi^*(q_i)$ can be derived, it is required to discuss the condition so that the total work of deformation and the extended total potential energy obey a potential. If the total work of deformation and the extended total potential energy can be expressed in the form of a potential, then it is possible to derive a variational principle in which the extended total potential energy functional is one of the generalized coordinates only. This means that the changes in structure, generally governed by the respective constitutive laws regarding the damage parameters ξ_k, are considered by the deformation behaviour obtained by solving the variational principle in the generalized coordinates.

2.2.1 Total work of deformation and extended total potential energy

In this section, the response of a mechanical system is described in terms of generalized displacements (α_m) and generalized forces (A_m). Consequently, it is necessary to differentiate between systems where the boundary is subjected to prescribed displacements (displacement-controlled) or prescribed loads (load-controlled).[6] In reversible processes, for prescribed displacements, the governing functional is the strain energy which is a function W_{rev} of the independent generalized displacements (α_m) and the current state of damage defined by K damage parameters (ξ_k), *i.e.*

$$W_{\text{rev}} = W_{\text{rev}}(\alpha_m, \xi_k). \tag{2.2.2}$$

On the other hand, when prescribed loads are present, the problem is described by the total potential energy which is a function of the independent generalized forces (A_m) and the damage parameters (ξ_k), *i.e.*

$$V = V(A_m, \xi_k). \tag{2.2.3}$$

By applying the theory presented in Section 1.2, the condition for describing the total work of deformation and the extended total potential energy only in terms of the generalized displacements and the generalized forces respectively is elaborated next.

2.2.1.1 Prescribed displacements

The total derivative of the strain energy function reads

$$\mathrm{d}W_{\text{rev}} = \left.\frac{\partial W_{\text{rev}}}{\partial \alpha_m}\right|_{\xi_k} \mathrm{d}\alpha_m + \left.\frac{\partial W_{\text{rev}}}{\partial \xi_k}\right|_{\alpha_m} \mathrm{d}\xi_k \quad \text{where} \quad f_k = -\frac{\partial W_{\text{rev}}}{\partial \xi_k}, \tag{2.2.4}$$

in which f_k is the thermodynamic force associated with the kth damage parameter. Since the strain energy is a constitutive potential of the generalized forces, the first term in Eq. (2.2.4) can be expressed as

$$A_m = \left.\frac{\partial W_{\text{rev}}}{\partial \alpha_m}\right|_{\xi_k}. \tag{2.2.5}$$

[6] A combination of prescribed displacements and prescribed loads is also covered by the framework. However, in order to provide a clear description, Section 2.2.1 distinguishes strictly between prescribed displacements and prescribed forces.

Rearranging Eq. (2.2.4) and employing Eqs. $(2.2.4)_2$ and (2.2.5) yields

$$A_m \, \mathrm{d}\alpha_m = \mathrm{d}W_{\mathrm{rev}} + f_k \, \mathrm{d}\xi_k, \tag{2.2.6}$$

from where it becomes obvious that whenever a change in structure occurs, the work done by the generalized displacements is not equal to the strain energy any more. However, a change in structure, *i.e.* $\dot{\xi}_k > 0$,[7] is only generated if the thermodynamic force reaches the threshold, as stated in Eq. (2.2.1). If this threshold is reached, then the total work of deformation W_{tot}—obtained by integrating Eq. (2.2.6) along the actual deformation path—is equal to the sum of elastic energy (W_{rev}) and energy associated with dissipation (W_{d}), thus

$$W_{\mathrm{tot}}(\alpha_m, \xi_k) = W_{\mathrm{rev}}(\alpha_m, \xi_k) + W_{\mathrm{d}}(\xi_k), \tag{2.2.7}$$

where the dissipative energy is assumed to be a state function depending on the damage parameters only. It is a potential of the forces required for a change in structure g_k, *i.e.*:

$$g_k = \frac{\partial W_{\mathrm{d}}}{\partial \xi_k}. \tag{2.2.8}$$

It should be noted that g_k may also be material parameters.

In order to express the total work of deformation in terms of a potential of the generalized forces, the damage parameters need to be derived as functions of the independent generalized displacements. This can be done, whenever, during the non-conservative deformation process, f_k equals g_k. Then, Eqs. $(2.2.4)_2$ and (2.2.8) yield

$$f_k(\alpha_m, \xi_k) = g_k(\xi_k) \Longrightarrow -\frac{\partial W_{\mathrm{rev}}}{\partial \xi_k} = \frac{\partial W_{\mathrm{d}}}{\partial \xi_k}. \tag{2.2.9}$$

From the set of equations in Eq. $(2.2.9)_2$, the damage parameters ξ_k may be derived in terms of the independent generalized displacements α_m, *i.e.* $\xi_k = \xi_k(\alpha_m)$ assuming that Eq. $(2.2.9)_2$ provides a unique solution for the damage parameters ξ_k, differentiable in α_m. Therefore, Eq. $(2.2.9)_2$ can be understood as the *evolution law* for the damage parameters ξ_k.[8]

By substituting $\xi_k(\alpha_m)$ in Eq. (2.2.7), W_{tot} is found as a function of the independent generalized displacements only, *i.e.* $W_{\mathrm{tot}} = W_{\mathrm{tot}}(\alpha_m)$. This means that the function W_{tot} considers the change in the respective damage parameters during the deformation process. Thus, with the derived relationship between the prescribed

[7] The dot symbolizes the change of the damage parameter from one loading step to another.
[8] With Eq. (2.2.9), the second term on the right hand side in Eq. (2.2.6) can be also determined resulting in Eq. (2.2.7).

generalized displacements and the damage parameters, W_{tot} characterizes an actual deformation process, where

$$W_{\mathrm{tot}} = \int A_m \, \mathrm{d}\alpha_m, \tag{2.2.10}$$

constitutes the total work of deformation which is a potential of the generalized forces, *i.e.*

$$A_m = \frac{\partial W_{\mathrm{tot}}}{\partial \alpha_m}. \tag{2.2.11}$$

It should be stressed that only if the condition of $f_k = g_k$ holds during an irreversible deformation process, the total work of deformation can be solely expressed in terms of the generalized displacements. Thus, $f_k = g_k$ is the sufficient condition, such that Eqs. (2.2.10) and (2.2.11) are valid.

2.2.1.2 Prescribed forces

As discussed in Section 2.1, the total potential energy characterizes isothermal reversible deformation processes in which generalized forces serve as the independent variables. In a similar manner to Section 2.2.1.1, first, the total derivative of the total potential energy, $V = V(A_m, \xi_k)$, is examined, *i.e.*:

$$\mathrm{d}V = \left.\frac{\partial V}{\partial A_m}\right|_{\xi_k} \mathrm{d}A_m + \left.\frac{\partial V}{\partial \xi_k}\right|_{A_m} \mathrm{d}\xi_k \quad \text{where} \quad f_k(A_m, \xi_k) = -\frac{\partial V}{\partial \xi_k}. \tag{2.2.12}$$

From Eq. (2.2.12) follows that the thermodynamic forces f_k are equal to the (negative) change of the total potential energy with respect to the damage parameters ξ_k. The forces required for a change in structure are determined, as in Section 2.2.1.1, by the change of the dissipative energy with respect to the kth damage parameter, thus:

$$g_k = \frac{\partial W_{\mathrm{d}}}{\partial \xi_k}. \tag{2.2.13}$$

Next, whenever during the non-conservative part of the deformation process the parameters f_k are equal to g_k, a set of equations in the form of

$$f_k(A_m, \xi_k) = g_k(\xi_k) \Longrightarrow -\frac{\partial V}{\partial \xi_k} = \frac{\partial W_{\mathrm{d}}}{\partial \xi_k}, \tag{2.2.14}$$

can be derived from which the damage parameters may be found as functions of the independent generalized forces, *i.e.* $\xi_k = \xi_k(A_m)$. Therefore, Eq. $(2.2.14)_2$ serves as the *evolution law* for ξ_k in load-controlled configurations.

The energy that characterizes the irreversible deformation process is denoted by V^* and consists of the total potential energy V and the dissipative energy W_d (assumed to be a state function of the damage parameters), *i.e.*:

$$V^*(A_m, \xi_k) = V(A_m, \xi_k) + W_\mathrm{d}(\xi_k). \tag{2.2.15}$$

Inserting the functions $\xi_k = \xi_k(A_m)$ into Eq. (2.2.15) yields that V^* depends on the generalized forces only. In the following, $V^* = V^*(A_m)$ will be referred to as the *extended total potential energy*. The extended total potential energy comprises the evolution of the damage parameters and therefore characterizes the actual deformation process. As a consequence, during an inelastic deformation process which fulfils the condition that $f_k = g_k$, the extended total potential energy can be obtained by the expression:

$$V^* = -\int \alpha_m \, \mathrm{d}A_m, \tag{2.2.16}$$

which describes a potential of the generalized displacements, thus

$$\alpha_m = -\frac{\partial V^*}{\partial A_m}. \tag{2.2.17}$$

In summary, Eq. (2.2.14) is the sufficient condition, such that Eqs. (2.2.16) and (2.2.17) hold for an irreversible deformation process, thus an extended total potential exists which depends on the generalized forces only.

2.2.2 Extended total potential energy principle

For now, it is assumed that during an irreversible deformation process the condition of equilibrium between f_k and g_k holds and that a potential form of the extended total potential energy, as described in Eqs. (2.2.16) and (2.2.17), could be found. For such processes, a variational principle in the form of $\delta\Pi^*(q_i) = 0$ may be derived; Π^* is the extended total potential energy functional comprising the total work of deformation and the work done by the external forces. Such a variational principle is not dissimilar to the principles described in [24, 25, 74, 75] for continuous problems, *i.e.*

$$\delta J(v_i) = \int_{\mathcal{B}} \delta E(\nabla v_i) \, \mathrm{d}V - \int_{\mathcal{S}_\mathrm{t}} \dot{t}_i \delta v_i \, \mathrm{d}A - \int_{\mathcal{B}} \rho \dot{b}_i \delta v_i \, \mathrm{d}V = 0, \tag{2.2.18}$$

in which J is a functional of the velocity field v_i, E is a potential of the stress rates, t_i are the surface tractions and b_i are the body forces. In Eq. (2.2.18), a dot denotes a differentiation with respect to time. However, as mentioned in the

introductory part of the current chapter, *time* may be regarded as a parameter characterizing the quasi-static deformation process rather than the *natural time*.

As discussed before, whenever the respective energies—total work of deformation or the extended total potential energy—may be expressed in the form of a potential, the deformation process exhibits path independence. Thus, a description in rate form, as done in Eq. (2.2.18), is not necessary. The deformation path for an irreversible process which complies with the condition of $f_k = g_k$ can be determined by a variational principle in terms of the displacement field u_i for respective prescribed magnitudes of loading. Thus, Eq. (2.2.18) can be rewritten as

$$\delta\Pi^*(u_i) = \int_{\mathcal{B}} \delta w_\mathrm{t}(\nabla u_i)\,\mathrm{d}V - \int_{\mathcal{S}_\mathrm{t}} t_i \delta u_i\,\mathrm{d}A = 0, \tag{2.2.19}$$

where Π^* can be regarded as the extended total potential energy functional in a continuous matter and the work done by the body forces is omitted. In Eq. (2.2.19), $\int w_\mathrm{t}\,\mathrm{d}V$ is the total work of deformation W_t (elastic plus dissipative energy contributions). Eq. (2.2.19) yields the Euler–Lagrange equations of systems under prescribed magnitudes of loading.

In the context of the discrete coordinate approach, Eq. (2.2.19) can be directly transformed into a description using I generalized coordinates q_i, for instance by applying continuous mode-forms as described in Section 2.1. Thus, the variational principle using the extended total potential energy functional Π^* reads

$$\delta\Pi^*(q_i) = \delta\Big(W_\mathrm{t}(q_i) - A_m\alpha_m(q_i)\Big) = 0. \tag{2.2.20}$$

It should be noted that in Eq. (2.2.20) the damage parameters are already considered and replaced by functions of the generalized forces A_m and the generalized coordinates q_i, *i.e.*

$$\xi_k = \xi_k(q_i, A_m), \tag{2.2.21}$$

using the condition $f_k = g_k$. In Eq. (2.2.21), the generalized coordinates are accounted for since the equilibrium path is not determined yet. Once the equilibrium path, $q_i(A_m)$, is obtained with the aid of Eq. (2.2.20), the evolution of the damage parameters are expressed in terms of the generalized forces only, as described in Section 2.2.1.2.

In comparison with Eq. (2.1.8), the dissipative energy (W_d) is added and the damage parameters are replaced. Thus, the extended total potential energy can

be written as

$$\begin{aligned}\Pi^*(q_i, A_m) &= W\Big(q_i, \xi_k(q_i, A_m)\Big) + W_\mathrm{d}\Big(\xi_k(q_i, A_m)\Big) \\ &\quad - A_m\alpha_m\Big(q_i, \xi_k(q_i, A_m)\Big) \\ &= W_\mathrm{t}(q_i, A_m) - A_m\alpha_m(q_i, A_m),\end{aligned} \tag{2.2.22}$$

in which the total work of deformation (W_t) is the sum of the reversible strain energy (W) and the dissipative energy (W_d) associated with a change in the damage parameters.

At the moment, regarding the variational principle in Eq. (2.2.20), it does not matter how the damage parameters are derived in the form of Eq. (2.2.21). The derivation of the damage parameters is explained in detail in the subsequent Section 2.3.

By solving Eq. (2.2.20), the deformation behaviour of mechanical systems is obtained in terms of $q_i(A_m)$ starting from the deformation state where damage propagation is initiated, thus where the condition $f_k = g_k$ is fulfilled first. Inserting the solution into the K damage parameters, $\xi_k(q_i(A_m), A_m)$, provides information about the damage propagation within the structure from one loading step to another. Hence, for processes which comply with the condition $f_k = g_k$, the variational principle proposed in Eq. (2.2.20) provides the equilibrium solution for prescribed magnitudes of loading and the corresponding evolution of the K damage parameters.

This variational principle differs from other approaches in the literature (*e.g.* [17, 21]) not only regarding its discrete manner but also its *a priori* incorporation of the damage evolution. Therefore, unlike the formulation proposed in the current work that yields the deformation behaviour (equilibrium equations) which already comprises the damage evolution, the variational principles described in [17, 21] give the macroscopic force balance and the yield criterion for damage propagation.

The condition $f_k = g_k$, herein assumed to hold during the irreversible processes investigated, embodies the yield criterion in the proposed formalism and is incorporated in the variational principle by replacing the damage parameters in the form of Eq. (2.2.21). This is in contrast to [17] where the yield criterion is an inequality, basically in the form of Eq. (2.2.1). Therefore, unlike the deformation processes considered in this work, the principles documented in [17, 21] do not require a potential form of the total work of deformation. As a consequence, the condition $f_k = g_k$, though applicable to certain damaging processes, allows a highly efficient description of the deformation process, *viz.* a variational problem in which only the deformation state is perturbed.

The difference in comparison with [17, 21] can be observed by examining the

total work of deformation, as done in [17], and assuming, for demonstration purposes, a one degree of freedom problem with a single damage parameter (ξ). Thus, following [17], both the deformation state and the damage state are perturbed, yielding a minimization problem which reads

$$W_{\mathrm{t}}(q,\xi) \leq W_{\mathrm{t}}(q+\eta,\xi+\chi), \tag{2.2.23}$$

in which η and χ are independent perturbations of the deformation and damage state respectively. However, in the framework proposed, the damage parameter is obtained *a priori* by means of the deformation state[9] which results in

$$W_{\mathrm{t}}(q,\xi) \leq W_{\mathrm{t}}\left(q+\eta,\xi(q+\eta)\right) \quad \text{with} \quad \xi=\xi(q) \quad \text{for} \quad f_k=g_k, \tag{2.2.24}$$

which holds starting from the deformation state where damage propagation is initiated, and the solution is a minimizer of the total work of deformation.

However, the solution must also comply with the *second law of thermodynamics*, *i.e.* healing of the structure is not allowed, so $\dot{\xi}_k \geq 0$ or in a quasi-static loading regime $\xi_k^i \supseteq \xi_k^{i-1}$ for i loading steps. This unilateral constraint is not included *a priori* in the formalism. However, as the damage parameters $\xi_k = \xi_k(q_i, A_m)$ have been predetermined, the variational principle provides one solution path on which the deformation state triggering inelastic deformation is located. Depending on the subsequent applied loading starting from the deformation state where the condition $f_k = g_k$ is fulfilled first, the solution path either complies with the *second law of thermodynamics* or violates it. Fig. 2.2 illustrates that matter with the aid of the well-known double cantilever beam (DCB) test.

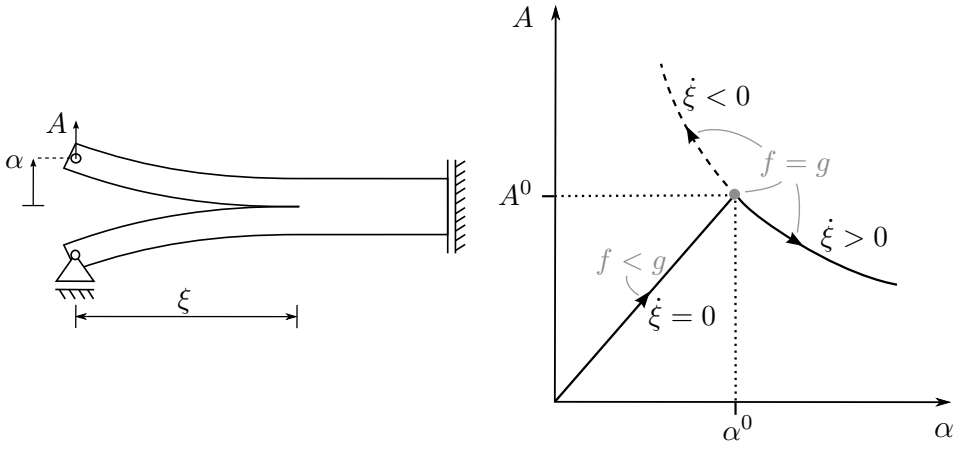

Fig. 2.2: Double cantilever beam test with the characteristic load–deflection response.

[9] As it is irrelevant for the variational principle, the dependence of the damage parameter on the loading parameter is neglected for demonstration purposes.

At the deformation state (α^0, A^0) growth of the damage parameter (ξ) is initiated and the solution of the variational principle would provide the deformation path starting from (α^0, A^0)—both dashed and solid line in Fig. 2.2. The loading path which fulfils the condition of non-healing damage—solid line in Fig. 2.2—is the actual deformation path of the system. The procedure to choose the correct path direction starting from (α^0, A^0) is readily implemented in a respective solving algorithm which evaluates for the first loading step of the respective path directions whether the response is associated with growth (actual deformation path) or healing (subsequently omitted). This *a posteriori* procedure is seen as advantageous for the framework, so that a variational principle of only the generalized coordinates can be employed for modelling the non-conservative part of the deformation processes considered in this work.

2.3 Structural stability analysis with damage propagation

In this section, the formalism of the structural stability analysis of mechanical systems S described by I generalized coordinates q_i, M loading parameters λ_m and K damage parameters ξ_k is presented. Therefore, Fig. 2.3 summarizes the analytical framework developed within this chapter.

Fig. 2.3 shows the strict distinction of the framework between the conservative and non-conservative part of a deformation process. It is assumed that the system contains a certain pre-existing state of damage definable by the K damage parameters ξ_k. Hence, damage initiation is not considered within the formalism. For instance, in multi-layered composite structures such pre-existing damage may be a transverse matrix crack or a delamination where ξ_k would be the crack area or the delamination area, respectively.

The formalism of the structural stability analysis commences by treating the system as conservative (segment "Conservative process" in Fig. 2.3), thus all damage parameters remain in its initial magnitude. Whether or not this actually applies for the respective deformation process will be determined once the thermodynamic forces for the current loading step are evaluated. The governing functional for the conservative part of the deformation process is the strain energy or the total potential energy which depends on whether independent generalized displacements or independent generalized forces act on the boundary. Both functionals may be expressed by Π in Fig. 2.3. In the following, the formalism is delineated using the total potential energy as the governing functional.

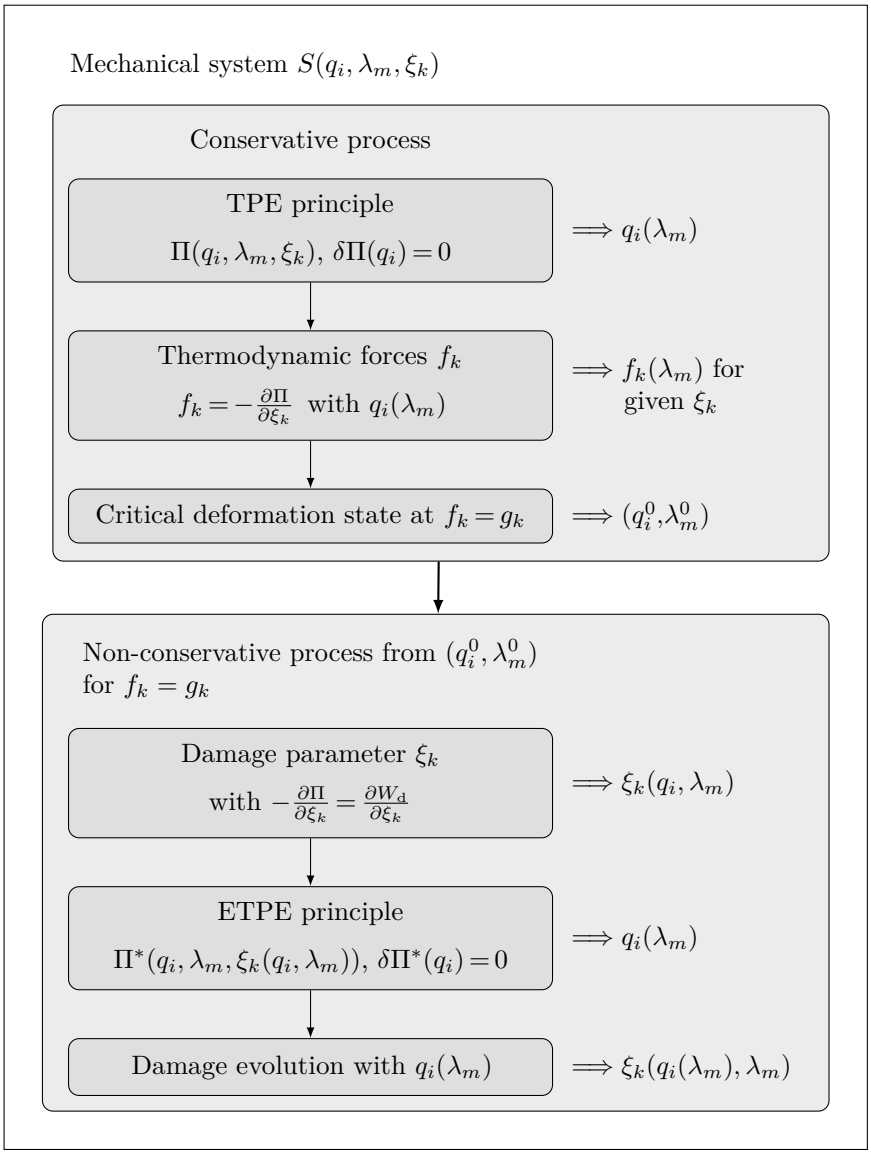

Fig. 2.3: Framework for the structural stability analysis of damageable structures; abbreviations: TPE – total potential energy, ETPE – extended total potential energy.

As illustrated in Fig. 2.3, first, with the aid of the conventional total potential energy principle, $\delta\Pi = 0$ (*cf.* Eq. (2.1.7) and Section 2.1.1), the deformation paths $q_i(\lambda_m)$ are determined for the given (constant) state of damage. Therefore, the following steps are performed referring to the first box within the conservative segment in Fig. 2.3.

- The displacement field is expressed in terms of the generalized coordinates. This can be done in a discrete manner or by continuous mode-forms as part of an approximation method (*e.g.* a Rayleigh–Ritz or Galerkin

formulation) whereby the respective boundary conditions defined by the mechanical system S have to be considered.

- The total potential energy is derived in terms of the generalized coordinates, the load parameters and the damage parameters.
- The set of algebraic equations resulting from the variational principle, $\delta\Pi = 0$, is solved either analytically (if possible) or numerically.

With the deformation path $q_i(\lambda_m)$, the thermodynamic forces associated with the K damage parameters, thus the forces available for producing a change in structure, are determined next (second box within the conservative segment in Fig. 2.3). As illustrated in Fig. 2.3 and described in Sections 2.1.2 and 2.2, therefore, the negative of the partial derivative of the total potential energy with respect to the damage parameters is calculated. This can be done without the knowledge of the deformation path, so that Π is used in Fig. 2.3. The thermodynamic forces are then readily determined by inserting the deformation path obtained by the total potential energy principle. As a result, the thermodynamic forces can be expressed in terms of the applied loading parameters.

In the next step, the deformation state is determined in which for the kth damage parameter the thermodynamic force f_k reaches the threshold g_k required for producing a change in the respective damage parameter (third box within the conservative segment in Fig. 2.3). The total potential energy principle is limited to this deformation state which is defined by a set of generalized coordinates (q_i^0) and the load parameters (λ_m^0), and is referred to as *damage state* rather than *critical state* to avoid confusion with the terminology of the structural stability analysis.

In order to determine the damage state, in addition to the information provided by the previous steps, the dissipative energy W_d has to be introduced. The dissipative energy is assumed to be a potential of the parameters g_k, *i.e.* the forces required for damage growth g_k can be determined by differentiating the dissipation potential with respect to the damage parameters ξ_k. On the other hand, the parameters g_k can also be material parameters which allows for a direct comparison with the thermodynamic forces. The formalism for the conservative process ends at the damage state (q_i^0, λ_m^0).

Before the non-conservative part of the deformation process can be modelled, it is required to verify that the condition $f_k = g_k$ holds during the subsequent non-conservative deformation. This can be done by analysing the behaviour of the thermodynamic forces with respect to the loading parameters and the damage parameters. If the condition $f_k = g_k$ is fulfilled, then the deformation path starting

from the damage state is determined by the formalism outlined in the segment "Non-conservative process" in Fig. 2.3.

As shown in the first box within the non-conservative segment in Fig. 2.3, Eq. $(2.2.14)_2$ is used to derive the respective (active) damage parameters ξ_k in terms of the generalized coordinates q_i and the loading parameters λ_m. If displacements are prescribed, the governing functional is the strain energy and Eq. $(2.2.9)_2$ is used instead. As mentioned before, Π is used rather than V (*cf.* Section 2.2.1.2) since the damage parameters depend on the deformation path $q_i(\lambda_m)$ that is to be determined. In general, it is not possible to obtain an explicit solution for the damage parameters from Eq. $(2.2.14)_2$, however, rewriting Eqs. $(2.2.14)_2$, such that

$$f_k - g_k = -\frac{\partial \Pi}{\partial \xi_k} - \frac{\partial W_\mathrm{d}}{\partial \xi_k} = 0, \tag{2.3.1}$$

yields the functions D_k, *i.e.*

$$D_k\Big(q_i, \lambda_m, \xi_k\Big) = 0. \tag{2.3.2}$$

From Eq. (2.3.2), $\xi_k(q_i, \lambda_m)$ is implicitly given assuming that a unique solution of $\xi_k(q_i, \lambda_m)$ exists, thus:

$$D_k\Big(q_i, \lambda_m, \xi_k(q_i, \lambda_m)\Big) \equiv 0. \tag{2.3.3}$$

In order to obtain an explicit form of $\xi_k(q_i, \lambda_m)$ a Taylor series approximation around the damage state (q_i^0, λ_m^0) is employed, thus

$$\begin{aligned}
\xi_k(q_i, \lambda_m) \;= \xi_k^0 &+ \left.\frac{\partial \xi_k}{\partial q_i}\right|_{\substack{q_i^0 \\ \lambda_m^0}} (q_i - q_i^0) + \left.\frac{\partial \xi_k}{\partial \lambda_m}\right|_{\substack{q_i^0 \\ \lambda_m^0}} (\lambda_m - \lambda_m^0) \\
&+ \frac{1}{2} \left.\frac{\partial^2 \xi_k}{\partial q_i \partial q_j}\right|_{\substack{q_i^0 \\ \lambda_m^0}} (q_i - q_i^0)(q_j - q_j^0) \\
&+ \frac{1}{2} \left.\frac{\partial^2 \xi_k}{\partial \lambda_m \partial \lambda_n}\right|_{\substack{q_i^0 \\ \lambda_m^0}} (\lambda_m - \lambda_m^0)(\lambda_n - \lambda_n^0) \\
&+ \left.\frac{\partial^2 \xi_k}{\partial q_i \partial \lambda_m}\right|_{\substack{q_i^0 \\ \lambda_m^0}} (q_i - q_i^0)(\lambda_m - \lambda_m^0) + \mathcal{O}(3),
\end{aligned} \tag{2.3.4}$$

in which ξ_k^0 is the pre-existing magnitude of the kth damage parameter. For the sake of clarity, the Taylor series in Eq. (2.3.4) is provided up to the 2nd order only. However, depending on the given problem, higher order terms may, of

course, be considered in the formalism which also results in higher computational demand.

With the aid of Eq. (2.3.3), the derivatives of ξ_k with respect to q_i and λ_m are obtained by implicit differentiation. Thus, differentiating Eq. (2.3.3) with respect to q_i and λ_m and applying the chain rule yields the derivatives of ξ_k used in Eq. (2.3.4), following some rearranging. For instance, the first order derivative with respect to q_i is obtained as follows:

$$\frac{\mathrm{d}D_k}{\mathrm{d}q_i} = \frac{\partial D_k}{\partial q_i} + \frac{\partial D_k}{\partial \xi_k}\frac{\partial \xi_k}{\partial q_i} \equiv 0 \Longrightarrow \frac{\partial \xi_k}{\partial q_i} = -\frac{\frac{\partial D_k}{\partial q_i}}{\frac{\partial D_k}{\partial \xi_k}}. \tag{2.3.5}$$

It should be noted that there is no summation of the index k in Eq. (2.3.5). The calculation for the derivative with respect to the loading parameters is analogous to Eq. (2.3.5) in which q_i is to be replaced by λ_m. The first order derivatives of the damage parameters provided by Eq. $(2.3.5)_2$ can then be used to determine the second order derivatives, thus

$$\frac{\partial^2 \xi_k}{\partial q_i \partial q_j} = -\frac{D_{k,_{ij}} + D_{k,_{ik}}\xi_{k,_j} + D_{k,_{jk}}\xi_{k,_i} + D_{k,_{kk}}\xi_{k,_i}\xi_{k,_j}}{D_{k,_k}}. \tag{2.3.6}$$

In Eq. (2.3.6), for the sake of clarity, partial derivatives are expressed in the form of $\partial(\bullet)/\partial q_i = (\bullet)_{,i}$ which applies also for the differentiation with respect to the K damage parameters and the load parameters; there is also no summation over the index k.

Subsequently, with the damage parameters given by Eq. (2.3.4), the extended total potential energy principle is applied (*cf.* second box within the non-conservative segment in Fig. 2.3 and Eq. (2.2.20)). The extended total potential energy Π^* consists of the total potential energy and the dissipative energy contributions associated with the respective active damage parameters in which these damage parameters are replaced by the functions in Eq. (2.3.4), *i.e.*:

$$\begin{aligned} \Pi^*(q_i, A_m, \xi_k(q_i, A_m)) &= W\big(q_i, \xi_k(q_i, A_m)\big) + W_\mathrm{d}\big(\xi_k(q_i, A_m)\big) \\ &\quad - A_m \alpha_m\big(q_i, \xi_k(q_i, A_m)\big) \\ &= W_\mathrm{t} - A_m \alpha_m. \end{aligned} \tag{2.3.7}$$

In Eq. (2.3.7), the loading parameter is replaced by the independent generalized forces A_m as the extended total potential energy is exemplarily considered. If the load parameters are the independent generalized displacements, the total work of deformation is the governing functional.

The variational principle using Eq. (2.3.7) reads

$$\delta\Pi^*(q_i) = \delta(W + W_\mathrm{d} - A_m\alpha_m) = \delta(W_\mathrm{t} - A_m\alpha_m) = 0. \tag{2.3.8}$$

The solution of Eq. (2.3.8) is the equilibrium path $q_i(A_m)$ for the non-conservative part of the deformation process in which $f_k = g_k$ holds starting from the damage state (q_i^0, A_m^0). The evolution of the damage parameters ξ_k is obtained by inserting the solution from Eq. (2.3.8) into Eq. (2.3.4).

Since the evolution of the damage parameters is approximated, the solution obtained from Eq. (2.3.8) is consecutively examined regarding whether the requirement $f_k = g_k$ is fulfilled. Once this is violated, the procedure restarts with a new damage state (q_i^0, A_m^0) which describes the deformation state for which the requirement $f_k = g_k$ was fulfilled last. This procedure is implemented in an iterative scheme which approximates the damage evolution and solves the extended total potential principle consecutively.

In summary, using the conventional total potential energy principle up to the damage state and subsequently applying the extended total potential energy principle enables the determination of the deformation and the stability behaviour of mechanical systems during an entire loading process depending on I generalized coordinates only.

With the analytical framework being developed, the next chapter is concerned with the application of the framework to a mechanical system which requires a structural stability analysis that considers damage growth, *viz.*: the problem of delaminated multi-layered composite struts subjected to compressive in-plane loading.

3 Non-linear buckling of a composite strut with a through-the-width delamination

The problem of delaminated composite struts under compressive in-plane loading has received much attention within the research community since the 1980s starting with the work of Chai *et al.* [10]. Such a delamination, *i.e.* the separation along the interfaces of a layered structure, may be barely detectable during the initial response of the structure when subjected to in-plane loading. However, its influence on the structural stability and integrity can be significant. Depending on size and location, such a delamination causes decreasing critical loads and possibly unstable post-buckling responses leading to a premature failure of the strut. These phenomena are, to a certain extent, documented within the literature. To date, the modelling of the post-buckling behaviour beyond the elastic limit is solely performed by comprehensive finite element simulations. Semi-analytical modelling approaches are hitherto restricted to non-growing—stationary—delaminations.

An illustration of a delaminated strut under compressive loading is provided in Fig. 3.1. The delamination is characterized by its length L and its depth h which are, in general, provided by their ratio with respect to the total length L_{tot} and the total thickness H of the strut, respectively.

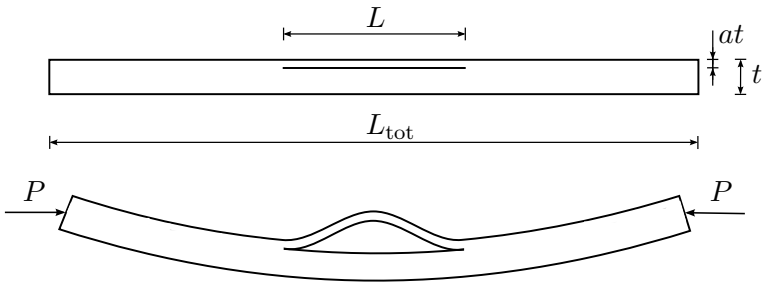

Fig. 3.1: Sketch of a delaminated strut subjected to an in-plane compressive load P.

In this chapter, post-buckling responses of delaminated composite struts without the restriction to stationary delaminations are semi-analytically modelled by employing the analytical framework developed in Chapter 2. As an outcome, possible additional load bearing capabilities as well as the structural and material

failure behaviour of composite struts are determined. This is performed in a highly efficient manner by means of four generalized coordinates only.

The chapter is arranged as follows. In Section 3.1, general phenomena of the buckling and post-buckling behaviour of struts are reviewed. This is followed by an overview of the state of research regarding the (post-)buckling behaviour of delaminated struts in Section 3.2. Section 3.3 presents the model description and the application of the framework. Results of the non-linear buckling responses for stationary and non-stationary delaminations are provided in Section 3.4. A discussion of the phenomena observed is included in Section 3.4. The chapter closes with concluding remarks (Section 3.5) regarding the results obtained and the application of the framework.

3.1 General buckling and post-buckling phenomena of struts

The section briefly reviews general phenomena of the buckling behaviour of struts without any pre-existing state of damage. This serves as an introduction regarding characteristic buckling responses of such structures and provides information helpful to highlight changes in the buckling behaviour when delaminated struts are considered.

Fig. 3.2 shows a one-dimensional representation of a strut. A strut is to be understood as a structural component characterized by a large length (L) to height (H) ratio[1] which is subjected to in-plane compressive loading.[2] The width of a strut (B) is also considerably smaller than the length, whereby the mechanical behaviour is, in general, assumed to be unchanged in the width dimension which is therefore neglected in most model descriptions (as done in Fig. 3.2). All reasonable

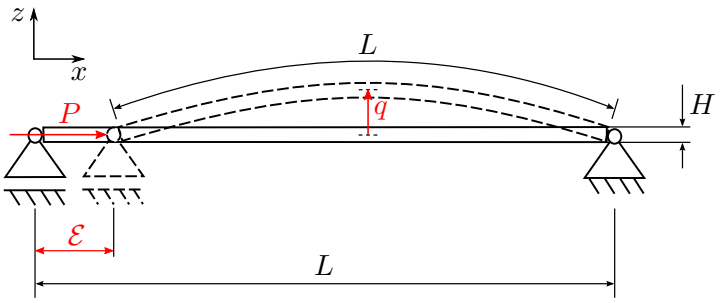

Fig. 3.2: Sketch of a strut subjected to an in-plane compressive load P.

[1] In general, the strut is taken to be a slender structure.

[2] Within the literature, the terms plate, beam, column and strut may be found when referring to the structure illustrated in Fig. 3.2. In this work the term *strut* will be used; however, no restriction with regards to other studies dealing with a structure as in Fig. 3.2 is implied in doing so.

combinations of clamped, hinged and free boundaries can be implemented; Fig. 3.2 shows a simply-supported strut for illustration purposes only.

The physical quantities often used within the structural stability analysis to describe the buckling and post-buckling behaviour, also referred to as linear and non-linear buckling, are highlighted in red in Fig. 3.2. The compressive load is denoted by P, its conjugate displacement, referred to as end-shortening [94], by $\mathcal{E}$ and the generalized coordinate describing the amplitude of the buckling displacement by q.

The linear and non-linear buckling response of a strut can be summarized with the aid of two plots showing the behaviour of the load against the end-shortening and the load against the amplitude of the buckling displacement. This is illustrated in Fig. 3.3 which provides characteristic responses of a strut.

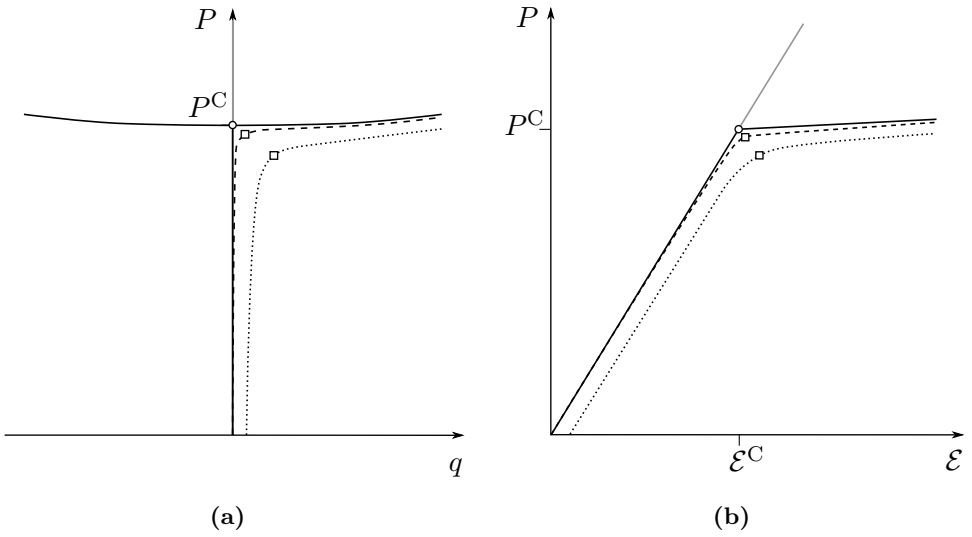

Fig. 3.3: Linear and non-linear buckling response of a strut; **(a)** compressive load (P) against out-of-plane deflection amplitude (q); **(b)** compressive load (P) against end-shortening ($\mathcal{E}$).

Each plot in Fig. 3.3 depicts three characteristic deformation paths: for an ideal strut (solid lines), a strut with stretching–bending coupling (dashed lines), which is regarded as a material imperfection,[3] and a strut with a geometric imperfection (dotted lines), *e.g.* an initial out-of-plane displacement.

The deformation path for the ideal strut exhibits a *critical point* denoted by P^{C} and the symbol "$\circ$" in Fig. 3.3, which is also referred to as branching point or bifurcation point [94]. At this deformation state, the fundamental equilibrium path, *i.e.* $q = 0$, loses its stability, which is illustrated in Fig. 3.3 by the grey

[3] This is specifically relevant for composite structures with an asymmetric layup. Further explanation is provided in Section 3.3.

coloured solid line, forcing the strut to leave its current configuration and to follow one of the bifurcation paths shown in Fig. 3.3a.

This behaviour is called *buckling*. Therefore, P^{C} is also referred to as *buckling load* or *critical load*. Determining the critical loads of a structure and its corresponding mode shapes, for instance the dashed strut in Fig. 3.2, comprises the *linear buckling behaviour* or the *critical behaviour*. The mechanical response beyond such critical points are referred to as *non-linear buckling behaviour*, *post-critical behaviour* or *post-buckling behaviour*.

A distinct critical behaviour, as for an ideal strut, does not exist when imperfections are present (dashed and dotted lines in Fig. 3.3). The initial response of a strut containing material imperfections (dashed lines), for instance in the form of stretching–bending coupling, may often be barely distinguishable from the ideal structure. In the case of stretching–bending coupling, the effects are initially comparably small and just scale up with increasing magnitudes of load. However, the compressive force P causes minor bending deformations (curvature) which vanishes the distinct critical behaviour. Therefore, as indicated in Fig. 3.3a, there is no bifurcation point as well as no transition of an equilibrium path from stable to unstable. Thus, the strut follows its initial path on which it will rather smoothly changeover in its buckled configuration. This changeover is also referred to as buckling. The buckling load or critical load is determined by the change in slope of the equilibrium path. In order to underline the difference with the bifurcation point of an ideal strut, the symbol "□" is used in Fig. 3.3 for the critical point of the imperfect systems.

Fig. 3.3 shows that the presence of imperfections is associated with a decrease of the buckling load and the loads describing the subsequent post-buckling path, whereas the qualitative behaviour stays mostly unaffected. This is visualized in Fig. 3.3 by the case of a geometric imperfection (dotted lines). However, the effect of decreasing critical and post-critical loads diminishes with larger imperfections.

In the post-buckling range (non-linear buckling behaviour), Figs. 3.3a and 3.3b delineate that the strut almost loses its entire stiffness against the compressive force, also referred to as post-buckling stiffness. The reason for that is the negligible contribution of in-plane stretching once the strut buckles. Therefore, it is often assumed that the strut—more precisely the neutral axis—is inextensional [94, 95] (*cf.* Fig. 3.2), thus the strut undergoes bending deformations only. In order to provide a realistic response of a strut, Fig. 3.3b considers in-plane deformations prior to buckling. The compressive strain of the strut at P^{C} is then assumed to retain its magnitude during the post-buckling response.

The post-critical behaviour of struts can be summarized as weakly stable. This implies that only minor increases of load are possible beyond P^{C}. It stands to

reason that such structures may be prone to defects and damage propagation. Thus, it is of great importance to model the buckling behaviour of struts containing a certain state of damage. This is performed in the following parts of the chapter for a composite strut with a delamination. Before proceeding to the model description and the application of the analytical framework the state of research regarding the linear and non-linear buckling behaviour of delaminated struts is reviewed next.

3.2 State of research

The problem of a delaminated strut under compressive in-plane loading was first studied by Chai *et al.* [10]. With the aid of a one-dimensional model, the work examines the behaviour of the strain energy and the strain energy release rate depending on the applied loading and the delamination length. Information regarding buckling loads and loads causing delamination growth is provided. The study presents a closed-form formulation for thin-film buckling.[4] A more general case without the restriction to thin-film buckling is also described. On the other hand, the work considers isotropic material behaviour which results in a distinct critical response, as described in Section 3.1. Moreover, the critical behaviour depending on the delamination depth as well as post-buckling responses in terms of load against amplitude or load against end-shortening are not provided. These phenomena have been the subject of investigation for a fairly large number of ensuing studies.

Therefore, the following review of the literature is subdivided into studies investigating:

- the critical behaviour,
- the post-critical behaviour and
- the delamination growth characteristics.

3.2.1 Critical behaviour

The buckling responses of homogeneous isotropic (*e.g.* [30]), homogeneous orthotropic (*e.g.* [12, 28, 89, 90]) and multi-layered orthotropic[5] (*e.g.* [8, 23, 36, 57,

[4] Thin-film buckling refers to a buckling response of a structure where the thickness of the delaminated part h is very small compared with the overall thickness H (*cf.* Fig. 3.1), *i.e.* $h \ll H$. A ratio of $h/H < 0.1$ is often taken as a requirement for thin-film buckling. In thin-film buckling, it is assumed that only the delaminated part experiences out-of-plane deflection, thus the buckling response of the thicker part is neglected.

[5] In most cases, the orthotropic struts are also transversally isotropic.

72, 106]) struts are presented within the literature. Analytical, numerical and experimental studies have been carried out.

With regards to analytical formulations, the delamination buckling is mostly described in two ways. On the one hand, the equilibrium equations of the forces and moments satisfying the respective boundary and continuity conditions are directly derived with the aid of free-body diagrams [28, 89, 90]. The buckling loads are then determined by employing a perturbation method, for instance as described in [86]. On the other hand, equilibrium equations and boundary conditions are derived by a variational principle using the total potential energy [12, 23, 53, 72].

Another approach is documented in [30] in which the buckling loads and the respective mode shapes are directly determined by evaluating the total potential energy. As discussed in Sections 1.2 and 3.1, the study uses the fact that at a critical state—buckling point—the HESSIAN matrix of the total potential energy becomes singular. Thus, the magnitudes of load for which this condition is fulfilled are the buckling loads.

Experimental work is provided in studies [23, 36, 53]. Samples of similar dimensions are used in which the length is approximately 50 times larger than the height and 5 times larger than the width. Refs. [36, 53] study unidirectional composite struts and present similar results in which the deviation between the experimental data and a finite element analysis [36] or an analytical model [53] respectively is significant for deep and small delaminations (up to approximately 30%) and becomes negligible for large and thin delaminations. The deviations decrease significantly up to 15% when a non-linear kinematic approach is implemented [36].

Multi-layered cross-ply $[0°/90°/90°/0°]_{12s}$ and angle-balanced laminates $[-45°/45°]_{9s}$ are investigated in [23].[6] In contrast with [36, 53], deviations of the experimentally determined critical loads are less than 10% compared with a linear analysis and less than 5% when shear effects and non-linearity are considered.

Even though partly significant quantitative deviations between experimental and computed data are documented, the qualitative behaviour of the buckling load modelled by means of analytical or numerical methods is verified by the experimental studies. The behaviour of the buckling load of delaminated composite struts can be described by an analysis against the delamination length and the delamination depth. The results obtained by the above-mentioned studies are summarized and visualized in Fig. 3.4.

[6] A numerical subscript indicates a multiplier of the stacking sequence in the brackets and the label “s” refers to a symmetric layup.

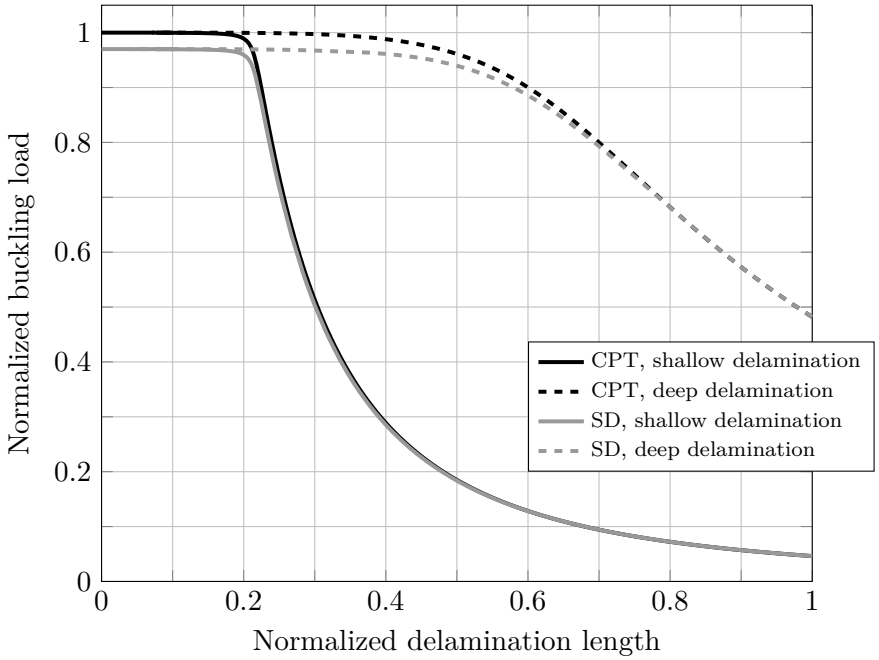

Fig. 3.4: Buckling load against delamination length for shallow and deep delaminations; CPT – Classical Plate Theory,[7] SD – Shear deformations considered; in normalized quantities.

All quantities shown in Fig. 3.4 are understood as normalized. The length of the delamination is normalized to the respective overall dimension of the strut and the buckling load of a non-damaged strut, *e.g.* the Euler load, is used for the normalization of the load. The effect of the delamination depth is visualized by considering two cases: shallow delaminations ($0 \leq h/H < 0.2$) and deep delaminations ($0.2 \leq h/H \leq 0.5$). For increasing delamination depths, the behaviour of the buckling loads transitions from the case "shallow delaminations" into the case "deep delaminations". The following conclusions can be drawn from Fig. 3.4:

- the delamination length for which the buckling load remains almost unaffected increases with deeper delaminations,
- the buckling load abruptly drops in the case of shallow delaminations when a certain delamination length is reached,
- in the case of deeper delaminations, the buckling load decreases more or less smoothly with larger delamination lengths and
- shear effects (grey lines in Fig. 3.4) lower the buckling loads compared with

[7] The specification Classical Plate Theory is used as an overall category combining all studies on homogeneous and multi-layered plates which obey the Kirchhoff–Love plate theory [76].

the Classical Plate Theory (black lines), which are more relevant for smaller delamination lengths. However, the overall length to height ratio of the strut strongly dictates whether or not shear effects may be neglected.

It should be stressed that the applicability of the results and modelling approaches reviewed in this section strongly depends on the layups investigated. Bifurcation analysis, *i.e.* assuming that the fundamental path is described by zero out-of-plane displacement, is not appropriate for laminates causing stretching–bending coupling. Symmetrically laid-up non-damaged struts can become asymmetric once delaminations are present yielding the aforementioned coupling effects. This does not count for isotropic and homogeneous struts. On the other hand, studies investigating multi-layered angle-plies are limited to cases in which the delamination causes two symmetric sublaminates [23, 72].

3.2.2 Post-critical behaviour

Post-buckling responses in terms of load against midpoint deflections or load against end-shortening were first documented by Whitcomb [107] employing a finite element simulation. In [107], thin-film buckling of a composite with a unidirectional layup ($[0°]_4$) on top of a thick isotropic sublaminate was investigated. The results of the finite element simulation were compared with experimental findings showing good correlations of the buckling point and the initial post-buckling behaviour while deviating significantly beyond the initial deflection.

Early analytical studies employ either a perturbation scheme [38, 39] or a variational principle using an energy formulation [12, 13, 88]. Unlike the buckling responses, second order terms are required to obtain initial post-buckling paths *via* the perturbation method. Most of the early work on delamination buckling [12, 13, 38, 39, 107] considers homogeneous or unidirectional laminates. Various stacking sequences were considered first in [88] in which the variational principle using the total potential energy was solved using a finite-difference scheme.

In [88], detailed information about the load against midpoint deflection behaviour is provided in which focus is placed on the influence of initial imperfections, stretching–bending coupling and cylindrical bending. Varying delamination lengths are also considered for an isotropic strut. The depth of the delamination is selected so that only one sublaminate exhibits stretching–bending coupling. This work is extended in [87] in which contact of both sublaminates is considered and plane strain and plane stress assumptions are compared. Furthermore, the influence of changes in the layup in the form of $[0°/(\theta/-\theta)_6/\theta/0°]$ with θ taking certain values in between 0° and 90° is investigated.

More recent analytical studies also investigate the post-buckling behaviour of

multi-layered angle-ply composite struts (*e.g.* [42, 71, 72, 87]). In these studies, either formulations are derived which employ a vast number of generalized coordinates in the form of a Rayleigh–Ritz method [42, 71, 72] or the variational principle is solved by means of purely numerical methods such as the finite difference method [87, 88] or the finite element method [58]. In contrast to these studies, Ref. [30] presents detailed information about the post-buckling response of an isotropic strut employing four generalized coordinates only. Post-buckling paths are obtained by a variational principle using the total potential energy and a Rayleigh–Ritz formulation.

All aforementioned studies provide post-buckling responses for stationary delaminations. The post-buckling behaviour beyond the deformation state causing delamination growth is mainly provided by means of finite element [3, 27, 62, 64] or finite strip [104, 112] analyses. Results are provided for unidirectional and cross-ply layups as well as laminates of the type $[0°/(\theta/-\theta)_n/\theta/0°]$.

In a recent work, Ref. [105] proposes an analytical formulation for a unidirectional bi-layered strut based on the thin-film buckling assumption which requires input from numerical studies in order to describe post-buckling responses which consider delamination growth. Comparisons with experimental work exhibit significant deviations in the critical and post-critical behaviour.

Experimental studies are documented in [23, 36, 40], whereby only unidirectional laminates are investigated in [36] and [40]. A specific support system is used in [40] in order to trigger local buckling responses. In [36], post-buckling responses in terms of load against end-shortening are provided for a laminate with a large delamination for different delamination depths. The work documented in [23] provides more detailed results. Cross-ply and balanced angle-ply layups are studied for near surface and midplane delaminations. Post-buckling responses in terms of load against end-shortening and load against midpoint deflections are presented.

Characteristic phenomena obtained in the above-mentioned studies are visualized in Fig. 3.5. The post-buckling response is shown in terms of compressive load against midpoint deflections.[8] Central delaminations which are not located in the middle of the layup (with respect to the depth) are considered. The black and grey lines describe the deflection of the lower and upper sublaminate respectively. The physical quantities are taken as normalized—the load against the Euler buckling load of an undelaminated strut and the midpoint deflection against the overall height of the strut.

[8] The midpoint deflection is the out-of-plane displacement at the centre of the strut. As symmetrically located delaminations are considered (with regards to the length dimension), this coincides with the midpoint deflections of the delaminated parts—the sublaminates.

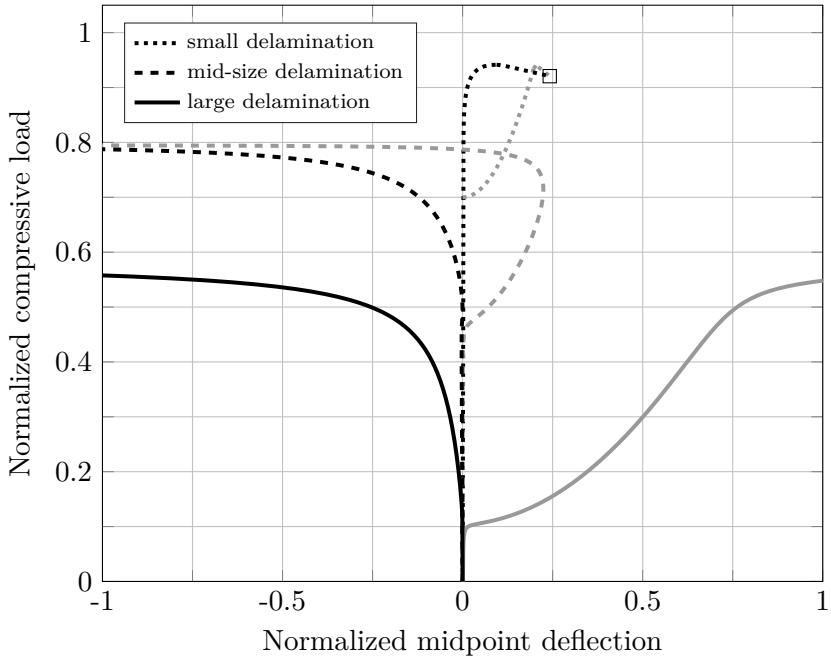

Fig. 3.5: Post-buckling response in terms of compressive load against midpoint deflection for small, mid-size and large delamination lengths; upper sublaminate (grey), lower sublaminate (black); in normalized quantities.

By considering three distinct qualitative cases of delamination length (small – dotted lines, mid-size – dashed lines, large – solid lines), Fig. 3.5 summarizes post-buckling responses of delaminated struts documented within the literature. It should be noted that all magnitudes used in Fig. 3.5 serve for illustration purposes only and that the delamination depth is not further specified since the responses associated with small, mid-size and large delaminations may be qualitatively obtained for various delamination depths. The post-buckling phenomena are subsequently reviewed by differentiating between post-critical deformation and post-critical stability.

However, first, it should be stressed that most studies provide only information about the case of large delaminations (solid lines). The response for mid-size delaminations (dashed lines) is described by studies incorporating imperfections in the form of initial out-of-plane deflections caused by the presence of the delamination [23, 58, 88].[9] This post-buckling behaviour is verified by experimental data documented in [23]. The case of small delaminations (dotted lines) is solely described by [30] which considers an isotropic strut and provides information about the amplitudes of the respective delaminated regions without considering the contribution of the undelaminated part.[10] Whether such behaviour is also

[9] Ref. [87] also considers such imperfections but provides post-buckling paths for large delaminations (solid lines in Fig. 3.5).

[10] The information provided in [30] is used to sketch the midpoint deflections for the strut (considering local and global contributions) in Fig. 3.5 (dotted lines).

present for composite struts is not discussed in the literature.

Post-critical deformation.

For all three post-buckling responses shown in Fig. 3.5 the less stiff (thinner) sublaminate buckles at first, thus exhibits significant larger deflections than the thicker more stiff laminate. However, the extent of this phenomenon is strongly dependent on the delamination length and delamination depth with larger and shallow delaminations amplifying this effect and *vice versa*. The buckling response as long as the thicker laminate remains mainly unaffected is referred to as local buckling.

Fig. 3.5 shows three distinct buckling responses when the thicker more stiff sublaminate starts to buckle. This phenomenon is called global buckling. For large delaminations, both sublaminates deflect in opposite directions once global buckling occurs.[11] This is different for mid-size delaminations (cases with imperfections). When global buckling is triggered, the less stiff sublaminate is pulled towards the direction of the stiffer sublaminate, so that both parts deflect into the same direction. It should be noted that both sublaminates still, relatively to each other, deflect in opposite directions. The response for mid-size and large delaminations is referred to as opening-mode buckling [30, 102].

The response for small delaminations shows that both sublaminates deflect in the same direction, which is referred to as closed-mode buckling [30, 102], exhibiting comparably small out-of-plane displacements. The post-buckling path displays a limit point from where the deformation behaviour changes abruptly. Large deflections are caused for the thicker more stiff laminate, so that both sublaminates get in contact with each other, indicated in Fig. 3.5 by the symbol "□". Deformations beyond this deformation state considering the contact of both sublaminates are not provided in [30] and are therefore omitted herein.

Post-critical stability.

Initially, the post-buckling response for all configurations of delaminations is stable. For the case of small delamination lengths, a changeover to an unstable response in the form of a limit point occurs which is associated with the initiation of the global buckling response. This phenomenon is illustrated in Fig. 3.5 by the dotted lines where the limit point is the peak value of the load. The subsequent path may only be traced in a displacement-controlled configuration.

Mid-size and large delaminations do not exhibit such a change in stability. During the local buckling response, most of the original stiffness of the system against compression is retained which can be readily examined by the increasing

[11] Some models concerning homogeneous plates [12, 38] present post-buckling responses in which the black lines in Fig. 3.5 for the case of large delaminations (solid lines) deflect in the opposite direction. So, in contrast with Fig. 3.5, such behaviour describes a closed-mode response.

magnitudes of load following the buckling point or the corresponding load against end-shortening plot, see for instance [30]. Nevertheless, for the mid-size delaminations the delaminated strut rather abruptly loses almost the entire post-buckling stiffness once global buckling is caused. This is visualized in Fig. 3.5 by the dashed lines which indicate the characteristic asymptotic behaviour of the load towards its maximum. This response is at most weakly stable if not neutrally stable.[12]

Large delaminations (solid lines) also converge towards a maximum load showing the characteristic weakly stable behaviour. With increasing delamination length, the post-buckling stiffness decreases less abruptly compared with the case of mid-size delaminations, however the respective maximum load decreases significantly.
Further remarks.
It should be noted that the classification in small, mid-size and large delamination lengths and therefore the corresponding phenomena described in this section strongly depend on the depth of the delamination. Thus, with changing depth, the three cases presented in Fig. 3.5 shift quantitatively towards smaller length (for shallow delaminations) or towards larger length (for deep delaminations). The classification of small, mid-size and large cannot be generally quantified. An analysis for all possible delamination depths is required to determine the respective quantitative measures. So far, this has not been done for delaminated composite struts. Such a classification is introduced by the author, such that a summary of the results for various configurations of delaminated struts is enabled.

Shear effects influence the post-buckling response by lowering the magnitudes of the load, similar to Section 3.2.1. However, the qualitative behaviour is not affected and therefore, for reasons of clarity, shear effects are not considered in Fig. 3.5. In general, the influence of the shear effects, as for the critical behaviour, depends on the overall dimensions of the strut.

As a final remark, in Fig. 3.5, post-buckling responses for stationary delaminations are summarized. Within the literature, information about post-buckling responses considering delamination growth is just provided for specific and limited configurations mainly following the examples given by [104]. Therefore, such limited case studies are herein excluded in the general review.

3.2.3 Delamination growth characteristics

The delamination growth characteristics comprise:

- the behaviour of the physical quantity governing the changes in structure and thus

[12] Neutrally stable refers to a deformation path exhibiting zero post-buckling stiffness (horizontal line).

- whether growth is stable or unstable.

As mentioned at the beginning of Section 3.2, the pioneering work of Chai *et al.* [10] already addresses both characteristics. With the aid of the energy release rate the questions whether or not delamination growth occurs and whether or not this growth would be stable or unstable are discussed. Therefore, the energy release rate is analysed with respect to the delamination length for certain constant magnitudes of the applied compressive strain.

Albeit subsequent studies enhance the general modelling of the post-buckling behaviour and extend it to multi-layered laminates, the analysis of the delamination growth characteristics remains similar. The energy release rate is the physical quantity used to describe the delamination growth behaviour. It is either determined with the aid of the *J integral* principle[13] [79] applied to the one-dimensional problem using the forces and moments at the delamination tip [13, 38, 39, 87, 89, 90, 109] or by differentiating the total potential energy with respect to the delamination length [10, 12]. All studies assume a Griffith-type crack problem [22] which is suitable for quasi-brittle material behaviour, *i.e.* growth is triggered if $G \geq G_\mathrm{c}$ with $G = -\partial\Pi/\partial A$ where G is the energy release rate, G_c is the critical energy release rate and A is the crack area.

For homogeneous struts, the mode decomposition of the energy release rate is employed in [39] using the concept of stress intensity factors and mode mixture as documented in [35]. Mode mixture for multi-layered composite struts has been considered in most finite element analyses starting with [107]. Detailed information about the energy release rate for mode I and mode II in the pre-growth range and during growth is documented in [104, 112] using a finite strip method. Most of the information available concerns unidirectional laminates. Refs. [87] and [104] present mode decompositions for mode I and mode II for cross-ply layups and laminates of the type $[0°/(45°/-45°)_n/45°/0°]$ respectively.

Furthermore, the analysis of the energy release rate against the applied loading is provided in most studies. This can be done for the energy release rate or its decomposed modes. Findings documented within the literature are therefore summarized by two plots showing the energy release rate against the applied forces (Fig. 3.6) and the energy release rate against the delamination length (Fig. 3.7). As performed in Sections 3.2.1 and 3.2.2, all quantities are normalized, the load against the Euler buckling load of an undelaminated strut, the energy release rate against its critical value causing delamination growth and the delamination length against the overall length of the strut.

[13] The *J integral* is a path-independent integral enclosing, for instance, a crack tip. In the original work [79], it is formulated in terms of a two-dimensional stress state.

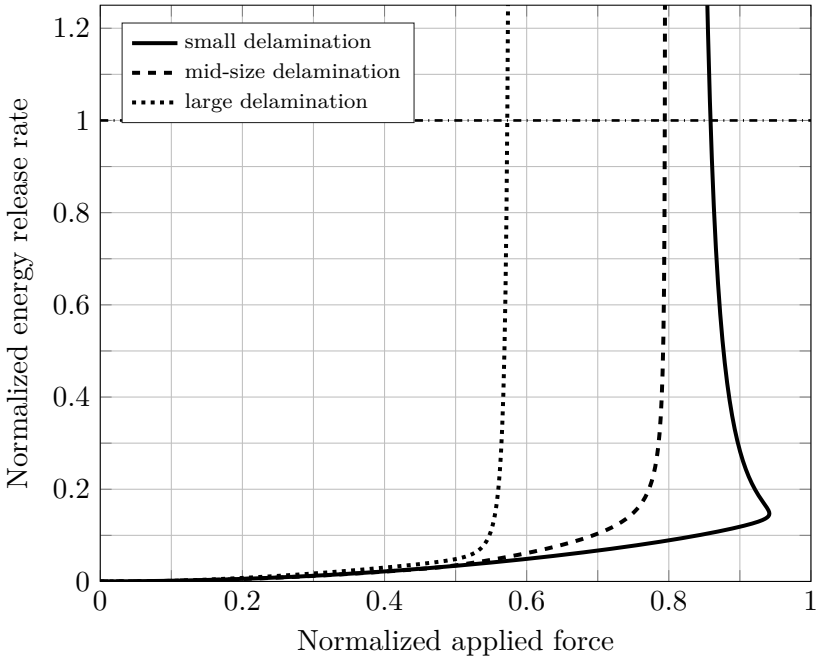

Fig. 3.6: Energy release rate against applied forces for small, mid-size and large delamination lengths; in normalized quantities.

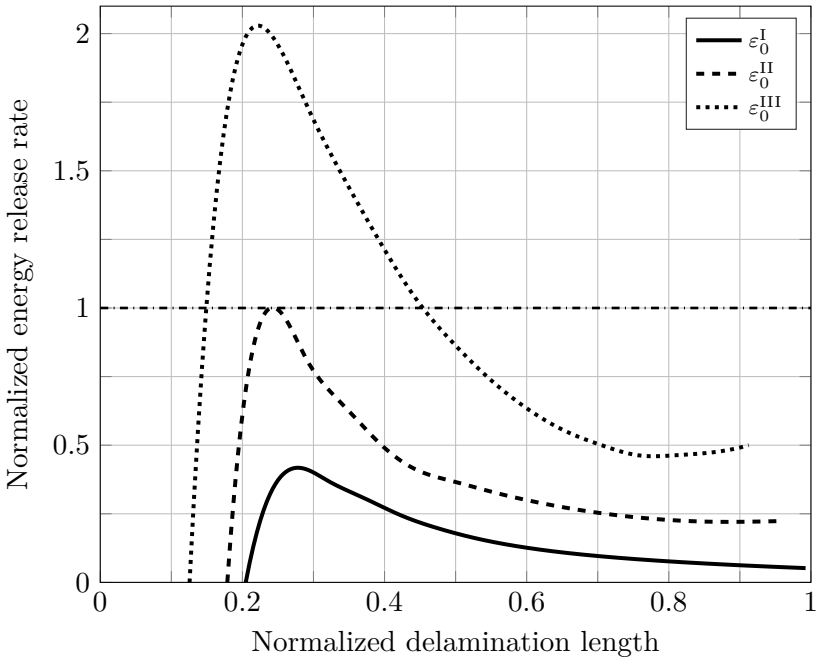

Fig. 3.7: Energy release rate against delamination length for three distinct prescribed magnitudes of load in the form of applied strain with $\varepsilon_0^{\mathrm{I}} < \varepsilon_0^{\mathrm{II}} < \varepsilon_0^{\mathrm{III}}$; in normalized quantities.

Fig. 3.6 comprises the behaviour of the energy release rate for three characteristic lengths of delamination (small – solid line, mid-size – dashed line, large – dotted

line), which correspond to Fig. 3.5. For each case, the energy release rate stays negligibly small as long as the strut does not buckle. A slight increase of the energy release rate is shown when local buckling occurs. In general, delamination growth is not caused during local buckling, which can be seen in Fig. 3.5 showing magnitudes of the energy release rate that are significantly smaller than the magnitude required to initiate growth which is indicated by the dot-dashed line.

The energy release rate increases significantly once global buckling occurs. As the load converges towards its maximum the corresponding energy release rate rises asymptotically. Thus, growth is generally initiated during the global buckling response of delaminated composite struts if opening-mode buckling responses such as those documented in Fig. 3.5 occur. For post-buckling deformations exhibiting a closed-mode response the energy release rate would remain small in comparison with its critical value [87].

The behaviour of the energy release rate against the delamination length for prescribed magnitudes of load is shown in Fig. 3.7, in which applied strains are exemplarily taken as the load input. Whenever the curve reaches the required magnitude of load (dot-dashed line), growth occurs. So, minimum magnitudes of load input required to cause delamination growth as well as the load inputs required to cause growth for certain given delamination lengths can be obtained from Fig. 3.7. Furthermore, it can be determined whether the delamination growth is stable or unstable. Therefore, the behaviour of the energy release rate for a constant state of loading is examined for an increase in delamination length. If the energy release rate decreases, growth is termed stable; otherwise it is unstable.[14]

3.2.4 Concluding remarks

With regards to the post-buckling behaviour of delaminated struts, it should be stressed that the majority of studies focus on certain configurations regarding delamination size and location. Few of these studies investigate specific effects such as shear deformations [12, 38, 39], contact conditions [72] or layups [88]. Refs. [13, 30, 58] analyse the influence of varying delamination length and depth, whereby only changes causing similar qualitative buckling responses are documented in [13, 58]. To the authors knowledge, only [30] presents a detailed analysis regarding the influence of delamination length and depth. However, [30] considers isotropic material behaviour and stationary delaminations.

Thus, a detailed analysis for delaminated composite struts is required, such that more general insight into the post-buckling behaviour comprising qualitative and quantitative changes regarding delamination length and depth can be gained.

[14] Detailed explanation about the behaviour of the energy release rate is provided in Section 3.4 in relation with the application of the analytical framework (*cf.* Fig. 3.18).

The study of the energy release rate, as documented in Section 3.2.3, mainly considers homogeneous struts. Information about the energy release rate for multi-layered struts in the form of Fig. 3.6 can be found in [87]. More recent studies focus instead on the modelling of post-buckling paths considering delamination growth which is, except in [105], entirely done by numerical simulations. Such simulations—though powerful—focus on specific and limited problem definitions mostly as documented in [104]. Ref. [105] employs the restricting case of thin-film buckling and considers bi-layered unidirectional struts. Moreover, additional input from purely numerical simulations is required in order to obtain post-buckling deformations with delamination growth.

An analytical modelling approach which determines post-buckling responses of multi-layered composite struts considering delamination growth has not been found. This is presented in the subsequent sections by employing the framework developed in Chapter 2.

3.3 Modelling approach

The application of the analytical framework (*cf.* Chapter 2) to the problem of a delaminated composite strut under compressive in-plane loading is presented in this section. First, the geometric model of a one-dimensional representation of the strut and the constitutive relations are described. Subsequently, the total potential energy principle is presented consisting of the derivation of the total potential energy as well as a Rayleigh–Ritz formulation in order to solve the variational principle for the conservative part of the deformation process. This is followed by the extended total potential energy principle (*cf.* Sections 2.2.2 and 2.3) comprising the derivation of the damage parameter and the extended total potential energy as well as the variational principle.

As an outcome, the deformation behaviour of the system as long as a conservative process is present (stationary delamination) and the post-buckling responses beyond the deformation state causing delamination growth (non-stationary delamination) are determined. Respective results are presented in Section 3.4.

For the geometric model presented in the upcoming Section 3.3.1, the description provided in [30] is taken as a benchmark model. The derivation of the displacement functions as well as the application of the analytical framework follow the studies [47, 48, 49] of the author.

3.3.1 Geometric model

The geometric model of the delaminated composite strut is shown in Fig. 3.8. Since the deformation behaviour will be described by a one-dimensional representation (refer to Sections 3.3.2 and 3.3.3), the width dimension of the strut (y-coordinate in Fig. 3.8) is not considered in the geometric model.

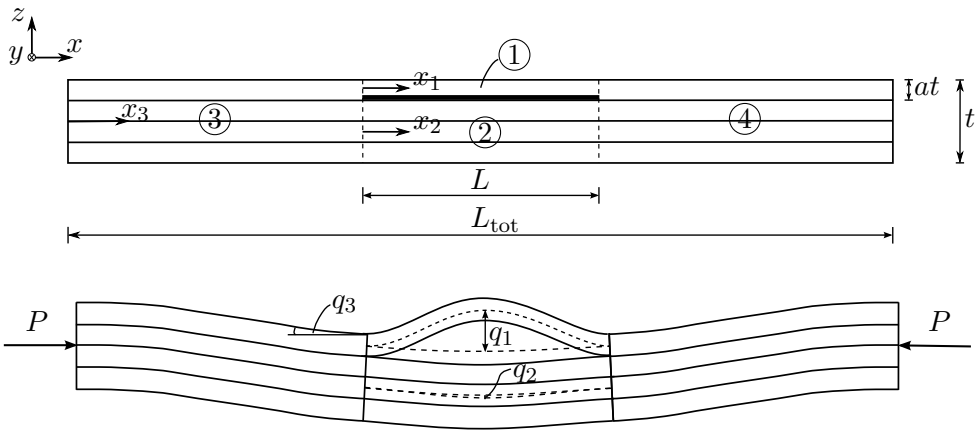

Fig. 3.8: One-dimensional model of a composite strut with a through-the-width delamination.

Clamped boundary conditions are studied even though the model may be easily reformulated for a simply supported case. It is assumed that the strut is subjected to a compressive in-plane load in the form of an independent generalized force P. The length of the strut is denoted by L_{tot}. A central delamination with the length L is assigned to the strut. Thus, as indicated in Fig. 3.8, the strut can be subdivided into four parts.

Each part is given its own coordinate system. Parts ① and ② are the upper and lower sublaminate respectively. Parts ③ and ④ describe the undelaminated region of the strut. Subsequently, owing to the symmetry, only part ③ will be considered for the undelaminated region. The depth of the delamination is described by the parameter a.

Four generalized coordinates q_i ($i = 1, ..., 4$) are employed to describe the deformation behaviour of the system. The generalized coordinates q_1 and q_2 are the amplitudes of the upper and lower sublaminate respectively (with respect to the neutral axis of the delaminated parts, see dashed lines in Fig. 3.8). The generalized coordinate q_3 is the rotation (also the slope) of the plane at the interface between the delaminated and undelaminated part, and q_4 (not shown in Fig. 3.8) describes the total end-shortening of the delaminated parts.

The following assumptions and simplifications are employed within the problem description.

- The dependence of the deformation behaviour with respect to the y-direction

is assumed to be negligible, thus a one-dimensional representation of the strut is employed. However, deformations caused by coupling effects are considered for the y-direction as well as the x-y-plane. This is accounted for by determining effective stiffness parameters which is described in Section 3.3.2.2.

- All parts of the strut are treated as independent laminates whose deformation behaviour complies with the respective boundary and continuity conditions.
- In-plane stretching of the undelaminated region is omitted as its influence on the (post-)buckling response is assumed to be small. This avoids the introduction of another degree of freedom (similar to q_4 for the delaminated region) and neglects non-linear strains during the post-buckling response.
- Thin delaminated struts are considered, so that shear deformations are neglected whose influence is assumed to be small.
- Contact of the sublaminates is not considered. In the case that both sublaminates get into contact, the problem description provides the post-buckling path up to the deformation state at which contact would occur.

3.3.2 Constitutive relations

The Classical Laminate Theory [76] is employed in the application example. Therefore, this section commences with a brief summary of the main derivation steps of the constitutive relations comprised by the Classical Laminate Theory. This provides an orientation regarding the calculation of the stiffness parameters used in the application example. An detailed derivation of the respective stiffness matrices can be found in established textbooks such as [76, 85].

In the second part of the section, the incorporation of deformation characteristics associated with various coupling effects into the one-dimensional problem description is presented.

3.3.2.1 Classical laminate theory

The materials used for the multi-layered struts are assumed to obey linear elastic behaviour, *i.e.* Hooke's law

$$\sigma_{ij} = C_{ijkl}\varepsilon_{kl}, \tag{3.3.1}$$

where the fourth order stiffness tensor C_{ijkl} relates the infinitesimal strains ε_{ij} with the Cauchy stresses σ_{ij}. Eq. (3.3.1) may be rewritten for non-linear kinematic

behaviour in terms of the GREEN–LAGRANGE strain tensor E_{ij} and the second PIOLA–KIRCHHOFF stress tensor S_{ij},[15] thus

$$S_{ij} = C_{ijkl} E_{kl}. \tag{3.3.2}$$

Struts consisting of unidirectional layers are considered. Such unidirectional layers exhibit transversally-isotropic material behaviour which is characterized by five independent material parameters. With the aid of VOIGT's notation [14, 76], the constitutive relation of a transversally-isotropic unidirectional layer can be expressed in matrix form, *i.e.*

$$\begin{pmatrix} \sigma_1 \\ \sigma_2 \\ \sigma_3 \\ \sigma_4 \\ \sigma_5 \\ \sigma_6 \end{pmatrix} = \begin{pmatrix} C_{11} & C_{12} & C_{12} & 0 & 0 & 0 \\ & C_{22} & C_{23} & 0 & 0 & 0 \\ & & C_{22} & 0 & 0 & 0 \\ & & & \frac{1}{2}(C_{22} - C_{23}) & 0 & 0 \\ & & & & C_{66} & 0 \\ \text{sym.} & & & & & C_{66} \end{pmatrix} \begin{pmatrix} \varepsilon_1 \\ \varepsilon_2 \\ \varepsilon_3 \\ \varepsilon_4 \\ \varepsilon_5 \\ \varepsilon_6 \end{pmatrix}, \tag{3.3.3}$$

where the following relation for the indices applies,[16]

$$\{1, 2, 3, 4, 5, 6\} \Longleftrightarrow \{11, 22, 33, 23, 31, 12\}. \tag{3.3.4}$$

In the subsequent text, the spatial coordinates $x_i = \{x, y, z\}$ may be used instead, whenever it is considered to provide a better understanding. It should be noted that Eq. (3.3.3) considers unidirectional layers in which the fibres are orientated in parallel to the x or the x_1-direction.

Since thin struts are investigated, the plane stress assumption is employed. Rewriting Eq. (3.3.3) by considering plane stress and effective material parameters[17] yields

$$\begin{pmatrix} \sigma_1 \\ \sigma_2 \\ \sigma_6 \end{pmatrix} = \begin{pmatrix} \frac{E_{11}}{1-\nu_{12}\nu_{21}} & \frac{\nu_{21}E_{11}}{1-\nu_{12}\nu_{21}} & 0 \\ \frac{\nu_{12}E_{22}}{1-\nu_{12}\nu_{21}} & \frac{E_{22}}{1-\nu_{12}\nu_{21}} & 0 \\ 0 & 0 & G_{12} \end{pmatrix} \begin{pmatrix} \varepsilon_1 \\ \varepsilon_2 \\ \varepsilon_6 \end{pmatrix}, \tag{3.3.5}$$

where E_{11} is the YOUNG's modulus in the fibre direction, E_{22} is the YOUNG's modulus in the transverse direction, ν_{21} is the minor POISSON's ratio, ν_{12} is

[15] Eq. (3.3.2) is commonly referred to as SAINT VENANT–KIRCHHOFF law.

[16] It should be noted that $\varepsilon_4 = 2\varepsilon_{23}$, $\varepsilon_5 = 2\varepsilon_{31}$ and $\varepsilon_6 = 2\varepsilon_{12}$; so-called *engineering shear strain*.

[17] The effective material parameters are either provided by the manufacturer of the unidirectional plies or may be calculated by micro-mechanical homogenization methods as well as empirical formulas based on the elastic properties of the two constituents [85].

the major Poisson's ratio and G_{12} is the shear modulus in the x-y-plane or x_1-x_2-plane.[18]

The matrix in Eq. (3.3.5) is referred to as the reduced stiffness matrix and will be denoted by $[Q]$ or Q_{IJ} (capital indices indicate Voigt's notation; for plane stress, $\{I, J\} = \{1, 2, 6\}$). The stiffness matrix $[Q]$ refers to the local coordinate system in which the fibres are always in parallel to the x-axis or x_1-axis. In order to obtain the reduced stiffness matrix with respect to the global coordinate system, the transformation matrix[19]

$$\Big[T\Big] = \begin{pmatrix} \cos^2\theta & \sin^2\theta & 2\cos\theta\sin\theta \\ \sin^2\theta & \cos^2\theta & -2\cos\theta\sin\theta \\ -\cos\theta\sin\theta & \cos\theta\sin\theta & \cos^2\theta - \sin^2\theta \end{pmatrix} \tag{3.3.6}$$

is considered. Using $[T]$ to transform the respective stresses and strains to the global coordinate system, the reduced transformed stiffness matrix can be determined as

$$\Big[\bar{Q}\Big] = \Big[T\Big]^{-1} \Big[Q\Big] \Big[T\Big]^{-\mathrm{T}}, \tag{3.3.7}$$

which is subsequently employed to calculate the laminate stiffness matrices of the multi-layered parts of the strut.

The Classical Laminate Theory characterizes the material behaviour of homogenized laminates,[20] for which shear effects are neglected, with the aid of three stiffness matrices: the in-plane stiffness matrix

$$\Big[A\Big] = \sum_{n=1}^{N} \int\limits_{Z^{(n)}} \Big[\bar{Q}\Big]^{(n)} \,\mathrm{d}z, \tag{3.3.8}$$

the coupling stiffness matrix

$$\Big[B\Big] = \sum_{n=1}^{N} \int\limits_{Z^{(n)}} \Big[\bar{Q}\Big]^{(n)} z \,\mathrm{d}z, \tag{3.3.9}$$

and the bending stiffness matrix

$$\Big[D\Big] = \sum_{n=1}^{N} \int\limits_{Z^{(n)}} \Big[\bar{Q}\Big]^{(n)} z^2 \,\mathrm{d}z. \tag{3.3.10}$$

[18] For plane stress, just four independent material parameters are present. The fifth independent material parameter—in the three-dimensional case—would be the Poisson's ratio ν_{23}.

[19] The transformation matrix is calculated with the aid of the rotation matrix $\mathcal{O}'_{ij}$ derived from a Euclidean transformation [65, 76] in which the stresses are transformed from the global (strut) coordinate system to the local (ply) coordinate system indicated by the symbol $'$, *i.e.* $\sigma'_{ij} = \mathcal{O}'_{ik}\mathcal{O}'_{jl}\sigma_{kl}$.

[20] The material parameters of the two constituents—fibre and matrix—are homogenized yielding the effective parameters used in Eq. (3.3.5).

In Eqs. (3.3.8) to (3.3.10), the summation index n refers to the nth layer of the respective part of the strut and $Z^{(n)}$ describes the integration range from the lower to the upper bound of the nth layer.

The in-plane stiffness matrix $[A]$ relates the in-plane strains

$$\{\varepsilon\} = \begin{Bmatrix} \varepsilon_1 \\ \varepsilon_2 \\ \varepsilon_6 \end{Bmatrix} = \begin{Bmatrix} \varepsilon_{xx} \\ \varepsilon_{yy} \\ 2\varepsilon_{xy} \end{Bmatrix} \tag{3.3.11}$$

to the in-plane force resultants (force per unit width)

$$\{n\} = \begin{Bmatrix} n_1 \\ n_2 \\ n_6 \end{Bmatrix} = \begin{Bmatrix} n_{xx} \\ n_{yy} \\ n_{xy} \end{Bmatrix}. \tag{3.3.12}$$

The bending stiffness matrix relates the curvatures

$$\{\kappa\} = \begin{Bmatrix} \kappa_1 \\ \kappa_2 \\ \kappa_6 \end{Bmatrix} = \begin{Bmatrix} \kappa_{xx} \\ \kappa_{yy} \\ \kappa_{xy} \end{Bmatrix} \tag{3.3.13}$$

to the moment resultants (moment per unit width)

$$\{m\} = \begin{Bmatrix} m_1 \\ m_2 \\ m_6 \end{Bmatrix} = \begin{Bmatrix} m_{xx} \\ m_{yy} \\ m_{xy} \end{Bmatrix}. \tag{3.3.14}$$

The coupling matrix $[B]$ couples the bending deformations (curvatures) with the in-plane force resultants and the in-plane strains with the moment resultants. This is commonly referred to stretching–bending coupling which occurs due to an asymmetric layup in multi-layered laminates. The Classical Laminate Theory can be summarized with the following equation,

$$\begin{Bmatrix} n_1 \\ n_2 \\ n_6 \\ m_1 \\ m_2 \\ m_6 \end{Bmatrix} = \begin{pmatrix} A_{11} & A_{12} & A_{16} & B_{11} & B_{12} & B_{16} \\ & A_{22} & A_{26} & & B_{22} & B_{26} \\ \text{sym.} & & A_{66} & \text{sym.} & & B_{66} \\ B_{11} & B_{12} & B_{16} & D_{11} & D_{12} & D_{16} \\ & B_{22} & B_{26} & & D_{22} & D_{26} \\ \text{sym.} & & B_{66} & \text{sym.} & & D_{66} \end{pmatrix} \begin{Bmatrix} \varepsilon_1 \\ \varepsilon_2 \\ \varepsilon_6 \\ \kappa_1 \\ \kappa_2 \\ \kappa_6 \end{Bmatrix}, \tag{3.3.15}$$

comprising all coupling effects between the deformation measures (in-plane strains and curvatures) and the force measures (in-plane force resultants and moment resultants).

3.3.2.2 One-dimensional multi-layered composite strut

Even though the problem of a delaminated strut is described with the aid of a one-dimensional model, various coupling effects comprised in Eq. (3.3.15) are considered in the subsequent derivation. Owing to such coupling effects ε_2, ε_6, κ_2 and κ_6 should not be neglected.

Therefore, entries responsible for bending–twisting (D_{16}, D_{26}), bending–bending (D_{12}) as well as stretching–shearing (A_{16}, A_{26}) and stretching–stretching (A_{12}) are considered and incorporated in the energy formulation by calculating effective parameters for the in-plane (A_{eff}), coupling (B_{eff}) and bending (D_{eff}) stiffness of the respective parts of the strut.

This is done by assuming that the forces n_{yy} and n_{xy} as well as the moments m_{yy} and m_{xy} are zero, thus

$$\begin{Bmatrix} n_{xx} \\ 0 \\ 0 \\ m_{xx} \\ 0 \\ 0 \end{Bmatrix} = \begin{pmatrix} A_{11} & A_{12} & A_{16} & B_{11} & B_{12} & B_{16} \\ & A_{22} & A_{26} & & B_{22} & B_{26} \\ \text{sym.} & & A_{66} & \text{sym.} & & B_{66} \\ B_{11} & B_{12} & B_{16} & D_{11} & D_{12} & D_{16} \\ & B_{22} & B_{26} & & D_{22} & D_{26} \\ \text{sym.} & & B_{66} & \text{sym.} & & D_{66} \end{pmatrix} \begin{Bmatrix} \varepsilon_{xx} \\ \varepsilon_{yy} \\ 2\varepsilon_{xy} \\ \kappa_{xx} \\ \kappa_{yy} \\ \kappa_{xy} \end{Bmatrix}, \tag{3.3.16}$$

from where the strains ε_{yy} and $2\varepsilon_{xy}$ as well as the curvatures κ_{yy} and κ_{xy} can be determined. Such strains and curvatures are subsequently replaced in the expressions for n_{xx} or m_{xx} determined from Eq. (3.3.16) yielding

$$\begin{Bmatrix} n_{xx} \\ m_{xx} \end{Bmatrix} = \begin{pmatrix} A_{\text{eff}} & B_{\text{eff}} \\ B_{\text{eff}} & D_{\text{eff}} \end{pmatrix} \begin{Bmatrix} \varepsilon_{xx} \\ \kappa_{xx} \end{Bmatrix}, \tag{3.3.17}$$

in which the effective stiffness parameters are smaller, thus less stiff, than the respective $(\bullet)_{11}$ entries due to the additional deformation considered in comparison with a purely one-dimensional representation. The formulas derived from Eq. (3.3.16) to determine the effective stiffness parameters are provided in Appendix B.

3.3.3 Total potential energy principle

First, the total potential energy Π (*cf.* Eqs. (2.1.3) and (2.1.6)) is derived. In order to obtain the strain energy W, the well-known formula for the strain energy of a multi-layered composite plate employing the Classical Laminate Theory

[76],[21] where:

$$W = \frac{1}{2} \int_x \int_y \left(\varepsilon_I^0 A_{IJ} \varepsilon_J^0 + 2\varepsilon_I^0 B_{IJ} \kappa_J + \kappa_I D_{IJ} \kappa_J \right) \mathrm{d}y \, \mathrm{d}x, \tag{3.3.18}$$

is applied to the one-dimensional formulation of a composite strut, thus

$$W = \frac{1}{2} b \int_x \left(\varepsilon_1^0 A_{11} \varepsilon_1^0 + 2\varepsilon_1^0 B_{11} \kappa_1 + \kappa_1 D_{11} \kappa_1 \right) \mathrm{d}x. \tag{3.3.19}$$

Next, Eq. (3.3.19) is rewritten, such that coupling effects in the y-direction and the x-y-plane are considered, by using the effective stiffness parameters derived in Section 3.3.2.2, *i.e.*

$$W = \frac{1}{2} b \int_x \left(\varepsilon_{xx}^0 A_{\mathrm{eff}} \varepsilon_{xx}^0 + 2\varepsilon_{xx}^0 B_{\mathrm{eff}} \kappa_{xx} + \kappa_{xx} D_{\mathrm{eff}} \kappa_{xx} \right) \mathrm{d}x, \tag{3.3.20}$$

where b denotes the width of the strut, ε_{xx}^0 the membrane strains in the x-direction and κ_{xx} the curvature in the x-direction.[22] It should be noted that in Eq. (3.3.20), the spatial coordinates have been used instead of Voigt's notation (*e.g.* $\varepsilon_1^0 \equiv \varepsilon_{xx}^0$).

Eq. (3.3.20) considers all coupling effects present in the Classical Laminate Theory, so that arbitrarily laid-up struts as well as asymmetric layups caused by a delamination can be investigated. By applying Eq. (3.3.20) to the problem description provided in Section 3.3.1, the reversible strain energy W comprising energy contributions from stretching and bending deformations of each part of the strut can be obtained, *i.e.*

$$\begin{aligned} W = \frac{1}{2} b \Bigg[& 2D_{\mathrm{eff}}^{③} \int_0^{L^*} \left(\kappa_{xx}^{③} \right)^2 \mathrm{d}x_3 \\ & + \int_0^{L} \left(D_{\mathrm{eff}}^{①} \left(\kappa_{xx}^{①} \right)^2 + A_{\mathrm{eff}}^{①} \left(\varepsilon_{xx}^{①} \right)^2 + 2B_{\mathrm{eff}}^{①} \kappa_{xx}^{①} \varepsilon_{xx}^{①} \right) \mathrm{d}x_1 \\ & + \int_0^{L} \left(D_{\mathrm{eff}}^{②} \left(\kappa_{xx}^{②} \right)^2 + A_{\mathrm{eff}}^{②} \left(\varepsilon_{xx}^{②} \right)^2 + 2B_{\mathrm{eff}}^{②} \kappa_{xx}^{②} \varepsilon_{xx}^{②} \right) \mathrm{d}x_2 \Bigg], \end{aligned} \tag{3.3.21}$$

in which $L^* = (L_{\mathrm{tot}} - L)/2$ and, as mentioned in Section 3.3.1, stretching contributions for the undelaminated part ③ are not considered.

Struts with a symmetric layup are investigated, thus no coupling effects occur

[21] The derivation of Eq. (3.3.18) is provided in Appendix C.

[22] It should be noted that the notation κ_{xx} refers to a moment around the y-axis denoted by m_{xx}.

for the undelaminated part, *i.e.* $B_{\text{eff}}^{\textcircled{3}} = 0$. For illustration purposes, the membrane strains ε_{xx}^{0} are stated as $\varepsilon_{xx}^{\textcircled{i}}$ in Eq. (3.3.21) indicating the respective part of the strut while omitting the symbol "0" used to refer to membrane strains.

The work done by the external loads is expressed in the form of a potential Φ,

$$\Phi = -P\mathcal{E}, \tag{3.3.22}$$

where P is the prescribed force and $\mathcal{E}$ denotes the end-shortening of the strut. Eqs. (3.3.21) and (3.3.22) define the total potential energy, $\Pi = W - P\mathcal{E}$, of the delaminated composite strut under compressive in-plane loading.

In general, the membrane strains and the curvatures in Eq. (3.3.21) as well as the end-shortening in Eq. (3.3.22) depend on derivatives of the in-plane (u) and out-of-plane displacement (w), so that a variational principle would yield differential equations whose solution are the displacement functions. However, as described in Chapter 2, the deformation behaviour of the problems to be studied with the analytical framework is expressed in terms of a set of generalized coordinates q_i. Thus, the variational principle provides a set of algebraic equations rather than differential equations.

In the present application example, a Rayleigh–Ritz formulation is employed. Continuous mode forms, which fulfil the geometric boundary and the continuity conditions for the case of clamped boundaries at the end of the strut as well as at the interface between the delaminated and undelaminated part, thus

$$\begin{aligned}
&w_3(x_3 = 0) &&= 0\,, && w_3(x_3 = L_{\text{tot}}) = 0\,,\\
&w_3(x_3 = L^*) = w_i(x_i = 0)\,, && w_i(x_i = L) &&= w_3(x_3 = L^* + L)\,,\\
&w_3'(x_3 = 0) &&= 0\,, && w_3'(x_3 = L_{\text{tot}}) = 0\,,\\
&w_3'(x_3 = L^*) = w_i'(x_i = 0)\,, && w_i'(x_i = L) &&= w_3'(x_3 = L^* + L),
\end{aligned} \tag{3.3.23}$$

with $i = 1, 2$, and $L^* = (L_{\text{tot}} - L)/2$, are used to approximate the out-of-plane displacements (buckling displacement of each part, ① – ③) by employing three generalized coordinates only, *i.e.*:

$$\begin{aligned}
w_i &= q_i \sin^2\left(\frac{\pi x_i}{L}\right) + C_0 x_i^3 + C_1 x_i^2 + C_2 x_i + C_3 \quad \text{with} \quad i = 1, 2, \quad \text{and}\\
C_0 &= \frac{q_3}{2L^3}\left[\frac{L_{\text{tot}}}{\pi}\tan\left(\frac{\pi L^*}{L_{\text{tot}}}\right) - \frac{L_{\text{tot}}}{\pi\cos\left(\frac{\pi L^*}{L_{\text{tot}}}\right)}\sin\left(\frac{\pi(L^* + L)}{L_{\text{tot}}}\right)\right],\\
C_1 &= \frac{1}{2}\left(-\frac{2q_3}{L} - 3C_0 L\right),\\
C_2 &= q_3, \quad C_3 = \frac{q_3 L_{\text{tot}}}{2\pi}\tan\left(\frac{\pi L^*}{L_{\text{tot}}}\right),
\end{aligned} \tag{3.3.24}$$

$$w_3 = q_3 \frac{L_{\text{tot}}}{2\pi \cos\left(\frac{\pi L^*}{L_{\text{tot}}}\right) \sin\left(\frac{\pi L^*}{L_{\text{tot}}}\right)} \sin^2\left(\frac{\pi x_3}{L_{\text{tot}}}\right).$$

In Eqs. (3.3.23) and (3.3.24), x_i and w_i ($i = 1, 2, 3$) denote the x-axis and the out-of-plane displacement of the parts of the strut respectively. The polynomial in Eq. (3.3.24), thus its coefficients $C_{0\ldots3}$, enforce the continuity conditions for the buckling displacements. In Eq. (3.3.23), a ($'$) denotes a differentiation with respect to the x-coordinate of the respective part.

The approximation of the out-of-plane displacements is based on the assumption that the delaminated sublaminates behave as being clamped in the undelaminated part of the strut. Therefore, the local buckling response is taken as the exact solution for a double-sided clamped EULER strut. The polynomial which enforces the continuity conditions also adds the global buckling response to w_1 and w_2. The physical interpretation of the generalized coordinates introduced in Section 3.1 can be retrieved from Eq. (3.3.24), where q_1 and q_2 are the amplitudes of the local out-of-plane displacement of the sublaminates respectively, and q_3 is the rotation at the interface between the delaminated and the undelaminated parts.

The curvature κ_{xx} for the respective parts are obtained by differentiating the out-of-plane displacements twice, *i.e.*

$$\kappa_{xx}^{\textcircled{i}} = -\frac{\partial^2 w_i}{\partial x_i^2}, \tag{3.3.25}$$

where the index i refers to the respective part of the strut, so that no summation is implied in Eq. (3.3.25).

In order to model the post-buckling response, a non-linear kinematic approach is required. Most studies employ the VON KÁRMÁN plate theory [76] which considers non-linear strains associated with the out-of-plane displacement. This follows the assumption of moderate rotations in the post-buckling range, where the strain contributions $(\partial w/\partial X_i)^2/2$ are not negligible whereas other non-linear terms are vanishingly small and thus omitted.[23] However, implementing the VON KÁRMÁN approach would result in a larger amount of generalized coordinates required to model the post-buckling response, which is discussed in Chapter 4.

The current approach follows a phenomenological model, described in [30, 95], and employs a single generalized coordinate q_4 which describes the end-shortening of the delaminated region. The modelling approach is not dissimilar to the VON KÁRMÁN theory, in such a way that a non-linear kinematic approach is considered. However, the modelling considers contributions to the shortening of the sublaminates rather than the in-plane displacement field. Thus, it assumes

[23] The VON KÁRMÁN plate theory is described in detail in Chapter 4. It should be noted that X_i refers to the coordinates system of the reference configuration.

that the in-plane strain is evenly distributed.

The total end-shortening of the delaminated region (q_4) comprises the axial shortening of the sublaminates, which is denoted by $u^{①}$ and $u^{②}$, and a purely geometric part associated with the buckling displacement.[24]

The stretching energy contribution to the strain energy is associated with the in-plane strain caused by the the axial shortening of the delaminated parts ($u^{①}$ and $u^{②}$), which can be expressed as

$$\begin{aligned} u^{①} &= q_4 - \frac{1}{2}\int_0^L \left(\frac{\partial w_1}{\partial x_1}\right)^2 \mathrm{d}x_1 - 2\left(\frac{1-a}{2}\right) t q_3\,, \\ u^{②} &= q_4 - \frac{1}{2}\int_0^L \left(\frac{\partial w_2}{\partial x_2}\right)^2 \mathrm{d}x_2 + 2\left(\frac{a}{2}\right) t q_3\,, \end{aligned} \tag{3.3.26}$$

where the second terms describe the aforementioned shortening associated with the buckling displacement. In addition, Eq. (3.3.26) considers the axial displacements associated with the rotation of the interface during the buckling response (third terms in Eq. (3.3.26)) due to the offset in between the neutral axis from the undelaminated region and the neutral axes of the sublaminates (*cf.* Fig. 3.8). This contribution to the shortening is approximated as the rotation angle q_3 multiplied by the distance between the respective neutral axes.

The respective in-plane strains ($\varepsilon_{xx}^{①}$, $\varepsilon_{xx}^{②}$) are then obtained by simple division with the respective length of the delaminated parts L owing to the aforementioned assumption of evenly distributed in-plane strain, *i.e.*:

$$\varepsilon_{xx}^{ⓘ} = \frac{u^{ⓘ}}{L}, \quad \text{with} \quad i = 1, 2. \tag{3.3.27}$$

Thus, all quantities required to determine the strain energy, *cf.* Eq. (3.3.21), in terms of the four generalized coordinates are determined.

The total end-shortening of the strut $\mathcal{E}$ required to describe the work done by the external forces is calculated as

$$\mathcal{E} = q_4 + \int_0^{L^*} \left(\frac{\partial w_3}{\partial x_3}\right)^2 \mathrm{d}x_3\,, \tag{3.3.28}$$

where the assumption that the undelaminated region does not undergo in-plane deformations is considered, such that the shortening of the undelaminated part

[24] The geometric part of the shortening of the delaminated parts, *cf.* the second terms in Eqs. (3.3.26) and (3.3.28), is the end-shortening—to the first order—of the respective part of the strut under the assumption of an inextensional neutral axis.

results entirely from the buckling displacement (the second term in Eq. (3.3.28)).

In terms of the notation of the analytical framework developed in Chapter 2, the prescribed force P and the total end-shortening of the strut $\mathcal{E}$ denote the conjugate variables A_1 and α_1 respectively. Regarding the current state of damage, it should be noted that by considering the width of the strut b—even if the problem is formulated as a one-dimensional model—the damage parameter is, in general, the delamination area (L times b). However, since the width of the delamination is constant, a change in structure is solely associated with the delamination length. This is why the delamination length is subsequently stated as the damage parameter of the current application example, *i.e.* $K = 1$ and $\xi_1 = \xi = L$.

Thus, with all quantities determined for a post-buckling analysis of stationary delaminations, Eq. (3.3.29) states the total potential energy of a composite strut with a through-the-width delamination:

$$\Pi(q_i, P, L) = W(q_i, L) - P\mathcal{E}(q_i, L) \quad \text{with} \quad i = 1, ..., 4, \tag{3.3.29}$$

where the delamination length L is treated as a constant and the deformation of the strut is determined for independent prescribed magnitudes of load with the variational principle

$$\delta\Pi(q_i) = \delta\left(W - P\mathcal{E}\right) = 0. \tag{3.3.30}$$

Eq. (3.3.30) yields a non-linear set of four algebraic equations

$$\frac{\partial\Pi}{\partial q_i} = 0, \quad \text{with } i = 1, ..., 4, \tag{3.3.31}$$

whose solution is the deformation paths $q_i(P)$ (in the following expressed in terms of $P(q_i)$).

The total potential energy and the set of algebraic equations are determined analytically using MATLAB [37]. The non-linear set of algebraic equations is solved numerically using the software AUTO-07P [18] which performs a continuous NEWTON method. As discussed in Chapter 2, the deformation path $P(q_i)$ resulting from Eqs. (3.3.30) and (3.3.31) applies only as long as the delamination is stationary, *i.e.* no growth is initiated, thus up to the deformation state (q_i^0, P^0) referred to as *damage state* (*cf.* Section 2.3 and Fig. 2.3).

3.3.4 Extended total potential energy principle

Delamination growth, *i.e.* a change in the damage parameter $\xi = L$, occurs, whenever the thermodynamic force associated with a change in the delamination length (f) reaches or exceeds the force required to produce delamination growth (g), thus:

$$f \geq g. \tag{3.3.32}$$

Regarding the current application example, the thermodynamic force is effectively the energy release rate G, *i.e.*

$$f = G, \tag{3.3.33}$$

which, following Section 2.3, can be determined by

$$f = G = -\frac{1}{b}\frac{\partial \Pi}{\partial L}, \tag{3.3.34}$$

where the multiplier $1/b$ results from considering the width of the strut.

A quasi-brittle fracture behaviour, thus a GRIFFITH-type damage process, is assumed for the delaminated composite strut which appears adequate when considering the laminates studied within this work.[25] Therefore, the dissipative energy can be expressed as

$$W_{\mathrm{d}} = W_{\mathrm{d}}(\xi = L) = G_{\mathrm{c}}(L - L^0)b, \tag{3.3.35}$$

in which L^0 is the initial delamination length and G_{c} is the critical energy release rate which is a material parameter that depends, in general, on the mode mixture [69]. However, for reasons of simplicity, G_{c} is assumed constant in the application example.

Thus, following Section 2.3, the force required for delamination growth can be determined by

$$g = \frac{1}{b}\frac{\partial W_{\mathrm{d}}}{\partial L} \tag{3.3.36}$$

yielding

$$g = G_{\mathrm{c}}. \tag{3.3.37}$$

With Eqs. (3.3.34) and (3.3.37), the condition for delamination growth (*cf.*

[25] Unidirectional layers of fibre reinforced plastics are investigated in which duroplastic materials are used as the matrix constituent. Such materials exhibit a brittle fracture behaviour.

Eq. (3.3.32)) can be stated in terms of the current application example, *i.e.*:

$$G \geq G_{\mathrm{c}}. \tag{3.3.38}$$

Thus, the behaviour of the energy release rate with respect to the prescribed load input as well as certain delamination lengths, *cf.* Figs. 3.6 and 3.7, can be analysed with Eq. (3.3.34) and the solution for the conservative behaviour $P(q_i)$ obtained from Eq. (3.3.31). Furthermore, the deformation state which causes growth—the *damage state* (q_i^0, P^0)—can be identified using Eq. (3.3.38). At the damage state, the total potential energy principle loses its validity. As described in Section 2.3, the extended total potential energy principle applies starting from the damage state (q_i^0, P^0).

An extended total potential energy exists, if the condition

$$f = g \tag{3.3.39}$$

holds during the non-conservative deformation process. Rewriting the condition for the existence of an extended total potential energy in terms of the application example yields

$$G = G_{\mathrm{c}} \quad \text{with} \quad G = -\frac{1}{b}\frac{\partial \Pi(q_i, P, L)}{\partial L}. \tag{3.3.40}$$

It should be stressed that in contrast to purely tensile loading, the condition of $G = G_{\mathrm{c}}$ does not necessarily lead to a catastrophic failure of the strut in the post-buckling regime, which is explained in detail in Section 3.4.

With the aid of Eq. (3.3.40), the damage parameter L is derived as a function of the generalized coordinates q_i and the applied force P. However, since an explicit form cannot be found from Eq. (3.3.40) it is rewritten, such that

$$D\left(q_i, P, L\right) = G - G_{\mathrm{c}} = 0, \tag{3.3.41}$$

from where the damage parameter, *i.e.* the delamination length $L = L(q_i, P)$, is implicitly given, thus

$$D\left(q_i, P, L(q_i, P)\right) \equiv 0. \tag{3.3.42}$$

Following the framework developed in Chapter 2, an explicit form of the damage parameter is then obtained by employing a TAYLOR series approximation around the damage state (q_i^0, P^0) up to the 2nd order, thus:

$$
\begin{aligned}
L(q_i, P) = L^0 &+ \left.\frac{\partial L}{\partial q_i}\right|_{\substack{q_i^0 \\ P^0}} (q_i - q_i^0) + \left.\frac{\partial L}{\partial P}\right|_{\substack{q_i^0 \\ P^0}} (P - P^0) \\
&+ \frac{1}{2} \left.\frac{\partial^2 L}{\partial q_i \partial q_j}\right|_{\substack{q_i^0 \\ P^0}} (q_i - q_i^0)(q_j - q_j^0) + \frac{1}{2} \left.\frac{\partial^2 L}{\partial P^2}\right|_{\substack{q_i^0 \\ P^0}} (P - P^0)^2 \\
&+ \left.\frac{\partial^2 L}{\partial q_i \partial P}\right|_{\substack{q_i^0 \\ P^0}} (q_i - q_i^0)(P - P^0) + \mathcal{O}(3),
\end{aligned}
\tag{3.3.43}
$$

in which L^0 is the initial pre-existing delamination length. The partial derivatives in Eq. (3.3.43) are obtained from Eq. (3.3.42) by implicit differentiation (*cf.* Section 2.3). The delamination length, as provided by Eq. (3.3.43), is subsequently incorporated in the extended total potential energy principle.

With the dissipative energy described in Eq. (3.3.35), all energy terms of the extended total potential energy are obtained. Subsequently, the damage parameter L in the form of Eq. (3.3.43) is replaced in the respective expressions for the strain energy (*cf.* Eqs. (3.3.21) and (3.3.29)), the dissipative energy (*cf.* Eq. (3.3.35)) and the work done by the external forces (*cf.* Eq. (3.3.22) and (3.3.29)), so that the extended total potential energy reads

$$
\Pi^*(q_i, P) = W\left(q_i, L(q_i, P)\right) + W_\mathrm{d}\left(L(q_i, P)\right) - P\mathcal{E}\left(q_i, L(q_i, P)\right). \tag{3.3.44}
$$

The variational principle using the extended total potential energy can then be written as

$$
\delta\Pi^*(q_i) = \delta\left(W + W_\mathrm{d} - P\mathcal{E}\right) = 0, \tag{3.3.45}
$$

which yields a set of four non-linear algebraic equations whose solution is the deformation path $q_i(P)$ starting from the damage state (q_i^0, P^0). The deformation path is obtained numerically by applying the Newton method. It should be stressed that the deformation path considers delamination growth. The behaviour of the damage parameter—the delamination length—can be obtained by inserting the solution $q_i(P)$ into Eq. (3.3.43).

Since Eq. (3.3.43) approximates the delamination length, the solution obtained from Eq. (3.3.45) will violate the condition $G = G_\mathrm{c}$ at a certain deformation state, which is determined by evaluating G with the aid of Eq. $(3.3.40)_2$ for each loading step.[26] The deformation state for which the condition is violated is taken as a

[26] A deviation of 0.5% in between G and G_c is taken as an error threshold indicating the violation of $G = G_\mathrm{c}$.

"new" damage state from where a new expression for the delamination length is determined with Eq. (3.3.43). This is implemented in an iterative scheme which consecutively derives the delamination length and solves the variational principle.

For the current application example, a TAYLOR series up to the second order was determined as optimal for the approximation of the delamination length. Such an approximation provides just a marginally smaller range of loading steps until the condition $G = G_c$ is violated than an expression with third order terms but requires significantly less computational cost.

The implementation of the extended total potential energy principle as well as the iterative scheme is performed by a MATLAB script.

3.4 Results

In this section, results obtained for the post-buckling behaviour of delaminated composite struts are presented. It will be distinguished between post-buckling responses for stationary delaminations (Section 3.4.2) and post-buckling responses comprising delamination growth and thus an entire loading process (Section 3.4.3).

The former is included in this work since the model description in Section 3.3 enables a detailed study of the post-buckling behaviour of delaminated composite struts similar to the study [30] investigating isotropic struts, so that general phenomena of the post-buckling behaviour and characteristic buckling responses of delaminated composite struts can be summarized. However, focus is placed on the latter in which findings from the application of the framework developed in the current work are presented. Post-buckling responses yet to be obtained by semi-analytical modelling approaches are documented whereby residual and additional load bearing capabilities are described as well as the stability of the post-buckling behaviour is investigated.

Before proceeding to the results, first, the modelling approach is verified in Section 3.4.1 by comparisons with findings documented within the literature for the case of stationary delaminations for an isotropic and a multi-layered orthotropic strut.

3.4.1 Verification of the model description

In order to verify the model description developed in Section 3.3, post-buckling responses obtained (without considering possible delamination growth) are compared with findings documented in [30] and [87] studying delaminated isotropic and multi-layered orthotropic struts respectively.

Fig. 3.9 shows the post-buckling response of a delaminated isotropic strut in terms of normalized compressive load *vs.* normalized end-shortening, $P_{\mathrm{norm}}(\mathcal{E}_{\mathrm{norm}})$.

A comparison with [30] is enabled by adjusting the model description in Section 3.3 to isotropic material behaviour and considering displacement functions for the simply supported case studied in [30]. The strut has a total length of $L_{\text{tot}} = 110\,\text{mm}$ and a thickness of $t = 2.13\,\text{mm}$. The delamination length is $L = 55\,\text{mm}$ and the delamination depth is given by $a = 0.235$ (*cf.* Fig. 3.8).

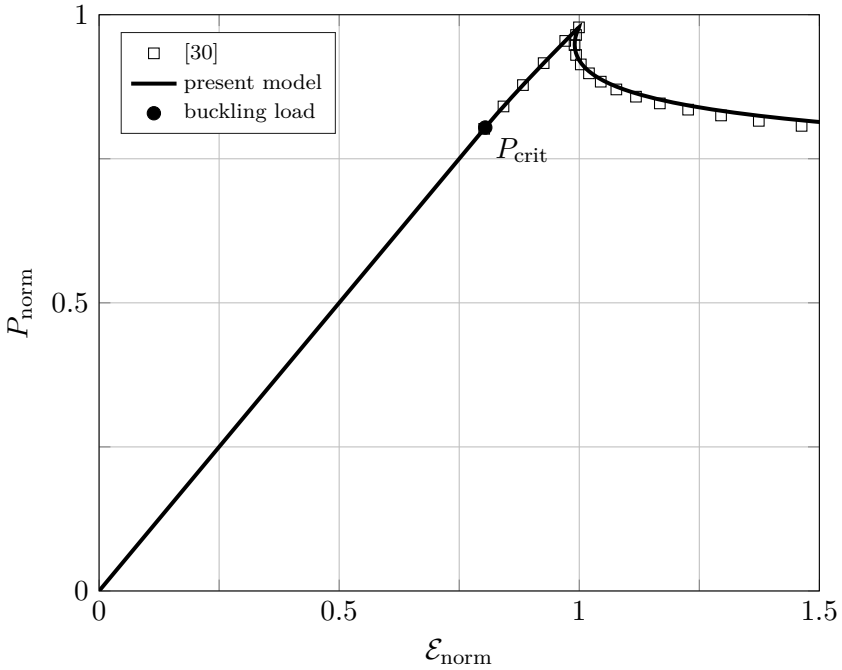

Fig. 3.9: Post-buckling response of a delaminated isotropic strut in terms of normalized load (P_{norm}) *vs.* normalized end-shortening ($\mathcal{E}_{\text{norm}}$) in comparison with results published in [30].

The normalization of the load and the end-shortening is carried out with respect to the corresponding EULER buckling load and the end-shortening for an undelaminated strut respectively, thus:

$$P_{\text{Euler}} = \frac{c\pi^2 EI}{L_{\text{tot}}^2} \quad \text{and} \quad \mathcal{E}_{\text{Euler}} = \frac{P_{\text{Euler}} L_{\text{tot}}}{EA}, \tag{3.4.1}$$

in which EI is the bending stiffness of an isotropic strut, EA is the in-plane stiffness, L_{tot} is the length of the strut and c is 1 for a simply-supported strut and 4 for a both-sided clamped strut.

Fig. 3.9 depicts that the model description provides results which are in very good agreement. The critical load and the post-buckling path show almost no deviations.

Fig. 3.10 describes the post-buckling response in terms of normalized compressive load *vs.* normalized midpoint deflections, $P_{\text{norm}}(w_{\text{norm}})$, for a multi-layered cross-ply composite strut with the layup $[0°/(90°/0°)_7]$, a delamination depth of

$a = 4/15$ and a delamination length of $L = 50.8\,\text{mm}$ (*cf.* Fig. 3.8). The strut is clamped on both sides and has a total length of $L_{\text{tot}} = 96.52\,\text{mm}$ and a thickness of $t = 1.337\,\text{mm}$.

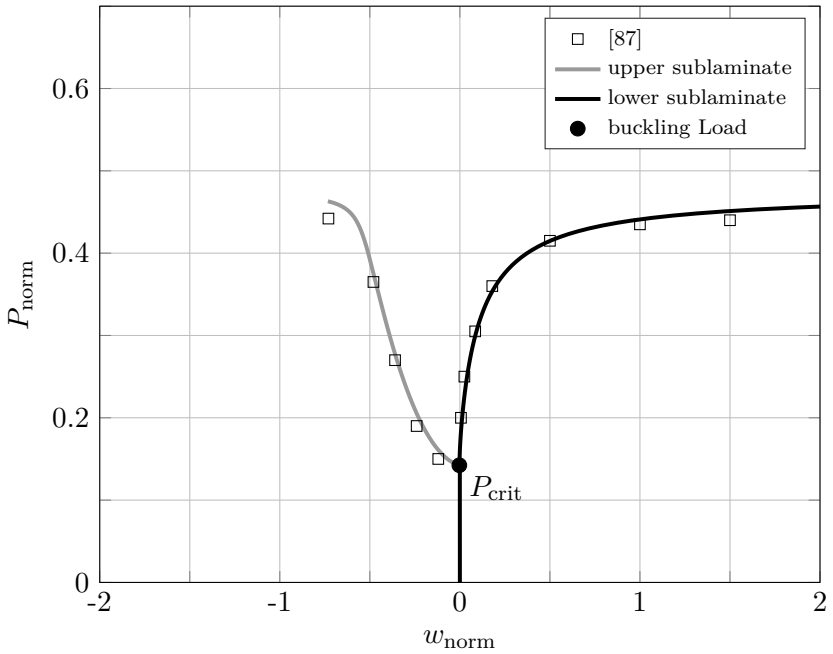

Fig. 3.10: Post-buckling response of a delaminated multi-layered composite strut in terms of normalized load (P_{norm}) *vs.* normalized midpoint deflections (w_{norm}) in comparison with results published in [87].

As in [87], an imperfection (assumed to be caused by the delamination) is considered in the form of an initial midpoint deflection. The imperfection is added to the energy formulation by assigning q_1 an initial value of $q^* = t/1000$ and subtracting its respective energy contributions (this is provided in detail in Appendix D). Such an imperfection is also considered for the results presented in Section 3.4.3.

Normalization of the load in Fig. 3.10 is carried out with respect to the EULER buckling load for an undelaminated strut with 0° degree layers only (as done in [87]), *i.e.*

$$P_{\text{Euler}} = \frac{c\pi^2 D_{11} b}{L_{\text{tot}}^2}, \tag{3.4.2}$$

where D_{11} is the bending stiffness against moment resultants around the y-axis (*cf.* Fig. 3.8) and b is the width of the strut.[27] The midpoint deflections are

[27] In Sections 3.4.2 and 3.4.3, the compressive load is normalized with respect to the actual layup of the strut and the effective bending stiffness D_{eff}, as introduced in Section 3.3.2.2, is employed.

normalized to the total thickness of the strut,[28] $w_{\text{norm}} = w_{1,2}(x_{1,2} = L/2)/t$.

The results shown in Fig. 3.10 are in very good agreement. The initial post-buckling solution almost coincides. Slight differences can be seen at larger deflections with deviations smaller than 4%. Based on such findings, the model developed in Section 3.3 appears to describe the buckling and post-buckling behaviour sufficiently well in the conservative range.

3.4.2 Stationary delamination

Even though focus of the current work is not on stationary delaminations, the section is included to exhibit the capabilities of the model description in Section 3.3 to enable detailed analyses regarding the post-buckling behaviour of delaminated composite struts. Therefore, the section summarizes post-buckling phenomena of delaminated transversally-isotropic composite struts with the aid of an illustrative example: a composite strut with a cross-ply layup and a symmetric stacking sequence $[0°/90°/0°/90°]_{\text{s}}$.

The dimensions of the strut are chosen, so that out-of-plane shear effects can be omitted with certainty. Each of the eight plies (unidirectional layers) consists of the same transversally isotropic material. In order to provide a realistic measure for the material parameters, it is assumed that the layers consist of Toho Tenax® UTS carbon fibres [97] and epoxy resin as matrix. The fibre volume fraction is taken as 0.58. The dimensions and the calculated effective material parameters are provided in Table 3.1, in which h describes the thickness of a single layer and t the total thickness of the strut.

Dimensions		**Material Parameters**	
L_{tot}	100.00 mm	E_{11}	141.00 GPa
b	10.00 mm	E_{22}	6.00 GPa
t	0.80 mm	G_{12}	2.60 GPa
h	0.10 mm	ν_{12}	0.27

Table 3.1: Dimensions and material parameters of the delaminated strut.

The post-buckling behaviour is described by examining general phenomena regarding the buckling modes[29] as well as by analysing the deformation paths for representative cases. In those cases, delaminations in between the fifth and sixth layer, *i.e.* $a = 0.375$ (*cf.* Fig. 3.8), are studied. Three delamination

[28] For the purpose of comparison, the coordinate system of [87] is used in Fig. 3.10. Thus, the signs of deflection are opposed to Fig. 3.8.

[29] Buckling modes are herein understood as characteristic buckling shapes rather than *eigen modes*. The terminology of [30] and [102] is adopted.

lengths, $L_{\text{norm}} = \{0.5, 0.62, 0.75\}$, are investigated. Such cases comprise most characteristics of the post-buckling behaviour for the stationary delaminations.

The results are provided in terms of normalized compressive load (P_{norm}) against normalized end-shortening ($\mathcal{E}_{\text{norm}}$) as well as normalized compressive load against normalized midpoint deflections (w_{norm}), which can be readily obtained from the deformation path $P(q_i)$ using Eqs. (3.3.28) and (3.3.24) respectively. Furthermore, the analysis of the load (P_{norm}) against the rotation angle (q_3) illustrates another advantage of the model description, such that single deformation characteristics can be readily analysed.

Normalization is carried out with respect to the EULER values for an undelaminated strut with the same stacking sequence in which the effective parameters for in-plane and bending stiffness are used—contrary to Eq. (3.4.2). The midpoint deflection is normalized to the thickness of the strut, $w_{\text{norm}} = w_{1,2}(x_{1,2} = L/2)/t$, and the delamination length to the total length of the strut, $L_{\text{norm}} = L/L_{\text{tot}}$.

3.4.2.1 General observations

The post-buckling behaviour can be described by examining the characteristic buckling modes occurring during the post-buckling response, as shown in Figs. 3.11 to 3.14. At the buckling load, a closed-mode buckling response, as illustrated in Fig. 3.11, is present for all possible delamination depth and length.[30] The response of the thicker sublaminate (grey line in Figs. 3.11) strongly depends on the delamination depth and on its in-plane stiffness. For thin delaminations, the thicker sublaminate remains unaffected (which is considered herein as closed-mode buckling).[31] Irrespective of the delamination length and depth, the initial (post-)buckling response (in the vicinity of the buckling load) is always stable.

Depending on the layup, the delamination length and the delamination depth, the post-buckling response of the strut may change from a closed-mode to an opening-mode response which is illustrated in Figs. 3.12 and 3.13.

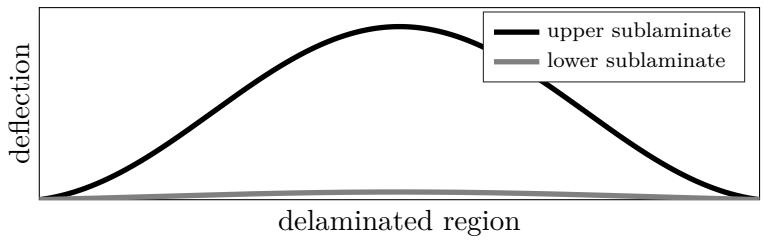

Fig. 3.11: Closed-mode buckling (initial response).

[30] Configuration which cause contact of both sublaminates are not considered.

[31] This is often referred to as thin-film buckling. As the present work considers global buckling responses, the post-buckling response in which just the thinner less stiff sublaminate exhibits out-of-plane deflection is subsequently referred to as local buckling rather than thin-film buckling.

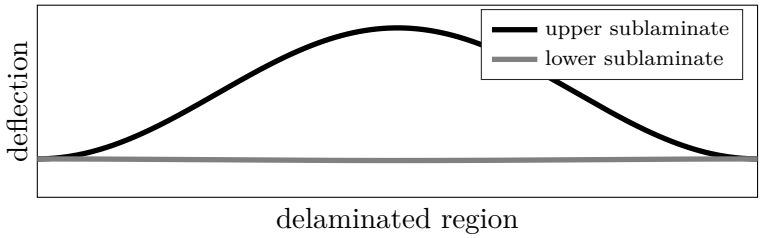

Fig. 3.12: Transition to opening-mode buckling.

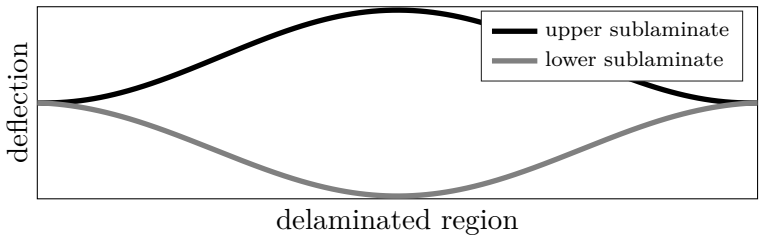

Fig. 3.13: Opening-mode buckling.

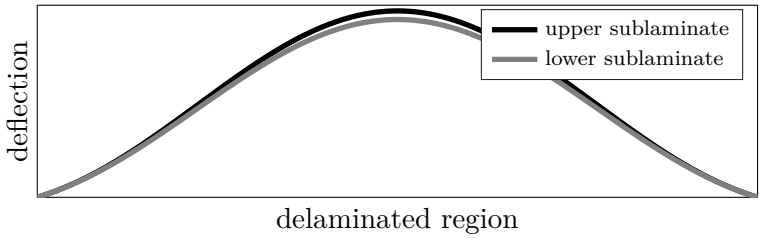

Fig. 3.14: Closed-mode buckling before contact.

Such a changeover is associated with the onset of global buckling and is more pronounced for deeper delaminations than for shallow delaminations. For shallow delaminations, the changeover occurs in the initial post-buckling response directly following the buckling load. For certain delamination configurations, *i.e.* the smaller and the deeper the delamination is, such a changeover does not occur.

Table 3.2 lists the delamination lengths (L_{change}) depending on the delamination depth (a) for which the buckling response changes from remaining in the closed-mode ($L < L_{\text{change}}$) to the transition from a closed-mode into an opening-mode response ($L \geq L_{\text{change}}$).

As can be seen, for increasing delamination depths the change in the buckling response occurs at larger delaminations. Furthermore, the delamination length L_{change} also provides a general indicator whether or not the strut loses its stability during the post-buckling response.

depth a	$L_{\text{change}}[-]$
$a = 0.125$	0.22
$a = 0.250$	0.46
$a = 0.375$	0.62
$a = 0.500$	no change

Table 3.2: Delamination length for the changeover in the buckling response.

For delamination length $L \geq L_{\text{change}}$, the post-buckling response remains stable throughout the deformation process (for stationary delaminations). For delamination length $L < L_{\text{change}}$, the system remains in the closed-mode but loses its stability during the post-buckling response in a load-controlled configuration. The loss of stability—the post-buckling response exhibits a limit point—is associated with the onset of global buckling. As a consequence, both sublaminates may get in contact with each other at a certain deformation state which is indicated in Fig. 3.14.

3.4.2.2 Post-buckling behaviour

Subsequently, characteristic phenomena of delaminated composite struts are described by studying the post-buckling responses of the aforementioned three cases of delaminated struts ($a = 0.375$, $L_{\text{norm}} = \{0.50, 0.62, 0.75\}$), as introduced in Section 3.4.2. Following Table 3.2, the three delamination lengths characterize configurations which are smaller than, equal to and greater than L_{change}, respectively.

Fig. 3.15 describes the post-buckling behaviour for the three cases considered in terms of the normalized compressive load (P_{norm}) against the normalized end-shortening of the strut ($\mathcal{E}_{\text{norm}}$). The corresponding behaviour of the normalized compressive load (P_{norm}) against the normalized midpoint deflections (w_{norm}) is provided in Fig. 3.16.

In Figs. 3.15 to 3.17, the buckling load (P_{crit}) for the cases studied is indicated by the symbols "●", "●" and "●", respectively. As expected, Figs. 3.15 and 3.16 show that larger delamination lengths cause smaller buckling loads. The drop of the buckling load is more significant in between $L_{\text{norm}} = 0.50$ and $L_{\text{norm}} = 0.62$ than $L_{\text{norm}} = 0.62$ and $L_{\text{norm}} = 0.75$. Such behaviour of the buckling load corresponds to the information provided in Section 3.2.1 in Fig. 3.4 for the case of deeper delaminations.

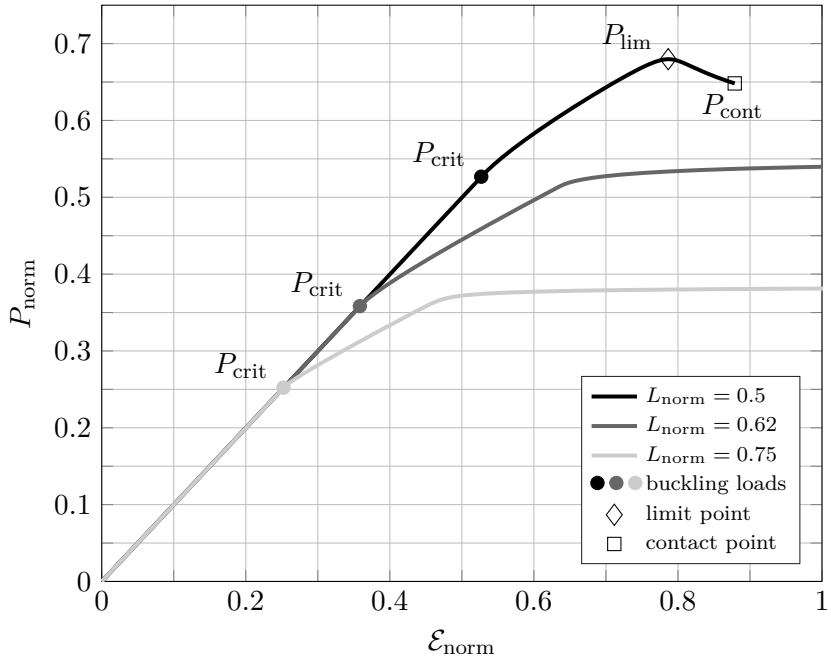

Fig. 3.15: Normalized load (P_{norm}) *vs.* normalized end-shortening ($\mathcal{E}_{\text{norm}}$); delamination depth $a = 0.375$; delamination lengths $L_{\text{norm}} = \{0.50,\ 0.62, 0.75\}$.

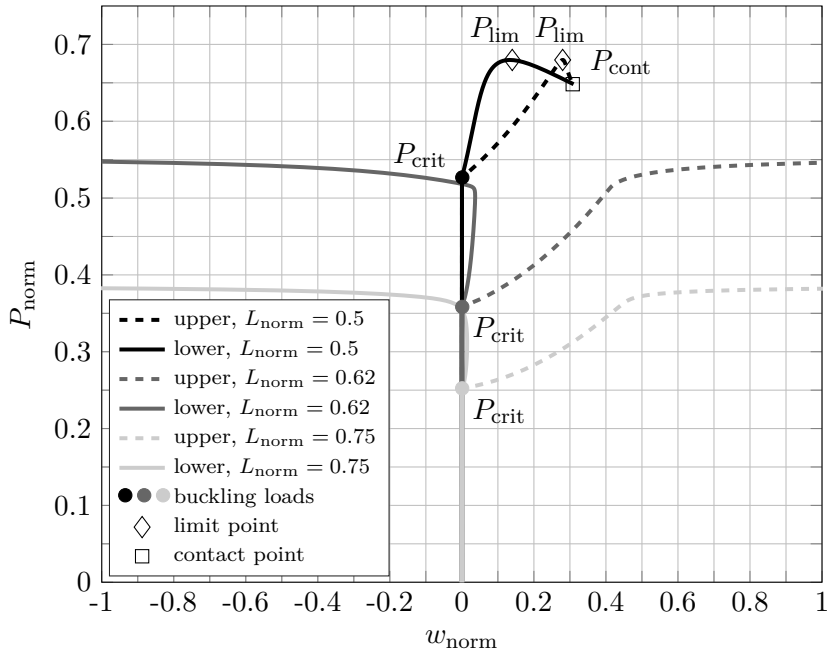

Fig. 3.16: Normalized load (P_{norm}) *vs.* normalized midpoint deflections (w_{norm}); delamination depth $a = 0.375$; delamination lengths $L_{\text{norm}} = \{0.50,\ 0.62, 0.75\}$.

Examining the case of $L_{\text{norm}} = 0.50$ (black lines), Fig. 3.15 shows that, initially, the post-buckling response is stable with a minor decrease in compressive stiffness of the strut. The post-buckling stiffness decreases further towards the maximum

load of $P_{\text{norm}} = 0.68$. At an end-shortening of $\mathcal{E}_{\text{norm}} = 0.78$ associated with the maximum load, the response changes from stable to unstable. This deformation state is a limit point (P_{lim}) illustrated by the symbol "$\diamond$" in Figs. 3.15 and 3.16. Thus, in a load-controlled configuration stability failure would occur at P_{lim}.

Fig. 3.16 depicts a closed-mode buckling response throughout the deformation process for $L_{\text{norm}} = 0.50$ whereby the upper less stiff sublaminate (dashed line) exhibits larger deflections than the lower sublaminate. As described in Section 3.4.2.1, after the loss of stability both sublaminates get in contact with each other which occurs shortly after the limit point is reached. The contact point is indicated in Figs. 3.15 and 3.16 by the symbol "$\square$".

As delineated by Table 3.2, such a post-buckling response occurs up to a delamination length of $L_{\text{norm}} = 0.61$ where the buckling load, the maximum load and the post-buckling stiffness would reduce consecutively without a change in the qualitative behaviour. At $L_{\text{norm}} = 0.62$, the post-buckling response of the strut changes. The deformation behaviour is described in Figs. 3.15 and 3.16 by the dark grey lines. As can be seen, no limit point is present and hence the deformation process is stable throughout the post-buckling response. The post-buckling response can be subdivided into two parts. The first part comprises the initial response which is characterized by a large post-buckling stiffness (Fig. 3.15) and a closed-mode buckling response where the thinner sublaminate exhibits significantly larger deflections than the thicker sublaminate (Fig. 3.16). The second part commences when the global buckling response is triggered, thus the thicker sublaminate also exhibits large deflections. The transition can be seen in Fig. 3.16 at a load of $P_{\text{norm}} = 0.52$. At this deformation state, the changeover from a closed-mode to an opening-mode response is initiated. Subsequently, both sublaminates deflect in opposite directions. Once the global buckling response is present, the post-buckling stiffness reduces significantly showing the characteristic weakly stable behaviour as for undelaminated struts where the load converges towards $P_{\text{norm}} = 0.55$.

If larger delamination lengths are present, the qualitative post-buckling behaviour does not change again. However, each part of the post-buckling response described for a delamination length of $L_{\text{norm}} = 0.62$ occurs at a different extent. This is depicted in Figs. 3.15 and 3.16 for a delamination length of $L_{\text{norm}} = 0.75$ (light grey lines). The initial post-buckling response in which both sublaminates deflect in the same direction (closed-mode response) associated with a small decrease in stiffness shortens ($P_{\text{norm}} = 0.36 - 0.52$ for $L_{\text{norm}} = 0.62$, $P_{\text{norm}} = 0.26 - 0.37$ for $L_{\text{norm}} = 0.75$). The transition to the second part of the post-buckling response is smoother than for $L_{\text{norm}} = 0.62$ as the changeover from closed-mode to opening-mode is already triggered during the initial post-buckling response (shortly after

the buckling load at $P_{\text{norm}} = 0.30$). The maximum load bearable by the system is also significantly reduced to $P_{\text{norm}} = 0.38$.

Since the generalized coordinates used within the model description provide further physical interpretation, Fig. 3.17 is analysed in which the normalized load (P_{norm}) is plotted against the rotation angle (q_3) at the connecting plane of the delaminated and undelaminated region. Whereas the rotation angle is always positive for a delamination length of $L_{\text{norm}} = 0.5$ (black line in Fig. 3.17), the changeover in buckling displacement from initially closed-mode to an opening-mode buckling response is documented for delamination lengths of $L_{\text{norm}} = 0.62$ (dark grey line) and $L_{\text{norm}} = 0.75$ (light grey line). As can be seen in Fig. 3.17, following buckling the rotation angle is positive associated with both sublaminates deflecting in the positive direction. The transition into the opening-mode buckling response is visualized by the rotation angle shifting to negative values which also indicates the onset of the global buckling response for the respective cases (*cf.* Figs. 3.15 and 3.16).

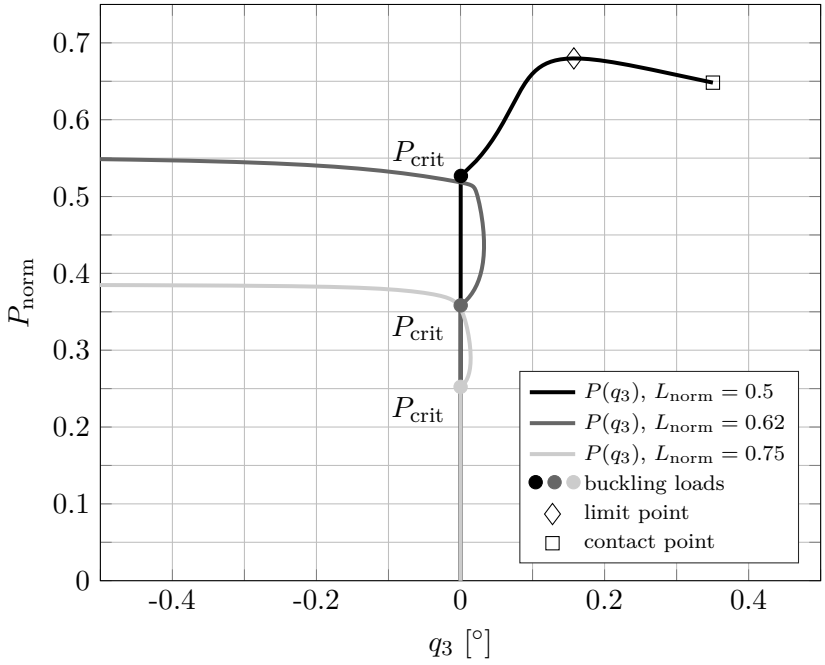

Fig. 3.17: Normalized load (P_{norm}) *vs.* rotation angle (q_3); delamination depth $a = 0.375$; delamination lengths $L_{\text{norm}} = \{0.50, 0.62, 0.75\}$.

3.4.2.3 Discussion of the results

The results obtained in Section 3.4.2 provide insight into the influence of delaminations on the post-buckling behaviour of composite struts. As it is, to a certain amount, random to what extent delaminations occur in composite struts

the results showed that minor changes in delamination length (*e.g.* as shown for $a = 0.375$ and $L_{\text{norm}} = 0.61 - 0.62$) may change the buckling response of the system (closed-mode to opening-mode) as well as, more importantly, the stability of the post-buckling deformation. Configurations of delaminations causing such a sudden change in the stability of the post-buckling response, and thus stability failure under prescribed forces, are determined and summarized in Table 3.2. Thus, with Table 3.2 and the characteristic post-buckling deformation paths (Figs. 3.15 to 3.17), the post-buckling behaviour of delaminated composite struts for stationary delaminations is described.

The characteristic post-buckling responses for delamination lengths $L_{\text{norm}} \geq L_{\text{change}}$ provided in Figs. 3.15 to 3.17 (dark grey and light grey lines) only change quantitatively for varying delamination depth with respect to the buckling load, the post-buckling stiffness and the out-of-plane deflections.

Post-buckling responses exhibiting a changeover in the buckling response from closed-mode to opening-mode that is associated with a loss in stability, as documented in [30] for isotropic struts, have not been obtained. Such a response is discussed in [30] as being related with a secondary bifurcation point which, on the one hand, can be neglected *a priori* for the current study owing to the stretching–bending coupling. On the other hand, a continuous change in the delamination depth as for homogeneous and isotropic struts does not apply for multi-layered composite struts. Thus, it remains to be investigated if for certain delamination depths which randomly match the depth of an interface in between two layers further post-buckling phenomena may be obtained.

Moreover, for smaller delamination depths than studied in Figs. 3.15 to 3.17 (shallow delaminations), a more pronounced local buckling response would be obtained. This, however, does not affect the general phenomena of the post-buckling behaviour presented in this section.

Imperfections in the form of an initial out-of-plane deflection, as it is partly assumed in the literature, are not considered. Thus, post-buckling responses as for mid-size delaminations in Fig. 3.5 are not present. Such imperfections would mainly affect delamination lengths $L_{\text{norm}} < L_{\text{change}}$ which, up to a certain smaller delamination length than L_{change}, cause stable post-critical behaviour exhibiting a post-buckling response similar to Fig. 3.5 (dashed lines). Such a case is included in the subsequent Section 3.4.3. The unstable post-buckling behaviour documented in this section would occur then for smaller delamination length as given in Table 3.2.

3.4.3 Non-stationary delaminations

This section presents the results following the application of the analytical framework developed in this work to the problem of delaminated composite struts under compressive in-plane loading.

Therefore, a laminate is chosen which is examined in [87] with respect to the post-buckling behaviour for stationary delaminations. The model description for a stationary delamination developed in Sections 3.3.1 and 3.3.2 has been verified by comparison with [87] in Fig. 3.10. The strut has a $[0°/(90°/0°)_7]$ cross-ply layup with a delamination at the depth $a = 4/15$.

The dimensions and material parameters of the delaminated strut are listed in Table 3.3 in which h describes the thickness of a single layer and t the total thickness of the strut.

Dimensions		**Material Parameters**	
L_{tot}	96.52 mm	E_{11}	137.90 GPa
b	12.70 mm	E_{22}	8.98 GPa
t	1.337 mm	G_{12}	7.20 GPa
a	4/15	ν_{12}	0.30
h	0.0889 mm	G_{c}^{I}	190 Nm/m^2

Table 3.3: Dimensions and material parameters taken from [87].

The results are compared with findings from finite element simulations using Abaqus [93]. The strut is built-up by shell elements (type S4R) with an element size of 0.2 mm by 0.2 mm and a total of 62790 nodes. Delamination propagation is modelled using the virtual crack closure technique [50, 51] incorporated in Abaqus.

First, the thermodynamic force—the energy release rate—is examined. With the aid of the energy release rate, the condition for the existence of an extended total potential energy is verified. Subsequently, post-buckling responses for two characteristic configurations are provided in terms of normalized compressive load against normalized midpoint deflections (P_{norm} *vs.* w_{norm}) and normalized compressive load against its corresponding end-shortening (P_{norm} *vs.* $\mathcal{E}_{\text{norm}}$). Post-buckling responses for an entire loading process, *i.e.* up to stability and/or material failure of the strut, are presented.

3.4.3.1 Energy release rate

Fig. 3.18 shows the normalized energy release rate, $G_{\text{norm}} = G/G_{\text{c}}^{\text{I}}$, with respect to the normalized delamination length, $L_{\text{norm}} = L/L_{\text{tot}}$, (used instead of the delamination area as the width b is constant) and increasing levels of constant end-shortening. The energy release rate is normalized with respect to the mode I critical energy release rate G_{c}^{I} provided in Table 3.3 where $G_{\text{norm}} = 1$, *i.e.* $G = G_{\text{c}} = G_{\text{c}}^{\text{I}}$, indicates delamination growth.[32] It is generally advisable to evaluate the energy release rate in terms of end-shortening $\mathcal{E}$ rather than forces as weakly stable or even unstable buckling phenomena can be analysed.

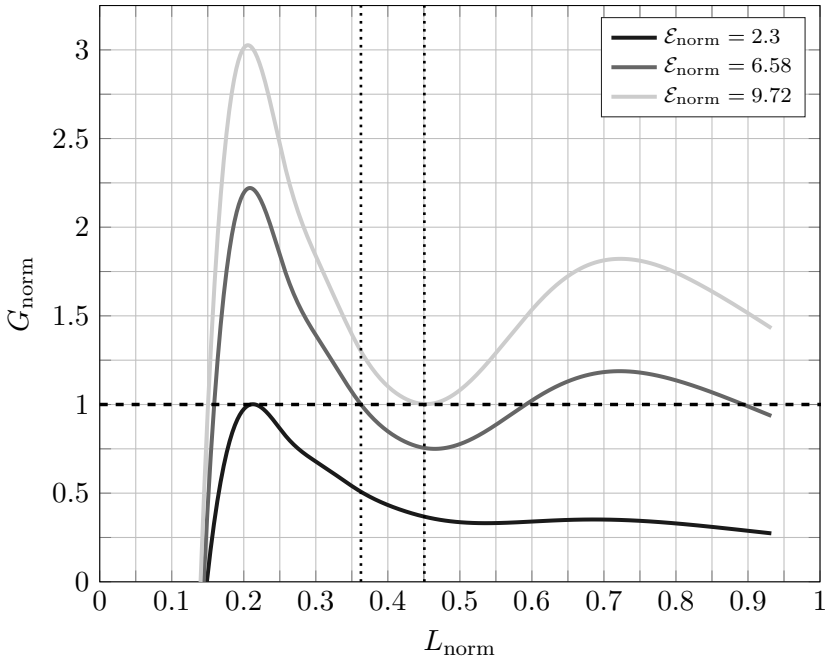

Fig. 3.18: Normalized energy release rate (G_{norm}) *vs.* normalized delamination length (L_{norm}) for increasing load levels in the form of normalized end-shortening ($\mathcal{E}_{\text{norm}}$); delamination depth $a = 4/15$.

Fig. 3.18 depicts a characteristic behaviour of the energy release rate for delaminated struts with a through-the-width delamination. Similar results are documented in the literature for homogeneous struts (*cf.* Fig. 3.7). The solid lines in Fig. 3.18 describe the energy release rate for respective constant values of end-shortening. The smallest value ($\mathcal{E}_{\text{norm}} = 2.3$) indicates the lowest level of "load input" for which delamination growth occurs. Thus, for an initial delamination length of $L_{\text{norm}} = 0.21$, growth is generated at $\mathcal{E}_{\text{norm}} = 2.3$. An initial delamination length of $L_{\text{norm}} = 0.45$ requires the highest value of end-shortening ($\mathcal{E}_{\text{norm}} = 9.72$) to cause growth. A vertical dotted line is added to Fig. 3.18 corresponding to a delamination length of $L_{\text{norm}} = 0.45$. The left vertical dotted line in Fig. 3.18

[32] The assumption $G_{\text{c}} = G_{\text{c}}^{\text{I}}$ constitutes a conservative measure.

indicates an arbitrary chosen initial delamination length of a strut ($L_{\text{norm}} = 0.36$) which is studied next.

At an end-shortening of $\mathcal{E}_{\text{norm}} = 6.58$, the energy release rate equals the critical value ($G = G_{\text{c}}$, $G_{\text{norm}} = 1$) for an initial delamination length of $L_{\text{norm}} = 0.36$. Once the critical energy release rate is reached, delamination growth occurs. Thus, for the current state of loading (quasi-static process) associated with the critical energy release rate G_{c}, the delamination length increases from L to $L + \Delta L$. For the new configuration, *i.e.* the constantly kept state of loading and a delamination length of $L + \Delta L$, the energy release rate changes from G_{c} ($G_{\text{norm}} = 1$) to another value, which is referred to as G_{new}. If the energy release rate decreases ($G_{\text{c}} > G_{\text{new}}$), growth stops and the process is termed stable. If $G_{\text{new}} > G_{\text{c}}$, unstable growth occurs causing catastrophic failure of the strut. If stable delamination growth occurs, further loading may be applied until G_{c} is reached again. Thus, the post-buckling response under stable delamination growth follows the condition of $G = G_{\text{c}}$ (horizontal dashed line in Fig. 3.18) which also dictates the load that may be applied to the system and embodies the requirement for deriving the extended total potential energy ($f_k = g_k$) used within the framework developed. With the study of Fig. 3.18, the existence of an extended total potential energy for delamination growth in buckled delaminated composite struts is verified.

Furthermore, by analysing Fig. 3.18, regions of stable or unstable growth for initial delamination lengths are obtained. For delamination lengths of $0.21 \leq L_{\text{norm}} < 0.45$ stable delamination growth occurs. Delamination lengths larger than $L_{\text{norm}} = 0.45$ but smaller than $L_{\text{norm}} = 0.73$ cause unstable growth. Stable growth occurs again if the delamination length is larger than $L_{\text{norm}} = 0.73$.

3.4.3.2 Post-buckling

The post-buckling behaviour of delaminated struts analysed in Fig. 3.18 ($a = 4/15$) is subsequently examined. Two cases of initial delamination lengths are considered ($L_{\text{norm}} = \{0.36, 0.67\}$) which provide characteristic post-buckling responses associated with a distinct damage growth behaviour. Furthermore, such cases refer to the classification of mid-size and large delaminations (*cf.* Fig. 3.5), thus configurations of struts which do not evoke a limit point, *i.e.* loss of stability, for the case of stationary delaminations.

First, the case of a delamination with the length $L_{\text{norm}} = 0.36$ ($L = 35\,\text{mm}$) and the depth $a = 4/15$ (in between the eleventh and twelfth layer, *cf.* Fig. 3.8) is studied. Fig. 3.18 shows that for such an initial delamination length growth will be stable until a delamination length of $L_{\text{norm}} = 0.45$ is reached (in between left and right vertical dotted line in Fig. 3.18).

In Figs. 3.19 and 3.20, the post-buckling behaviour is studied by examining the load P_{norm} against the midpoint deflection of the sublaminates w_{norm}. The

normalization of the load is performed with respect to the EULER buckling load of the undelaminated strut and the midpoint deflection is normalized against the total thickness of the strut.

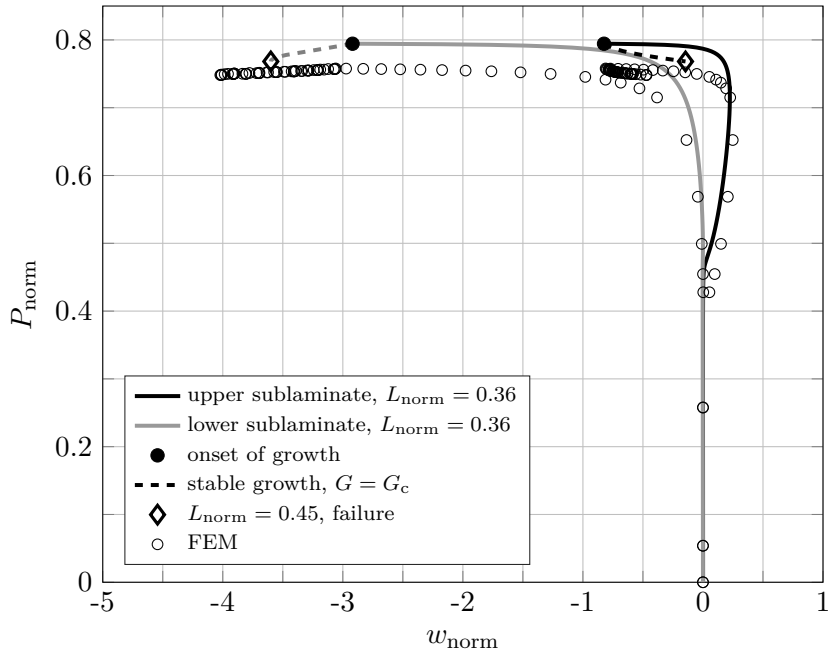

Fig. 3.19: Normalized load (P_{norm}) *vs.* normalized midpoint deflections (w_{norm}); initial delamination length $L_{\text{norm}} = 0.36$; delamination depth $a = 4/15$.

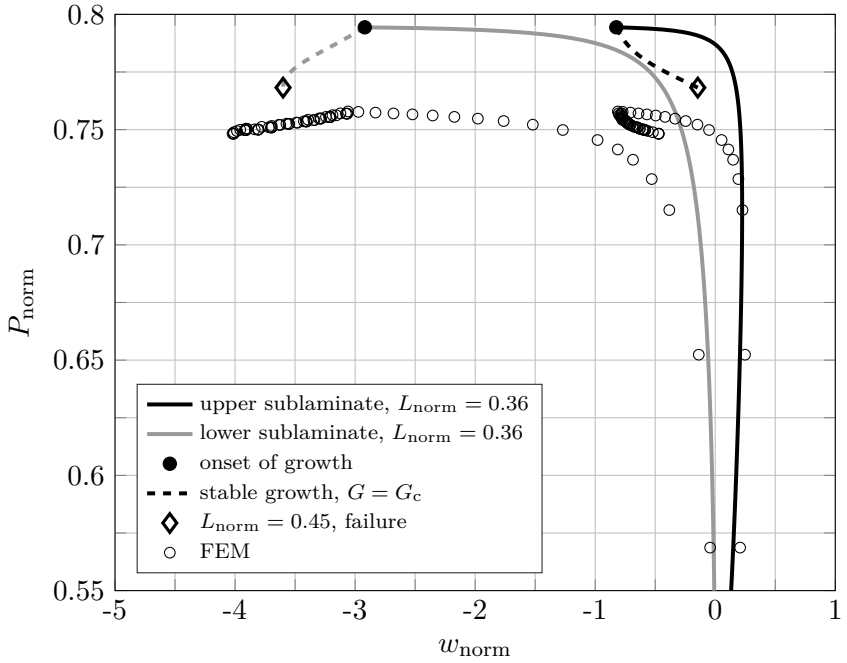

Fig. 3.20: Normalized load (P_{norm}) *vs.* normalized midpoint deflections (w_{norm}); initial delamination length $L_{\text{norm}} = 0.36$; delamination depth $a = 4/15$; closer look at the non-conservative part.

Fig. 3.19 shows a characteristic post-buckling response as long as the delamination does not grow (up to the symbol "•"). A local buckling response is shown at around $P_{\text{norm}} = 0.45$ where the upper delaminated part (thinner and less stiff than the lower part) buckles whereas the lower part stays unaffected. Once the global buckling response is triggered the lower sublaminate deflects in the negative direction causing an opening-mode buckling response. The global buckling response (buckling of the undelaminated and lower sublaminate) yields that the midpoint deflection of the upper sublaminate also shifts into the negative direction. However, the structure remains in an opening-mode response as the delamination opens further, *i.e.* both parts deflect in opposite directions with respect to each other, even though both parts show a negative deflection.

As documented in Fig. 3.19, the finite element simulation ("FEM" in Figs. 3.19 to 3.24) shows the same qualitative behaviour compared with the model whereas quantitatively the respective local buckling load as well as the global buckling differ by approximately 4%. This appears to be plausible since the model does not incorporate out-of-plane shear deformations and neglects in-plane contributions from the undelaminated region.

A changeover in the buckling response can be seen once delamination growth occurs. This is illustrated in Fig. 3.20 which takes a closer look at the buckling response around the deformation state where delamination growth is caused ("•").

Fig. 3.20 shows that once the delamination grows both sublaminates deflect in opposite directions associated with a slightly decreasing load. The dashed line shows the deformation path as long as delamination growth is stable. At "⋄", the delamination reaches a length of $L_{\text{norm}} = 0.45$ at which unstable growth is triggered causing failure of the strut. The same qualitative behaviour is obtained by the finite element simulation with the load being approximately 4% smaller. The midpoint deflections at the onset of growth almost coincide and just minor deviations are shown during delamination growth.

Fig. 3.21 shows the post-buckling response in terms of the normalized compressive load (P_{norm}) *vs.* the normalized end-shortening ($\mathcal{E}_{\text{norm}}$). Initially, a typical "conservative" buckling response is shown where the post-buckling stiffness of the strut remains unaffected during local buckling and almost reaches zero at global buckling illustrating the characteristic weakly stable behaviour. However, in contrast to other (semi-)analytical models, the deformation behaviour is also determined once delamination growth occurs.

As predicted by Fig. 3.18, delamination growth is initiated at $\mathcal{E}_{\text{norm}} = 6.58$ indicated by "•" in Fig. 3.21. The dashed line following "•" describes stable damage growth as it was predicted by Fig 3.18. Once damage growth is caused a slight drop in load occurs. In the range from $\mathcal{E}_{\text{norm}} = 6.58$ (•) to $\mathcal{E}_{\text{norm}} = 9.72$ (⋄),

the strut loses approximately 3.3% of the maximum load. Up to an end-shortening of $\mathcal{E}_{\text{norm}} = 9.72$, corresponding to a delamination length of $L_{\text{norm}} = 0.45$, the delamination propagation is stable, *i.e.* the strut does not fail. However, at an end-shortening of $\mathcal{E}_{\text{norm}} = 9.72$ ($\diamond$) the delamination grows unstably. Thus, for this configuration, sudden failure of the strut occurs once end-shortening reaches $\mathcal{E}_{\text{norm}} = 9.72$ which may be understood as the "failure displacement" of the system (indicated by the vertical dot-dashed line in Figs. 3.21 and 3.22).

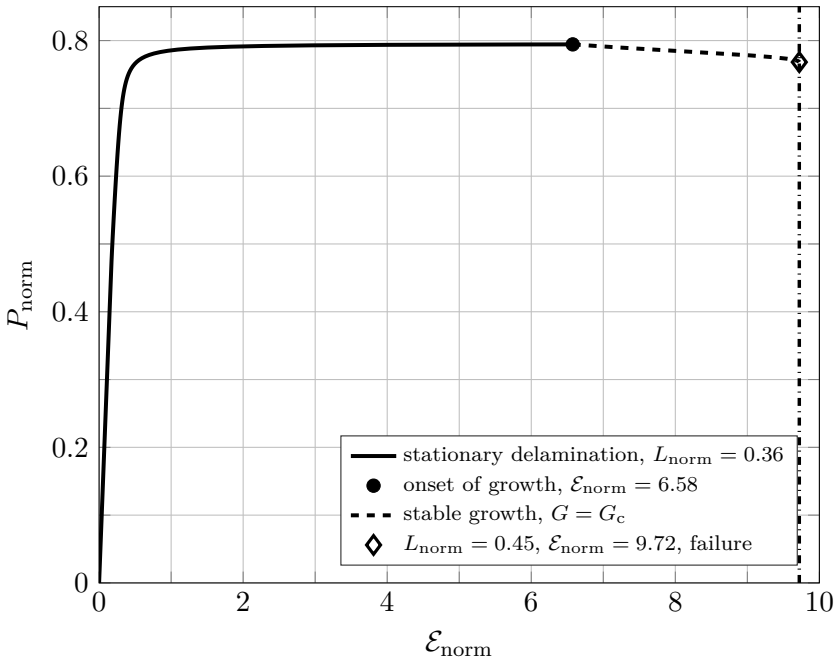

Fig. 3.21: Normalized load (P_{norm}) *vs.* normalized end-shortening ($\mathcal{E}_{\text{norm}}$); initial delamination length $L_{\text{norm}} = 0.36$; delamination depth $a = 4/15$.

Regarding the stability analysis, the initiation of delamination growth is important. For a load-controlled problem, "$\bullet$" exhibits a limit point from which the system will lose its stability causing a dynamic snap and thus stability failure. If the problem is displacement-controlled (end-shortening), the loss of structural stability coincides with the initiation of unstable delamination growth at "$\diamond$".

In order to enable a comparison with the finite element simulation, the axial shortening of the undelaminated part of the strut (not considered in the model description) has to be considered. This is done in Fig. 3.22, in which the axial shortening corresponding to the compressive load is added by means of a pure squashing contribution, such that the total end-shortening of the strut is increased in comparison with Fig. 3.21.

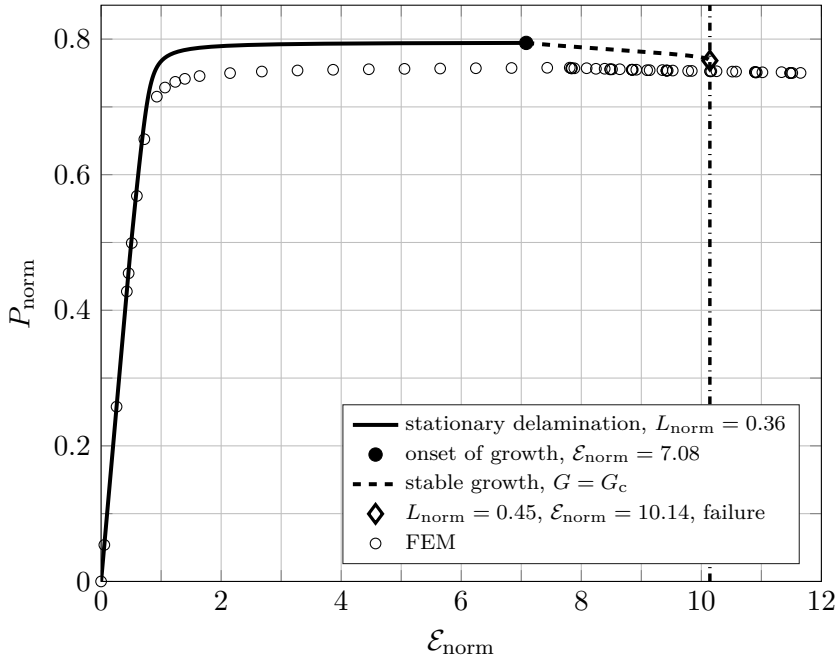

Fig. 3.22: Normalized load (P_{norm}) *vs.* normalized end-shortening ($\mathcal{E}_{\text{norm}}$); initial delamination length $L_{\text{norm}} = 0.36$; delamination depth $a = 4/15$; shortening of undelaminated part considered.

Despite the rough consideration of the axial shortening of the undelaminated part, Fig. 3.22 shows good agreement. The results coincide for the fundamental path and for the local buckling response. The global buckling response is initiated at a slightly smaller load in the finite element simulation and the subsequent path, as mentioned before, deviates by approximately 4%. The deviations between the finite element simulation and the results obtained for the onset of delamination growth and the prediction of the material failure (unstable growth) in terms of end-shortening are 8.5% and 12% respectively.

The second case of a delaminated strut—larger initial delamination length ($L_{\text{norm}} = 0.67$) but the same depth ($a = 4/15$)—is studied in Figs. 3.23 and 3.24. From the behaviour of the energy release rate shown in Fig. 3.18 follows that once growth is initiated, it is unstable for such a configuration. However, interestingly Fig. 3.18 also depicts that such growth would stop at a larger delamination length and henceforth proceed in a stable regime (this is similar to the case shown for $\mathcal{E}_{\text{norm}} = 6.58$ in Fig. 3.18 at $L_{\text{norm}} = 0.58$). Thus, contrary to the previously discussed case, post-critical behaviour causing initially unstable delamination growth but no complete failure is documented in Figs. 3.23 and 3.24.

Fig. 3.23 shows the normalized compressive load (P_{norm}) against the normalized end-shortening ($\mathcal{E}_{\text{norm}}$). As before, the symbol "•" indicates where delamination growth occurs, *i.e.* at $\mathcal{E}_{\text{norm}} = 5.95$. As discussed, unstable delamination growth

is caused at "•". This is associated with a sudden increase in delamination from $L_{\text{norm}} = 0.67$ to 0.77 and a drop in load of approximately 12% which is indicated by the vertical dotted line from "•" to "□" in Fig. 3.23. The model provides the solution for the condition $G = G_{\text{c}}$ (dashed line in Fig. 3.23) which is violated for unstable growth. Thus, the structure would follow the vertical dotted line and would not undergo the snap-back response indicated in Fig. 3.23. At "□", growth would follow a stable regime (corresponding to increasing end-shortening) up to the symbol "◇" which is illustrated by the dashed line. At "◇", the delaminated parts of the strut are completely separated.

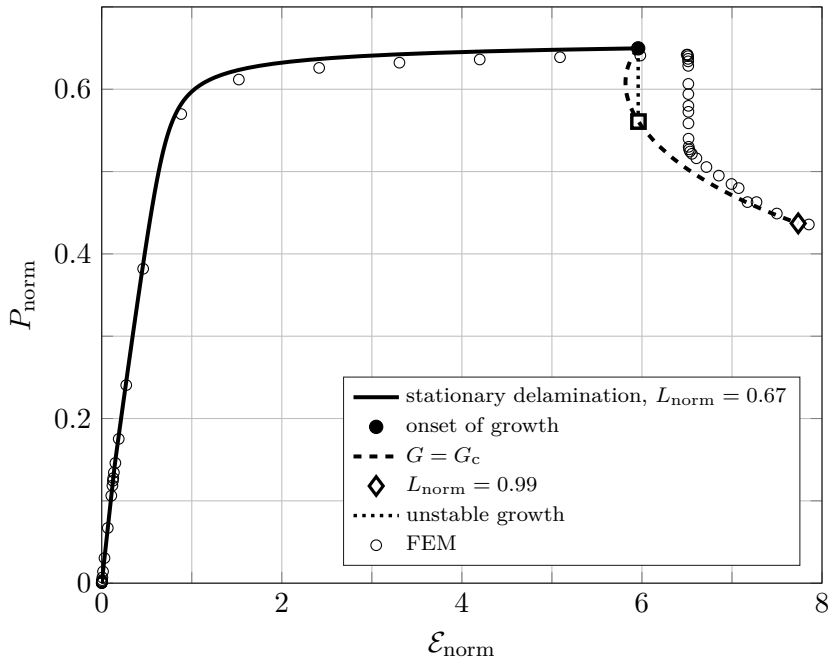

Fig. 3.23: Normalized load (P_{norm}) *vs.* normalized end-shortening ($\mathcal{E}_{\text{norm}}$); initial delamination length $L_{\text{norm}} = 0.67$; delamination depth $a = 4/15$.

The results obtained by the analytical model are in very good agreement with the findings from the finite element simulation. Minor deviations in load of approximately 1% are documented. The end-shortening at which growth occurs shows slight differences between the models. However, the characteristic drop in load is also illustrated by the finite element simulation and the points of complete separation almost coincide.

In a load-controlled configuration, "•" would correspond to the failure load of the system causing stability failure. The deformation path shown in Fig. 3.23 could be followed in a displacement-controlled setup. However, regarding the quasi-brittle damage behaviour assumed and present in such composites, the system would most likely not recover to a stable regime once unstable growth is initiated.

The corresponding load against midpoint deflection behaviour is shown in Fig. 3.24. The local buckling as well as the global buckling response are in very good agreement with the findings from the finite element simulation. The larger delamination length almost diminishes the shear deformation effects which are not considered in the model description. In contrast with Figs. 3.19 and 3.20, both sublaminates deflect in opposite directions, without that the undelaminated part pulls both sublaminates into the negative direction. The deflection at which growth occurs ("•") as well as the point of complete separation ("◇") almost coincide between the analytical model and the finite element simulation.

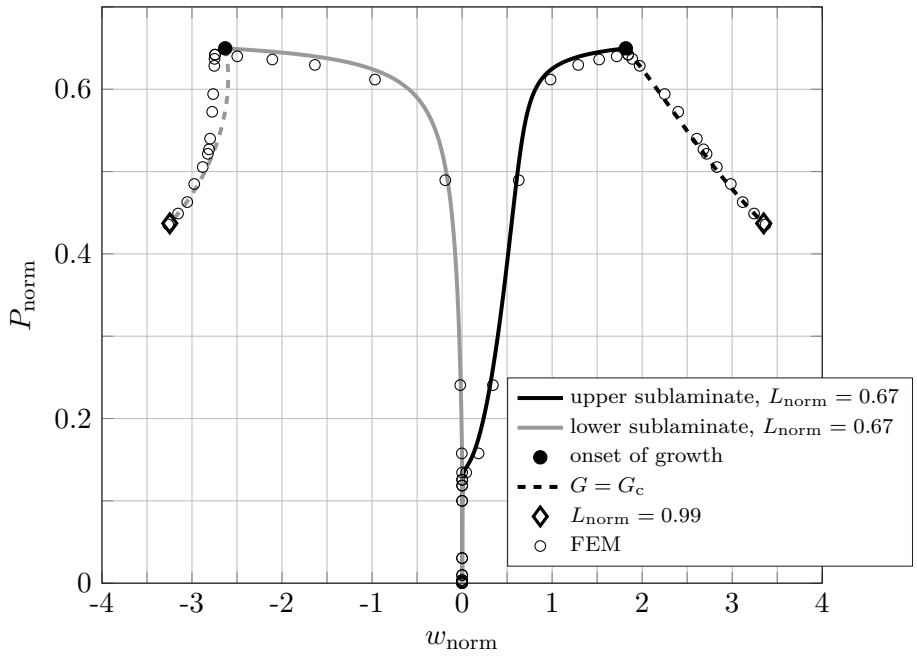

Fig. 3.24: Normalized load (P_{norm}) *vs.* normalized midpoint deflections (w_{norm}); initial delamination length $L_{\text{norm}} = 0.67$; delamination depth $a = 4/15$.

3.4.3.3 Discussion of the results

The model used to describe the buckling and post-buckling phenomena by means of four generalized coordinates incorporates several simplifying assumptions such as omitting out-of-plane shear deformations and the in-plane stiffness of the undelaminated part. Such simplifications affect more the response of struts with smaller delamination lengths (Figs. 3.19 to 3.22) than with larger delamination lengths (Figs. 3.23 and 3.24). This appears plausible and was expected due to the larger length-to-thickness ratio of the respective delaminated parts. In spite of these simplifications, the results provided in Section 3.4.3 are in very good agreement with findings from finite element simulations.

In Figs. 3.22 and 3.23, the corresponding in-plane displacement of the undelaminated part has been added to the solution in order to enable the comparison with the finite element simulation. This should be regarded as a rough approximation of the in-plane stretching contribution of the undelaminated part. Furthermore, it can be expected that this is a more precise approximation for smaller lengths of the undelaminated part (Fig. 3.23) than for larger lengths (Fig. 3.22).

As described in Section 3.4.3.1, mode mixture is not considered and the critical energy release rate of mode I is taken as G_c. However, for "deep" delaminations mode I is dominant, for which the simplification of $G_c = G_c^I$ in the cases studied is an acceptable choice.

The results presented indicate that delamination growth in delaminated composite struts occurs once global buckling is triggered. However, the deformation state where growth is initiated strongly depends on the material parameter G_c.

Regarding the stability of the post-buckling response, the results provided in Section 3.4.3 depict that delamination growth in delaminated composite struts is associated with a decrease in load, so that the deformation state causing growth is also a limit point in a load-controlled configuration (prescribed forces) yielding stability failure of the strut.

Such post-buckling paths are traceable in a displacement-controlled configuration (prescribed end-shortening), so that additional load bearing capacities of the systems are present and documented by the application of the framework. Material failure characterized by unstable delamination growth can also be directly derived from the results as it is associated with a loss in stability in a displacement-controlled system. Thus, with the aid of the post-buckling paths as well as the behaviour of the energy release rate (Fig. 3.18), besides the post-buckling behaviour, damage growth and failure characteristics (stability and/or material failure) can be examined for a given delaminated strut.

Even if not specifically investigated within the current work, savings of computational cost are tremendous using the framework. The commercial finite element code (specifically in the damaging process) requires hours for solving the given problem (Intel® i7, 3.4 GHz 16 GB RAM), whereas the implementation of the framework solves the four degree of freedom model within a few minutes.

3.5 Concluding remarks

3.5.1 Stationary delaminations

The post-buckling analysis for stationary delaminations presented in Section 3.4.2 shows that the model description developed in Section 3.3 provides an efficient approach to obtain detailed information about the critical and post-critical

behaviour of delaminated composite struts under the assumption of stationary delaminations.

This has been achieved by employing four generalized coordinates where the end-shortening of the delaminated part (q_4) describes a passive coordinate, such that it could be replaced for the case of stationary delaminations. As an outcome, the (post-)buckling response is obtained by solving a set of just three non-linear algebraic equations. The small number of generalized coordinates enables a highly efficient analysis of the influence of delaminations on the (post-)buckling behaviour of composite struts which, except [30] for isotropic material behaviour, has not been done in the proposed manner yet. Therefore, the modelling of the stationary case may be regarded as an extension of the study in [30] to multi-layered composite struts with transversally isotropic material behaviour. Furthermore, in contrast with [30], another approach regarding the displacement functions as part of the Rayleigh–Ritz formulation has been employed.

The model allows for arbitrary delamination lengths and depths which guarantees an applicability to arbitrary types of laminates (*e.g.* symmetric or asymmetric). The description of the post-buckling behaviour by means of a one-dimensional formulation simplifies the calculation but is regarded as sufficient as well as expedient since it may be argued whether a two-dimensional formulation of the problem provides further insight.

3.5.2 Non-stationary delaminations

The novel analytical framework comprising the extended total potential energy principle has been successfully applied to the problem of a composite strut with a through-the-width delamination under a compressive in-plane load.

Post-buckling responses with delamination growth have been modelled using four generalized coordinates only. Hence, the deformation behaviour, the stability analysis and the damage propagation have been determined by solving a set of just four non-linear algebraic equations. This has provided insight into the initiation of delamination growth, the structural stability during growth and the possibility of stable and unstable delamination growth. Deformation paths for an entire loading process (stationary and non-stationary delaminations up to failure) have been compared with finite element simulations. The results are in very good agreement and the quantitative differences obtained (up to 4%) are directly linked to the simplifications made in the model description of the composite strut.

For composite struts, thus far such information is not provided by semi-analytical models. Moreover, with the results obtained in the current chapter, for all configurations of delaminations, *i.e.* small, mid-size and large delaminations (following the classification introduced in Section 3.2), the structural stability

behaviour can be described and the type of failure can be predicted.

Concluding, employing the framework with just a few generalized coordinates allows for fast solutions with demonstrably good accuracy, while demanding low computational cost. This indicates the capability of the framework developed in this work. The model description of a delaminated composite strut comprising the analytical framework developed in Chapter 2 embodies an engineering tool which can be used to predict the deformation behaviour of such structures considering structural stability and damage mechanics phenomena. As a consequence, the current structural stability analysis contributes to a better understanding of the post-buckling behaviour of delaminated struts.

With the structural stability behaviour of delaminated composite struts being determined, the next chapter is concerned with an extension of the problem to delaminated multi-layered composite plates with embedded delaminations.

4 Non-linear buckling of a composite plate with an embedded delamination

The problem of a composite plate with an embedded delamination under compressive in-plane loading is studied in this chapter. It embodies an extension to the problem investigated in Chapter 3 towards a wider range of applications. In contrast to composite struts with a through-the-width delamination, growth of embedded delaminations in plates is not necessarily, at first, associated with decreasing loads bearable by the system and thus stability failure under prescribed forces. This might give rise to wrong conclusions of safe post-buckling responses, whereas damage growth can be already present potentially yielding unexpected and sudden failure of the structure. This underlines further the need for efficient modelling approaches describing the post-buckling behaviour considering delamination growth. In the current chapter, characteristic post-buckling responses of elliptically delaminated composite plates considering delamination growth are modelled providing insight into the structural stability behaviour, additional load bearing capabilities as well as the material failure behaviour. On the other hand, unlike Chapter 3, a general analysis of the post-buckling behaviour of delaminated plates is not intended.

Composite plates with embedded delaminations have been the subject of investigation of various studies whereof just a few employ semi-analytical modelling approaches. Furthermore, such models are restricted to stationary delaminations and, in most cases, consider local buckling responses only.

In the current chapter, besides the modelling of post-buckling responses by applying the analytical framework developed in this work, the general issue regarding the semi-analytical modelling of such a geometrically more complex application example is addressed. Therefore, two modelling approaches are analysed and the amount of generalized coordinates required to describe the deformation behaviour efficiently is determined.

The chapter commences in Section 4.1 with a brief review regarding general phenomena of the (post-)buckling behaviour of plates. This is followed by an overview of the state of research (Section 4.2) regarding the post-buckling be-

haviour of delaminated composite plates considering delamination growth. The semi-analytical model is presented in Section 4.3 which contains three parts. First, two modelling approaches considered for determining the post-buckling responses are reviewed and compared. Then, the model description is presented followed by the energy formulation used to determine the post-buckling responses for the case of stationary and non-stationary delaminations. In Section 4.4, results of non-linear buckling responses are presented. The chapter closes with concluding remarks regarding the phenomena observed and the application of the framework to the given problem.

4.1 General buckling and post-buckling phenomena of plates

An illustration of the problem of plates under in-plane compressive loading is shown in Fig. 4.1. For illustration purposes, Fig. 4.1 only depicts compressive loading along the x-axis as well as the case of simply-supported boundaries.[1] As often used to describe the two-dimensional plate problem (*cf.* [96]), the force resultants[2] in the x-direction n_{xx} and the corresponding displacements u_0 are provided in Fig. 4.1 in addition to the quantities introduced in the previous chapters: compressive force P and end-shortening $\mathcal{E}$.

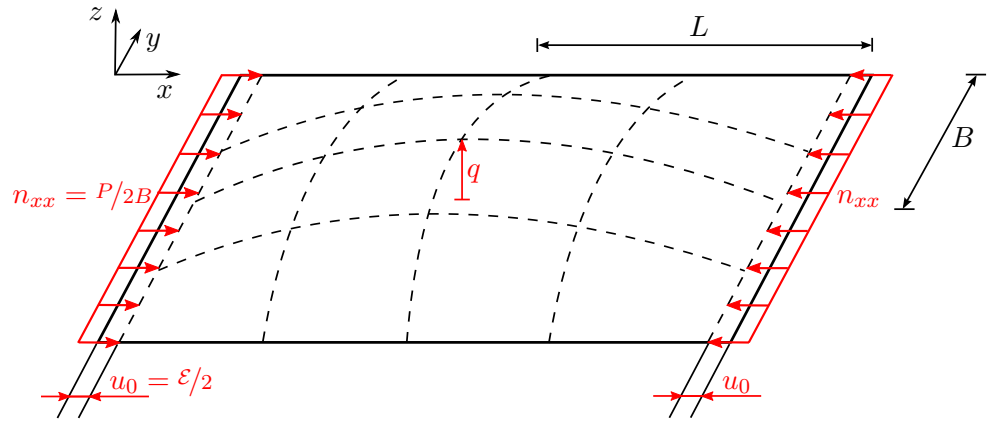

Fig. 4.1: Illustration of a plate subjected to in-plane compressive loading (n_{xx}).

As in Chapter 3, all physical quantities used for the structural stability analysis are highlighted in red in Fig. 4.1. The buckling displacement is sketched by the dashed lines. It should be noted that such a response refers to plates with similar

[1] The case of restrained edges is illustrated in Fig. 4.1, *i.e.* the boundaries are capable of withstanding in-plane forces, thus no transverse in-plane displacements occur at the longitudinal boundaries (along the x-axis in Fig. 4.1).
[2] The unit of the force resultants is N/m.

dimensions in length ($2L$) and width ($2B$), which are considered in this chapter. The out-of-plane displacement of the plate may be adequately described by a single generalized coordinate q representing the amplitude of the buckling displacement. As will be discussed in Section 4.3.1, in contrast to the strut, further generalized coordinates are usually required to describe the in-plane displacements of the plate, so that the post-buckling behaviour can be appropriately determined. Such additional generalized coordinates are omitted in Fig. 4.1.

The linear and non-linear buckling response of a plate is summarized in Fig. 4.2 with the aid of two plots showing the behaviour of the compressive load against the amplitude of the out-of-plane displacement (Fig. 4.2a) and the compressive load against the end-shortening of the plate (Fig. 4.2b). Besides the illustration of the general phenomena of plate buckling, this also serves to underline the differences in the post-buckling responses between struts (*cf.* Fig. 3.3 in Section 3.1) and plates.

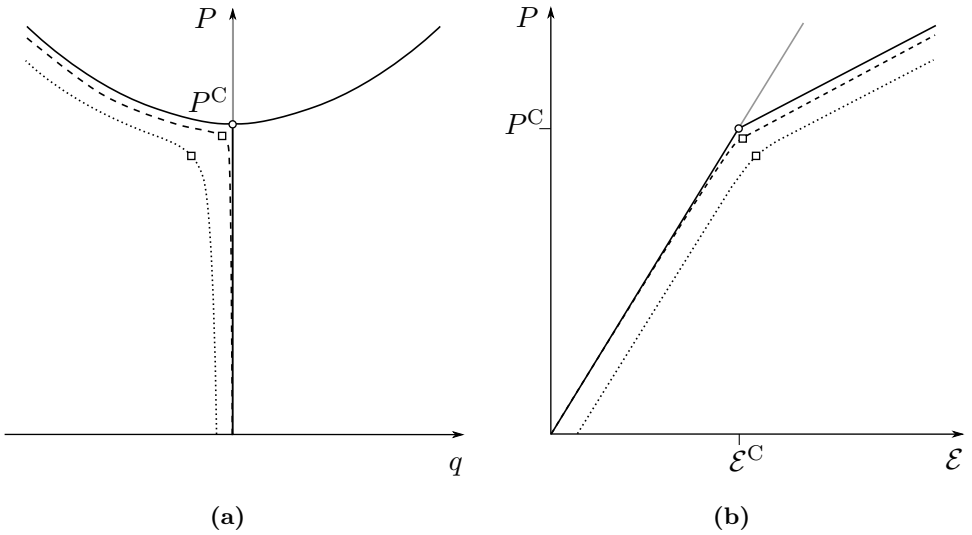

Fig. 4.2: Linear and non-linear buckling response of a plate; **(a)** compressive load (P) against out-of-plane deflection amplitude (q); **(b)** compressive load (P) against end-shortening ($\mathcal{E}$).

As in Chapter 3 for struts, Figs. 4.2a and 4.2b display deformation paths for an ideal plate (solid lines), plates with stretching–bending coupling (material imperfection, dashed lines) and the (post-)buckling response when geometric imperfections, such as an initial out-of-plane deflection, are present (dotted lines).

The buckling loads (P^{C}) for the ideal case can be determined analytically for homogeneous isotropic and specifically laid-up orthotropic laminates[3] by solving the equation of motion governing the buckling deflection and omitting non-linear

[3] A detailed overview of the respective laminates is given in [76].

terms (*e.g.* Navier and Lévy method [76, 96]) or by approximate methods (*e.g.* Ritz and Galerkin method [76, 96]).

The fundamental path of the ideal plate ($q = 0$ in Fig. 4.2a) loses its stability at the buckling load (indicated in Fig. 4.2 by the grey lines) forcing the plate to undergo out-of-plane deflections following either of the branches shown in Fig. 4.2a. As for struts, the critical deformation state describes a stable bifurcation point. However, this distinct critical point does not exist once imperfections are present. The influence of the imperfections on the critical behaviour is alike the buckling of struts, as described in Section 3.1, and is therefore not elucidated again.

Unlike struts, plates exhibit a considerably large post-buckling stiffness and are able to withstand loads far beyond the critical limit (neglecting material failure). This can be seen in Fig. 4.2b following the buckling load. How much compressive stiffness is retained depends strongly on the boundary conditions. In the present work, plates are considered which are supported along all edges. For such systems, a plate with all sides being simply-supported in such a manner that in-plane displacements at the boundaries along the longitudinal axis (x-axis in Fig. 4.1) are not restrained exhibit the lowest post-buckling stiffness of 0.408 times the original compressive stiffness (of the fundamental path) [46, 95].

The post-buckling stiffness is, in general, not affected by imperfections as illustrated in Fig. 4.2b, such that imperfect systems may also be loaded beyond the buckling load. The qualitative post-buckling behaviour of the plates with imperfections remains unaffected, thus the corresponding post-buckling paths more or less converge onto to the response of an ideal plate depending on the type of imperfection (material or geometric) and its extent.

4.2 State of research

Owing to the evident similarities with the problem studied in Chapter 3 as well as the objective of the current chapter, *viz.* the modelling of characteristic post-buckling responses of multi-layered delaminated composite plates without the restriction to stationary delaminations, the subsequent review of the state-of-the-art comprises only

- the post-critical behaviour considering delamination growth and
- the delamination growth characteristics.

The linear buckling behaviour remains qualitatively similar to the problem of delaminated struts, so that the buckling loads may also be represented by Fig. 3.4 in Chapter 3 in which the delamination length is replaced by the delamination area for distinct aspect ratios between delamination length and width. The

post-buckling behaviour also exhibits the characteristic opening and closing-mode responses depending on the delamination depth, shape and size. Such information can be found, for instance, in [15, 26, 43, 44, 56, 59] for the critical behaviour and in [44, 67, 71, 110, 111] for the post-critical behaviour.

Since the delamination shape embodies a new parameter to be considered when studying embedded delaminations, Table 4.1 classifies studies referring to the aforementioned criteria for rectangular, elliptical and circular delaminations.

Shape	**Post-buckling**	**Energy release rate**
rectangle	[26, 27, 98, 102]	[2]
ellipse	[92]	[9, 41, 45, 73, 108, 110, 111]
circle	[1, 52, 68, 69, 70]	[2, 6, 7, 45, 52, 68, 69, 70, 73] [77, 108, 110, 111]

Table 4.1: Overview of the studies investigating the post-buckling responses during delamination growth and/or the behaviour of the energy release rate.

As illustrated in Table 4.1, the majority of studies investigate circular and elliptical delaminations, whereby the case of circular delaminations can also be regarded as a special case of the elliptical delaminations. However, only [92] provides post-critical responses during delamination growth for elliptical delaminations. The experimental study in [11] has demonstrated that elliptical delaminations are caused by transverse impact scenarios in which a circular delamination is initially generated which grows during the impact into an elliptical shape. Similar reasoning is not provided for the case of rectangular delaminations.[4] Subsequently, with the aid of the references in Table 4.1 the aforementioned criteria are reviewed.

4.2.1 Post-critical behaviour considering delamination growth

To the author's knowledge, Refs. [98, 102] comprise the only semi-analytical modelling approach aiming at post-buckling paths during delamination growth. In these studies, post-buckling responses for the case of stationary delaminations (no growth is allowed) and non-stationary delaminations are determined with the aid of a Rayleigh–Ritz formulation in which the out-of-plane displacement is approximated by trigonometric functions. The non-linear strains generated during post-buckling are considered by Airy stress functions for the respective

[4] An example for rectangular delaminations could be sensors inserted in between layers of composite plates. Furthermore, delaminations could be defects caused during the manufacturing process. Such delaminations would also more likely fit an elliptical shape rather than a rectangular shape.

parts of the plate. Growth is assumed to occur uniformly in width and length direction and is modelled by a discrete cohesive zone method assuming spring elements along the plane of the delamination yielding an iterative solving scheme for each segment of springs. Comparisons with solutions suppressing growth show that delamination growth is generated during the initial post-buckling response and yields large deviations compared with the stationary solution regarding the load bearing capacities. Furthermore, for the cases presented, initially unstable post-buckling responses are associated with delamination growth.

Except [98, 102], post-critical responses comprising delamination growth are solely modelled by comprehensive finite element simulations. The majority of studies consider circular delaminations [1, 52, 68, 69, 70, 78, 81, 92]. Elliptical delaminations with aspect ratios of 0.5 and 2 are studied in [92].[5] Rectangular delaminations are investigated in [26, 27].

All aforementioned studies, with the exception of [1] for circular, [92] for elliptical and [26, 27] for rectangular delaminations, investigate plates with clamped boundary conditions on two opposite sides and free conditions on the remaining sides (subsequently referred to as CFCF). Thus, the post-buckling responses documented are very similar to the behaviour of struts, *i.e.* weakly stable behaviour once global buckling is caused (see for instance the behaviour of stationary delaminations in Figs. 3.19 and 3.21 in Chapter 3).

Refs. [69, 70] show that delamination growth for CFCF plates is strongly related with the initiation of the global buckling response. Loads causing growth are almost equal to the maximum load bearable by the system. On the other hand, in contrast with the results provided in Chapter 3, initial growth of embedded delaminations does not necessarily cause decreasing loads, so that the system remains in a stable deformation process. Findings documented in [68, 69, 70] for cross-ply laminates ($[90°/0°/90°]_{16}$ in [68] and $[(90°/0°)_{17}/90°]$ in [69]) and quasi-isotropic laminates ($[90°/\mp 45°/0°_2/\pm 45°/90°/0°/\pm 45°/90°_2/\mp 45°/0°]_2$ in [70]) are verified by comparisons with experimental work. Teflon films with a normalized radius of 0.4 (with respect to the total width and length of the plate) were inserted in between two layers to manufacture the desired delaminations. Very good agreement was obtained for the post-buckling responses and the onset of delamination growth.

Post-buckling responses of CFCF plates exhibiting unstable behaviour are presented in [81] (delamination radius of 0.3) considering local buckling responses only. However, as described in [69] by comparing local and global buckling responses, significantly higher loads than the global buckling load are required to cause

[5] Regarding elliptical delaminations, the aspect ratio describes the ratio of the lengths of the major and minor axis of the ellipse.

delamination growth if the modelling is limited to local responses. The possibility of unstable delamination growth is also documented in [70] once growth reaches a certain extent. Such behaviour was observed for a delamination depth of 0.28 (normalized with respect to the overall height). In general, delamination depths of 0.09 to 0.33 are investigated. Except [81], stable post-buckling responses are documented for depths up to 0.2. Post-buckling responses for deeper delaminations are limited to the case of 0.28 in [70] and 0.33 in an experimental study of fatigue loading in [52].

As mentioned before, the post-buckling behaviour of delaminated composite plates with all boundaries constrained in their out-of-plane displacement is limited to the work in [1, 26, 27, 92] performing finite element simulations of fully clamped (CCCC) uniaxial loaded plates with restrained edges[6] in [1, 92] and unrestrained edges[7] in [26, 27]. Ref. [92] also provides results for plates with all boundaries being simply supported (SSSS) and Ref. [1] provides findings from an experimental study. For these plates, in contrast with the CFCF plates, a large ratio of its compressive stiffness is retained in the post-buckling range, as described in Section 4.1 and illustrated in Fig. 4.2.

The plate configurations used in studies investigating delaminated composite plates in which the out-of-plane displacement at the boundaries is constrained are summarized in Table 4.2.

Mainly cross-ply laminates are investigated. The length-to-thickness ratio of the plates ranges from 25 to 42. The ratio of the thickness of the delaminated part to the overall thickness of the plate is, in all cases, smaller than 0.25 (this ratio is often considered as a parameter describing the delamination depth).

Results are presented in [1, 26, 27] in terms of compressive force against end-shortening and in [92] in terms of applied strain against midpoint deflection. Refs. [26, 27] also provide information in terms of compressive force against midpoint deflection.

[6] Restrained edges refer to boundaries at which in-plane displacements transverse to the boundary are suppressed.

[7] Unrestrained edges refer to boundaries at which in-plane displacements transverse to the boundary are enabled (the edges are not required to remain straight).

Ref.	Layup	Dim. [mm]	BC	DS	DC [mm]
[1]	UD-1	150 × 100 × 4	CCCC-1	circle (radius, r)	$t_\mathrm{d} \approx 0.56$ $r = 20$
	CP-1				
	AB-1				
[26]	CP-2	24 × 24 × 0.8	CCCC-2	rectangle (square) ($l \times l$)	$t_\mathrm{d} = 0.2$ $l = 10$
	CP-3				
	CP-4				
	CP-5	100 × 100 × 2.4			$t_\mathrm{d} = 0.2$ $l = \{20, 40, 70\}$
[27]	UD-2 AB-2	60 × 40 × 1.6	CCCC-2	rectangle ($l \times b$)	$t_\mathrm{d} = 0.2$ $l = 20, b = 10$
[92]	CP-6	100 × 100 × 4.06	CCCC-1	ellipse ($l \times b$)[8]	$t_\mathrm{d} \approx 0.5$ $l = \{15, 30\}$ $b = \{15, 30\}$
			SSSS-1		

Table 4.2: Summary of composite plates and their delamination configurations investigated in the literature; Layup: (UD – unidirectional, CP – cross-ply, AB – balanced angle ply): UD-1: $[0°]_{28}$, UD-2 $[0°]_{16}$, CP-1: $[0°_4/90°_{10}]_\mathrm{s}$, CP-2: $[90°_2/0°_2/0°_2/90°_2]_\mathrm{s}$, CP-3: $[0°_2/90°_2/90°_2/0°_2]_\mathrm{s}$, CP-4: $[0°/90°/90°/0°]_\mathrm{s}$, CP-5: $[0°_3/90°_3/90°_3/0°_3]_\mathrm{s}$, CP-6: $[0°_2/90°_2]_{4\mathrm{s}}$, AB-1: $[\pm 45°/\mp 45°/90°_{10}]_\mathrm{s}$ AB-2 $[0°/-45°/45°_2/-45°/90°/0°_2]_\mathrm{s}$; Dim. – Dimensions: $2L \times 2B \times t$, *cf.* Fig. 4.1; BC – boundary conditions: CCCC-1 – clamped boundaries, restrained edges, CCCC-2 – clamped boundaries, unrestrained edges, SSSS-1 – simply supported boundaries, restrained edges, DS – delamination shape, DC – delamination configuration: t_d – depth of delamination and r – radius.

Findings of the studies can be summarized as follows:

- all post-buckling responses before delamination growth is caused are stable,[9]
- the deformation state at which growth is initiated depends on the layup and the delamination depth and size,
  - after global buckling (unidirectional layup in [1]),
  - with global buckling (cross-ply layup in [1]),
  - after local buckling, before global buckling (angle-balanced layup in [1] and cross-ply layup in [92] for all sizes and aspect ratios considered),

[8] The parameters l and b describe the semi major and semi minor axis respectively, *cf.* Fig. 4.3.
[9] This is confirmed by studies investigating post-buckling responses for stationary delaminations such as [44, 52, 71].

- stable and unstable deformation processes under prescribed forces are documented for propagating delamination growth,
  - stable behaviour throughout the range of loads considered (unidirectional [1, 27] and balanced-angle layup in [1, 27] and cross-ply layup in [26, 92]),
  - changeover from stable to unstable after certain growth is generated (cross-ply layup in [1]),
- the initiation of unstable delamination growth is not documented.

4.2.2 Delamination growth characteristics

As for delaminated composite struts, the delamination growth characteristics comprise

- the behaviour of the physical quantity governing delamination growth, *i.e.* the energy release rate G, and thus
- whether delamination growth is stable or unstable.

Regarding semi-analytical modelling approaches, the work of Chai and Babcock [9] may be regarded as the foundation for most of the ensuing studies (*e.g.* see [6, 7, 9, 73, 77, 110, 111]). In all modelling approaches, the delamination area is described by the axes of the ellipse (circle), such that growth can be modelled in two directions, as visualized in Fig. 4.3.

All studies implement a Rayleigh–Ritz formulation and, except [41], determine the energy release rate by differentiating the total potential energy with respect to the delamination area for growth along either axis of the ellipse.[10] Furthermore, the thin-film buckling assumption is employed in the modelling approaches.

In comparison with [9], the determination and analysis of the energy release rate remains unchanged, however, the ensuing studies implement more comprehensive approximations of the displacement field such as higher order displacement functions up to the seventh order [110] as well as shear deformations resulting in 56 degrees of freedom [73].[11]

The work in [6, 7, 77] employs main features of the one-dimensional model of Chai [10] in order to subdivide circular delaminations into finite strips, so that thresholds of applied strain causing delamination growth can be determined with the aid of a numerical software tool and a chosen stiffness reduction for the post-buckling regime.

[10] Ref. [41] determines delamination growth with the aid of the von Mises criterion by considering the resin in between the layers only.
[11] All studies apply polynomial displacement functions.

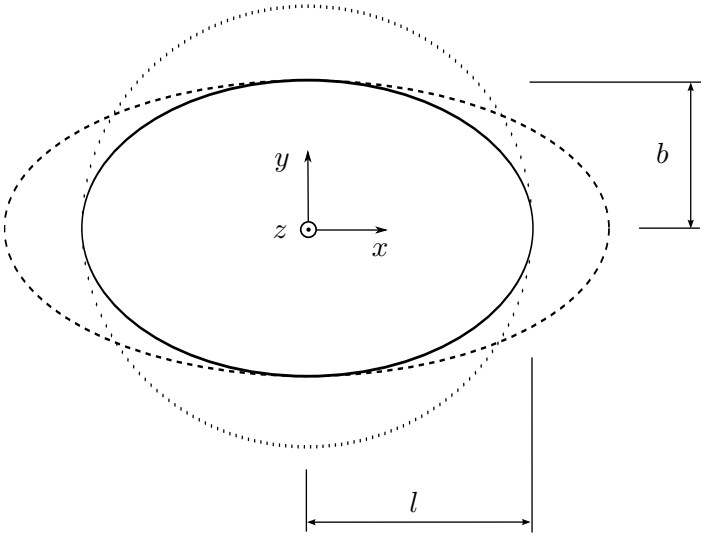

Fig. 4.3: Visualization of possible delamination growth incorporated in semi-analytical modelling approaches (x-y-plane is the plane of the plate); solid line – initial delamination, dashed line – growth along x-axis (l-direction), dotted line – growth along y-axis (b-direction).

A detailed analysis of the energy release rate can be found in [9] and in [110, 111], whereas comparisons with experimental tests regarding applied strains causing growth for multiple layups are provided in [6, 7, 77].

The behaviour of the energy release rate can be studied, as done for delaminated struts, by evaluation against the delamination area and the applied load. The behaviour against the applied load does not add insight in comparison with Fig. 3.6 in Chapter 3 and is therefore not reviewed further. The possibility of growth into two directions requires specific care when studying embedded delaminations. This is visualized in Fig. 4.4 by showing the energy release rate against the aspect ratio for certain magnitudes of applied strain which is adopted from [9].

Fig. 4.4 shows that the energy release rate governing growth in the width direction (G_b, solid lines) behaves similar to the energy release rate documented for delaminated struts (*cf.* Fig. 3.7). In contrast, the energy release rate for growth in the length direction (G_l, dashed lines) does not exhibit a peak value. Thus, for the aspect ratios considered in Fig. 4.4, growth in the length direction will be unstable. The peak values in the G_b-plots in Fig. 4.4 indicate the transition from unstable to stable delamination growth.

What kind of delamination growth is present depends on the critical threshold for growth which is not specifically indicated in [9]. The y-axis in Fig. 4.4 shows the energy release rate normalized against the critical energy release rate times a multiplier required to be determined for each case to be studied.[12] The results

[12] The multiplier used in [9] includes the length of the ellipse, the height of the plate, the critical energy release rate and the YOUNG's modulus in the loading direction.

shown in Fig. 4.4 apply to delaminations in a homogeneous isotropic plate which is also the case for most of the semi-analytical studies providing information in the form of Fig. 4.4.

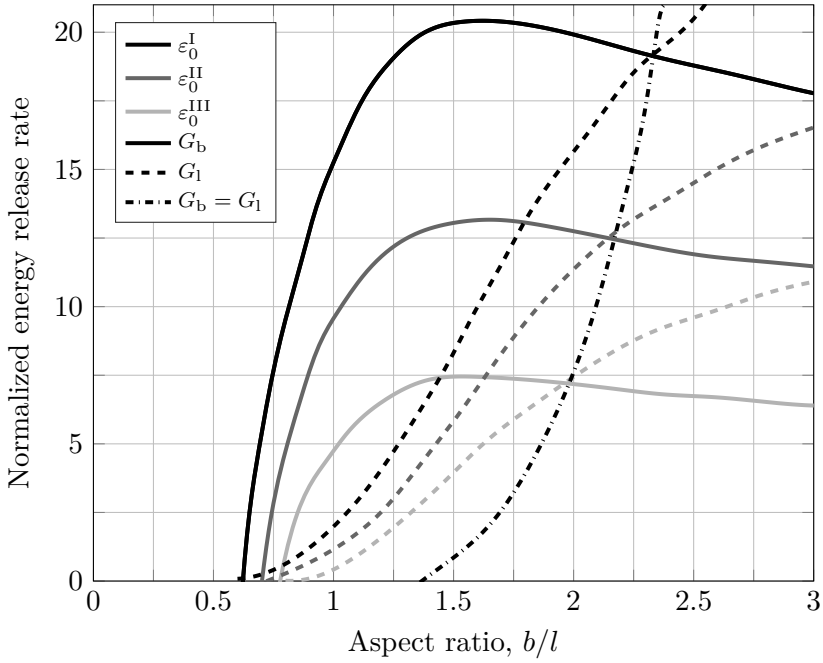

Fig. 4.4: Energy release rate against delamination aspect ratio for three distinct prescribed magnitudes of load in the form of applied strain with $\varepsilon_0^{\mathrm{I}} < \varepsilon_0^{\mathrm{II}} < \varepsilon_0^{\mathrm{III}}$; G_{b}, energy release rate for growth in width direction (solid lines); G_{l}, energy release rate for growth in length direction (dashed lines); $G_{\mathrm{b}} = G_{\mathrm{l}}$, energy release rate for simultaneous growth in both directions (dot-dashed line); in normalized quantities; adopted from [9].

It should be noted that Fig. 4.4 contains another plot showing the energy release rates where G_{b} equals G_{l} (dot-dashed line), *i.e.* for simultaneous growth in length and width direction. It follows that whenever a deformation state is reached for which this condition is fulfilled, growth will be unstable as the plot is strictly increasing for larger aspect ratios.

As aforementioned, insight into the behaviour of the energy release rate provided by semi-analytical modelling approaches is almost entirely bound to the work of Chai and Babcock [9]. Additional information is provided in [110, 111] determining the energy release rate in the form of Fig. 4.4 for the case of *local* growth, where local is to be understood as at a certain point of the boundary of the ellipse. Growth in transverse and longitudinal direction of the ellipse, *i.e.* at the vertices, is analysed. This was done with the aid of the *J integral* technique. Though, missing a direct comparison with the *global* growth behaviour (delamination growth defined by increasing length or width of the ellipse), Ref. [111] points out that partly significant deviations may be obtained in between both

methods.

As conducted in [111] for two points along the boundary of the delamination, studies implementing the finite element method (*e.g.* see [2, 45, 52, 68, 69, 70, 108]) provide detailed information about the energy release rate along the entire boundary of the embedded circular or elliptical delaminations.

Except in [108], where a three dimensional model is implemented, finite element simulations employ the Reissner–Mindlin plate theory or higher order shear deformation theories [2]. In most cases, delamination growth is modelled with the aid of a virtual crack closure technique (*e.g.* [2, 45, 52, 78, 108]). Refs. [68, 69, 70] determine the energy release rate using the energy momentum tensor.

Subsequently findings will be summarized with the aid of two figures showing the distribution of the energy release rate along the boundary of the delamination for a certain state of loading (Fig. 4.5) and during delamination growth for increasing magnitudes of applied strain (Fig. 4.6).

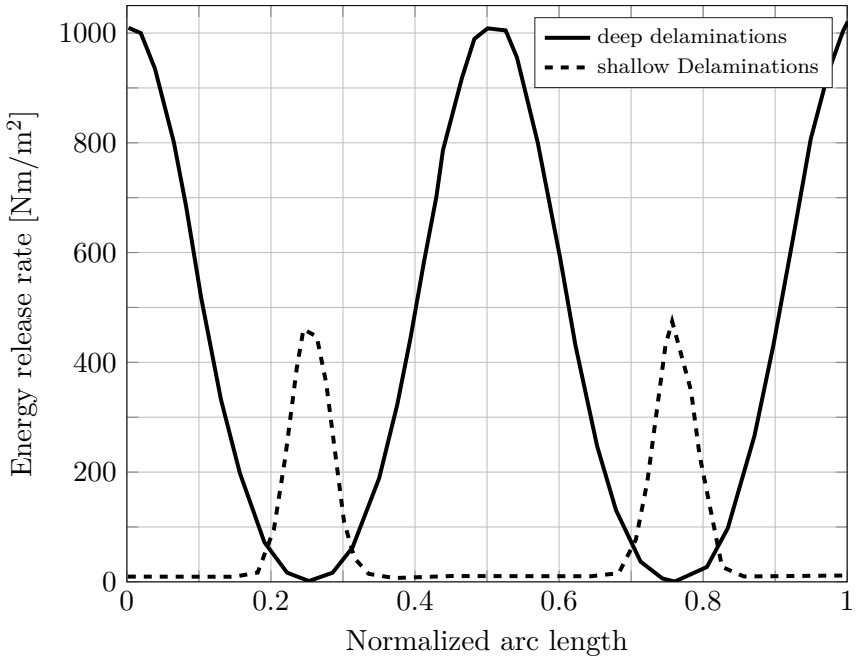

Fig. 4.5: Energy release rate against arc length of the boundary of the delamination for shallow and deep delaminations; x-axis normalized to the total length of the boundary; adopted from [70].

Fig. 4.5 shows the energy release rate along the boundary of a circular delamination of a uniaxially loaded CFCF plate with the layup $[90°/\mp 45°/0°_2/\pm 45°/90°/0°/\pm 45°/90°_2/\mp 45°/0°]_2$, in which the case of the deep delamination is associated with a normalized depth of 0.2812 (in between 0° and 45° layers) and the shallow delamination refers to a depth of 0.1562 (in between −45° and 90° layers). The arc length is normalized to the length of the

boundary of the delamination where 0 and 1 refer to the point $(l, 0)$ in Fig. 4.3.

It can be seen that growth occurs for the case of deep delaminations along the direction of loading and for shallow delaminations in the transverse direction. Furthermore, it is visualized that growth is initiated at the vertices of the circular delaminations (locally) and that the energy release rate diminishes along the rest of the boundary. However, in [70], the direction of growth is associated with the depth of delamination without considering further examples and examining the influence of the stacking sequence. In the cases provided in [70] and in Fig. 4.5, growth is also associated with 0° and 90° layers respectively.

In Fig. 4.6, the distribution of the energy release rate along the boundary of a circular delamination for increasing values of applied strain is delineated. A cross-ply laminate is investigated (layup of the sublaminate: $[0°/90°]_s$) and the thin-film buckling assumption is employed. Fig. 4.6 is included in this review since it provides important information regarding the applicability of the analytical framework developed in this work.

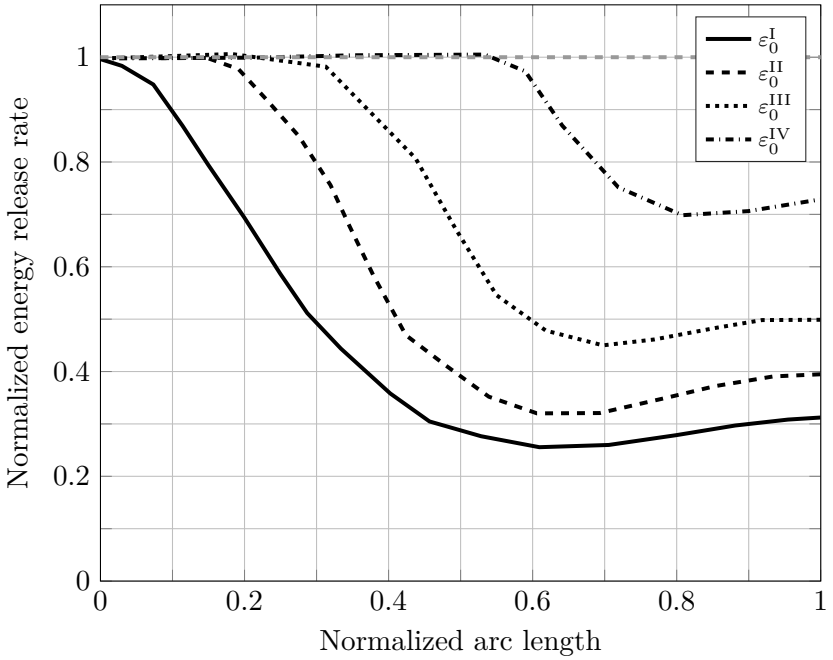

Fig. 4.6: Energy release rate against arc length of the boundary of the delamination for four distinct prescribed magnitudes of load in the form of applied strain with $\varepsilon_0^{\mathrm{I}} < \varepsilon_0^{\mathrm{II}} < \varepsilon_0^{\mathrm{III}} < \varepsilon_0^{\mathrm{IV}}$; in normalized quantities; adopted from [45].

Fig. 4.6 shows that growth is initiated at $\varepsilon_0^{\mathrm{I}}$ at an arc length of 0 which corresponds to the point $(0, b)$ in Fig. 4.3. In contrast with Fig. 4.5, the energy release rate is normalized against its critical magnitude and the arc length against the quarter of the length of the boundary using the symmetry of delamination growth, as also illustrated in Fig. 4.5. As can be seen in Fig. 4.6, further loading

in the form of increasing applied strains yields that growth proceeds along the boundary whereby the energy release rate remains at its critical value. Such behaviour proceeds for further loading as illustrated in Fig. 4.6 for the strains $\varepsilon_0^{\mathrm{III}}$ and $\varepsilon_0^{\mathrm{IV}}$.

It is also documented in [45] that once unstable growth is caused, this behaviour is violated and the energy release rate exceeds its critical value. Thus, in relation with the current work, the findings from [45], which may also be found in [69, 70], underline the applicability of the analytical framework, such that equality in between the energy release rate and its critical value holds during stable delamination growth.

4.2.3 Concluding remarks

The modelling of the post-buckling behaviour of multi-layered delaminated composites plates appears to constitute a mechanical problem which entails several difficulties when encountered by means of semi-analytical approaches. Such issues may be summarized as follows:

- an adequate description of the displacement field requires significantly more generalized coordinates than, for instance, the problem of a delaminated strut,
- the geometric description of the delamination area by global coordinates limits the modelling of the delamination growth characteristics[13] and
- the problem of mode mixture of the delamination growth would, in general, require both a detailed approximation of the displacement field and the evaluation of the energy release rate along the boundary.

On the other hand, as pointed out by [110, 111], computational cost is significantly lower for those modelling approaches in comparison with finite element simulations. However, the mandatory limitations are not addressed nor analysed with respect to qualitative and quantitative deviations, specifically regarding the behaviour of delamination growth. Furthermore, it may be argued whether model descriptions incorporating more than 300 degrees of freedom [71] (stationary delaminations investigated) still relate to the objective of semi-analytical formulations.

Regarding the mode decomposition of the energy release rate, studies in [34] and [35] provide characteristic equations describing the mode mixture for simplified cases of orthotropic bi-layered beams as well as the case of thin-film delamination

[13] It should be noted that growth is, in fact, not modelled by any semi-analytical approach considering circular or elliptical delaminations. To date, only the energy release rate is determined.

which may yield adequate approximations for the plate problem as stated in [70]. However, as described in [16, 84], in general, mode decomposition requires the consideration of shear deformation in the displacement field.

As aforementioned, to the author's knowledge, Refs. [98, 102] considering rectangular delaminations describe the only semi-analytical approach which models post-buckling responses for the case of non-stationary delaminations. However, the modelling approach is bound to isotropic material behaviour, simultaneous and uniform growth along the boundary of the delamination as well as an iterative solving scheme for discrete pre-determined changes in the delamination area. In [98], a pilot study is included investigating non-simultaneous delamination growth in the longitudinal and the transverse direction to the applied loading.

In general, information is sparse regarding delaminated plates being constrained in the out-of-plane displacement along all sides of the boundary. However, as stated in Section 4.2.1, such boundary conditions cause the characteristic post-buckling behaviour of plates in which a significant amount of the compressive stiffness is retained in the post-buckling regime. Especially when considering delamination growth for such plates (CCCC), the system's response may change from thoroughly stable to unstable and consequently unexpected failure, which has not been investigated thus far.

The literature review revealed that a lack of semi-analytical modelling approaches regarding the post-buckling behaviour of delaminated plates is present. However, such a mechanical problem associated with a more comprehensive description regarding the geometry and the mechanical behaviour requires a clear definition and analysis of the mandatory limitations to be employed in a modelling approach. This is aimed at in the subsequent sections yielding a model description which accomplishes the objective of predicting post-critical responses of delaminated plates while addressing mandatory restrictions and approximations in comparison with comprehensive finite element models.

4.3 Semi-analytical modelling

The current section is arranged in order to derive an efficient modelling approach for predicting post-buckling responses of delaminated multi-layered composite plates. Therefore, initially, two modelling approaches are evaluated for describing the post-buckling behaviour of plates. Subsequently, the geometric model of the delaminated plate is described and the amount of generalized coordinates required to approximate the post-buckling responses efficiently is determined. In the last part of the section, the energy formalism for modelling the post-buckling responses for stationary and non-stationary delaminations is presented.

4.3.1 Modelling approaches for non-linear plate buckling

The problem of a delaminated composite strut presented in Chapter 3 underlines one of the main advantages of the formalism of THOMPSON and HUNT which thus also applies for the framework developed in this work: computational efficiency while employing a considerably small amount of generalized coordinates. However, most of the applications of the structural stability formalism of THOMPSON and HUNT focus on one-dimensional problems such as struts, bars or frames, or problem descriptions which allow a simplified approach, so that, for instance, two-dimensional formulations may be transformed into one-dimensional descriptions.

In [95], THOMPSON and HUNT propose a simplified approach for the non-linear buckling of plates which was used in [30] by HUNT *et al.* and is therefore subsequently referred to as the modelling approach "HUNT". The approach aims at considering non-linear in-plane strains which occur during the post-buckling response without using further generalized coordinates for the in-plane displacements. Thus, the post-buckling behaviour of plates may be described only by a set of generalized coordinates approximating the out-of-plane displacements.

The modelling approach is based on the assumption that the in-plane strain is evenly distributed (constant) over the length of the plate,[14] where the in-plane displacement is expressed in terms of a resulting end-shortening rather than a displacement field $u(x,y)$.[15] Thus, the resulting axial shortening of the plate can be determined as (using the coordinate system shown in Fig. 4.8)

$$u = q_{\text{end}} - \int_{-L}^{L} \frac{1}{2} \left(\frac{\partial w(x,y)}{\partial x} \right)^2 \mathrm{d}x, \tag{4.3.1}$$

where q_{end} is the total end-shortening of the plate, yielding the in-plane strain

$$\varepsilon_{xx} = \frac{u}{2L}, \tag{4.3.2}$$

with the dimensions of the plate given in Figs. 4.1 and 4.8. The second term in Eq. (4.3.1) represents the end-shortening—to the first order—associated with a buckling process in which the neutral plane is inextensional. Thus, subtracting this contribution from the total end-shortening q_{end} yields the axial shortening u.

However, in general, the assumption of an inextensional neutral plane does not hold in non-linear plate buckling. Only in the vicinity of the buckling load, where the bending energy stored equals the membrane energy released [95, 96],[16] the

[14] Ref. [95] states that this is reasonable in the absence of transverse and shear stresses.

[15] In-plane contributions are just considered along the axis of the application of the load. Therefore, the in-plane displacement and strain are expressed for the x-direction only (*cf.* Figs. 4.1).

[16] This refers to the change in length from the pre-buckled length to the buckled length under fixed end conditions.

end-shortening under inextensional conditions (the first order approximation is given by the second term in Eq. (4.3.1)) adequately describes the contribution to the in-plane displacement.

Therefore, the modelling approach "HUNT" should be regarded as a rough approximation of the non-linear buckling of plates which, however, requires a minimal amount of generalized coordinates. Whether the approach is applicable strongly depends on the problem description and the information intended to be obtained. Before this is delineated by studying an application example, the second modelling approach for describing the non-linear plate buckling is discussed.

The second approach adopts a non-linear kinematic formulation used in the continuum-mechanical description of solids undergoing finite strains. Thus, the strain can be expressed as

$$E_{ij} = \frac{1}{2}\left(\frac{\partial u_i}{\partial X_j} + \frac{\partial u_j}{\partial X_i} + \frac{\partial u_m}{\partial X_i}\frac{\partial u_m}{\partial X_j}\right), \tag{4.3.3}$$

where E_{ij} is the GREEN–LAGRANGE strain tensor and X_i refers to the reference configuration [76]. However, all non-linear strain components referring to in-plane displacements remain negligible small during plate buckling [76], such that only the out-of-plane contributions are considered. Thus, the strains associated with the plane stress assumption can be written as

$$\begin{pmatrix} E_{xx} \\ E_{yy} \\ 2E_{xy} \end{pmatrix} = \begin{pmatrix} \frac{\partial u}{\partial X} + \frac{1}{2}\left(\frac{\partial w}{\partial X}\right)^2 \\ \frac{\partial v}{\partial Y} + \frac{1}{2}\left(\frac{\partial w}{\partial Y}\right)^2 \\ \frac{\partial u}{\partial Y} + \frac{\partial v}{\partial X} + \frac{\partial w}{\partial X}\frac{\partial w}{\partial Y} \end{pmatrix}, \tag{4.3.4}$$

which are referred to as VON KÁRMÁN strains, so that subsequently the modelling approach is termed "VON KÁRMÁN". Therefore, unlike the approach HUNT (Eq. (4.3.1)) the VON KÁRMÁN modelling approach requires the description of the displacement field considering the in-plane displacements, *i.e.*

$$u_i = \begin{pmatrix} u(x,y) \\ v(x,y) \\ w(x,y) \end{pmatrix}. \tag{4.3.5}$$

As a consequence, the approach requires more generalized coordinates. The derivation of the respective energy terms of the total potential energy remains unchanged in comparison with Chapter 3 distinguishing between stretching and bending contributions.

Both modelling approaches are subsequently compared with each other by studying the post-buckling responses of an all-sided simply-supported plate in

terms of normalized load against normalized midpoint deflections (Fig. 4.7a) as well as normalized load against normalized end-shortening (Fig. 4.7b).

Two cases of boundary conditions are considered in Fig. 4.7. Case "SSSS 1" suppresses in-plane displacements at the boundaries (except for the compressive shortening of the applied load) which are referred to as restrained edges, whereas case "SSSS 2" enables in-plane displacements at the longitudinal boundaries (with respect to the direction of the applied load, *i.e.* along the x-axis in Fig. 4.1) which are referred to as unrestrained edges. Thus, the following displacements are employed (with respect to the coordinate system shown in Fig. 4.8),

$$\begin{pmatrix} u(x,y) \\ v(x,y) \\ w(x,y) \end{pmatrix} = \begin{pmatrix} \varepsilon_0 x + q_1 \sin\left(\frac{\pi x}{L}\right) \cos\left(\frac{\pi y}{2B}\right) \\ q_2 \sin\left(\frac{\pi y}{B}\right) \cos\left(\frac{\pi x}{2L}\right) \\ q_3 \cos\left(\frac{\pi x}{2L}\right) \cos\left(\frac{\pi y}{2B}\right) \end{pmatrix}, \tag{4.3.6}$$

in which only $w(x,y)$ is used for the approach HUNT. The applied strain ε_0 is taken as the loading parameter,[17] so that the modelling approach HUNT employs one generalized coordinate whereas the modelling approach VON KÁRMÁN requires three.[18] In case SSSS 2, the additional contribution to the displacement in the y-direction, $v(x,y)$, is approximated by the term $a_0 y \cos(\pi x/(2L))$ where a_0 is a passive coordinate which can be replaced by solving the condition $\partial\Pi/\partial a_0 = 0$ with respect to a_0.

A symmetrically laid-up cross-ply laminate with the material parameters given in Table 3.3 in Chapter 3 and the dimensions 96.52 mm × 96.52 mm × 1.335 mm ($2L \times 2B \times t$, *cf.* Fig. 4.8) is taken as an application example. The responses are also compared with findings from a finite element simulation (S4R elements, 1 mm x 1 mm element size, 11294 nodes) indicated by the symbols "∘" and "□" in Fig. 4.7 for the cases SSSS 1 and SSSS 2 respectively.[19]

As can be seen from Fig. 4.7a, the midpoint deflections for the VON KÁRMÁN approach and the finite element simulation almost coincide for both cases with the case of restrained edges (SSSS 1) showing almost no deviations. For both cases, the approach HUNT yields the same response. This is expected, as in-plane displacements apart from the end-shortening are not considered. Thus, a different post-buckling response is only caused when other boundary conditions with respect to the out-of-plane displacements are studied.

[17] The generalized coordinate q_{end} in Eq. (4.3.1) is equal to $2\varepsilon_0 L$ and describes the loading parameter in a displacement-controlled configuration for the approach HUNT.

[18] The amount of generalized coordinates used describes the minimum, such that adequate post-buckling responses can be obtained. Further generalized coordinates may be required when studying other boundary conditions.

[19] As commonly done for non-linear buckling problems (*e.g.* [68, 69]), an imperfection in the form of a transverse load at the midpoint of the plate is incorporated in the finite element model, so that the post-buckling path can be traced.

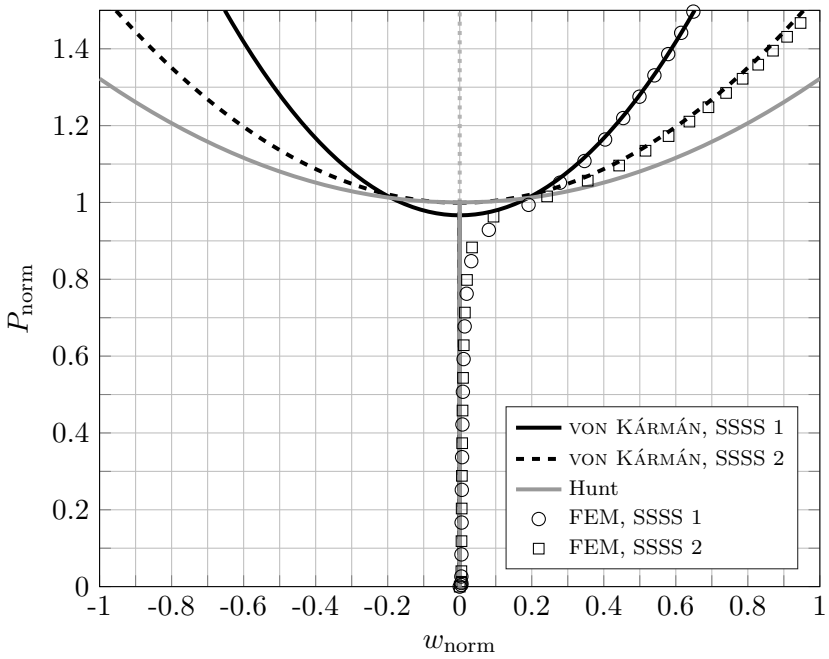

(a)

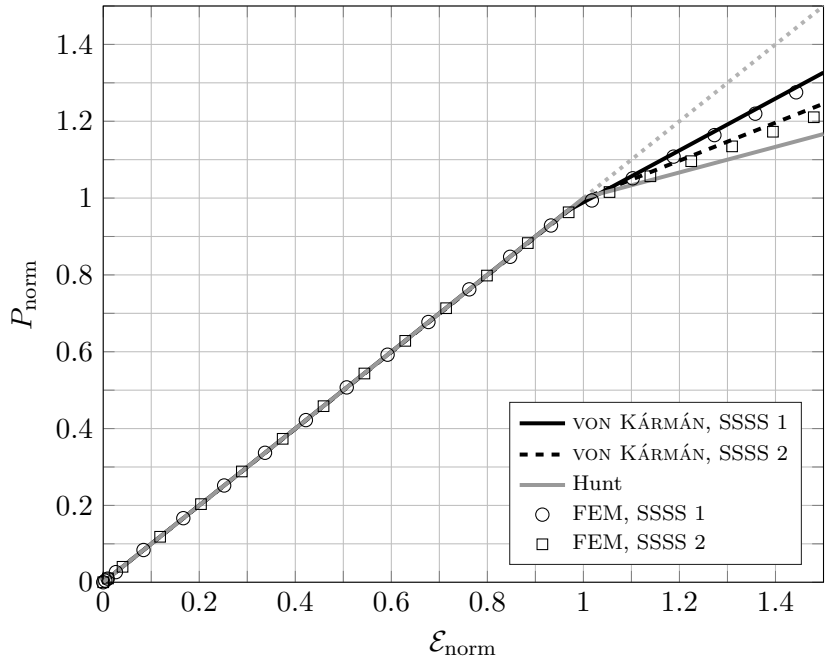

(b)

Fig. 4.7: Comparison of the modelling approaches "Hunt" and "von Kármán" for an all-sided simply-supported plate (SSSS); SSSS 1: restrained edges, SSSS 2: unrestrained edges; **(a)** normalized compressive load (P_{norm}) *vs.* normalized midpoint deflections (w_{norm}); **(b)** normalized compressive load (P_{norm}) *vs.* normalized end-shortening ($\mathcal{E}_{\text{norm}}$).

The post-buckling responses in terms of normalized load against normalized end-shortening (Fig. 4.7b) underline the deviations between the two approaches. Whereas the VON KÁRMÁN approach is in very good agreement with the finite element simulation, partly significant deviations are documented in comparison with the approach HUNT. It appears that only case SSSS 2 can be roughly approximated by the approach HUNT.

The post-buckling stiffness of the finite element path shown in Fig. 4.7b for the case SSSS 2 ("○") is 0.402 which is very close to the exact value of 0.408 [46, 95]. The stiffness of the approach HUNT is 0.33, as also stated in [46, 95].

From the insight gathered in this section, the following concluding remarks can be made.

- The approach HUNT may only provide arguably acceptable deviations, when the deformation of the system is least restricted, *i.e.* for certain boundary conditions, specifically in terms of the in-plane displacements. This appears plausible as the approach employs the condition of an inextensional neutral plane which is "more suitable" when the in-plane displacements at the boundaries are enabled (unrestrained edges).

- Since the approach HUNT considers only the axial shortening of the plate, *i.e.* in-plane boundary conditions are omitted, the post-buckling responses are only altered by a change of the out-of-plane boundary conditions. Thus, one deformation path is obtained for various types of in-plane boundary conditions. Regarding the results provided in Fig. 4.7, the single path may roughly approximate the deformation behaviour for the case SSSS 2 but fails to predict the post-buckling response for the case SSSS 1 adequately.

- The approach VON KÁRMÁN provides results which are in very good agreement with the finite element simulation. Furthermore, various in-plane conditions at the boundaries can be considered. However, more generalized coordinates are required since all components of the displacement field have to be approximated. This may seem negligible reviewing the case presented, but may become relevant when studying other boundary conditions such as an all-sided clamped plate as well as problem descriptions naturally comprising more degrees of freedom.

Furthermore, it should be stressed that the approach HUNT requires a certain geometry which enables the application of the generalized coordinate describing the end-shortening of the respective part. This may become cumbersome when studying non-rectangular geometries.

As a final remark, regarding the application to a composite plate with an embedded delamination, the prediction of the onset of delamination growth as well

as the growth itself requires the adequate description of the in-plane displacement field. Hence, studies employing an approach similar to HUNT consider thin-film-buckling as well as a geometric split into various strip elements which enables the aforementioned description (*e.g.* see [6, 7, 77]).

Concluding, for the study of the post-buckling behaviour considering delamination growth of non-rectangular delaminations the approach HUNT appears to be too restrictive, so that the VON KÁRMÁN approach is employed henceforth understanding the higher computational effort to be expected.

4.3.2 Model description

Fig. 4.8 shows the geometric model of a plate with an embedded delamination. As can be seen, the plate is subdivided into three parts, two sublaminates and one undelaminated region. Parts ① and ② describe the upper and lower sublaminate respectively. The undelaminated part of the plate is denoted by ③. The delamination is visualized in Fig. 4.8 by a grey shaded area.

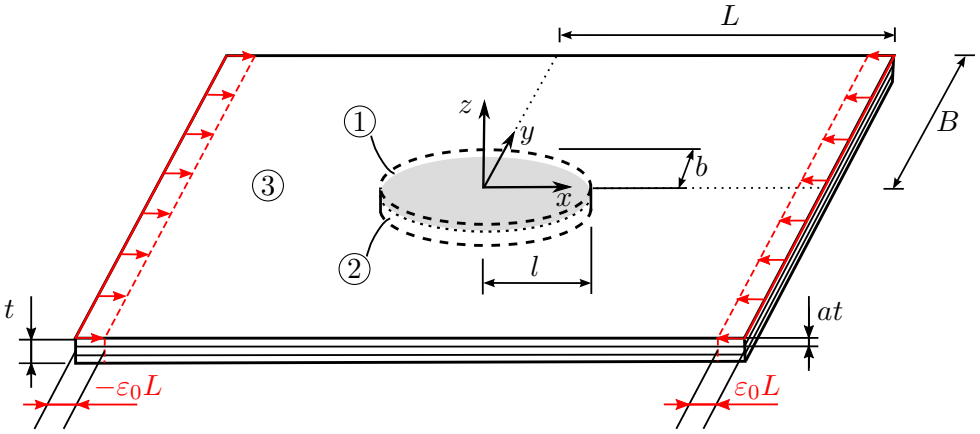

Fig. 4.8: Geometric model of a composite plate with an embedded elliptical delamination.

An elliptical delamination is chosen since experimental proof is existent for such a shape (*cf.* [11]). On the other hand, information about the post-buckling behaviour of elliptically delaminated composite plates is comparably sparse within the literature (*cf.* Table 4.1). The elliptical delamination is defined by the measures l and b describing the length and width of the ellipse (semi major and semi minor axis) respectively. The overall dimensions of the plate are denoted by $2L \times 2B \times t$ (length $\times$ width $\times$ thickness). The depth of the delamination is described by the parameter a.

A uniaxial loading is applied to the plate in the x-direction in the form of an applied strain such that the boundaries at (L, y) and $(-L, y)$ are subjected to the displacements $\pm\varepsilon_0 L$ respectively (*cf.* Fig. 4.8), *i.e.* a displacement-controlled

configuration is studied. The plate is taken to be clamped at the boundaries with in-plane displacements being restrained except for the applied compressive shortening. These boundary conditions are denoted in Table 4.2 by CCCC-1 and are described in the experimental test standard [91].

The Classical Laminate Theory is employed, as described in Section 3.3.2.1 (*cf.* Eq. (3.3.15)). In the current chapter, plate dimensions are chosen such that the effect of shear deformations is assumed to be small. Therefore, out-of-plane shear contributions are omitted in the description of the displacement field.[20] The boundary and continuity conditions for the displacement field $\boldsymbol{u} = \{u(x,y), v(x,y), w(x,y)\}^{\mathrm{T}}$ can be expressed as

$$
\begin{aligned}
&\underline{\text{in-plane, } u\text{:}} \\
&u_3(\pm L, y) = \pm\varepsilon_0 L, && u_3(x, \pm B) = \varepsilon_0 x, \\
&\qquad u_3(\Gamma) = u_i(\Gamma) - u_i^{\mathrm{rot}}, \\
&\underline{\text{in-plane, } v\text{:}} \\
&v_3(\pm L, y) = 0 && v_3(x, \pm B) = 0, \\
&\qquad v_3(\Gamma) = v_i(\Gamma) - v_i^{\mathrm{rot}}, && \qquad (4.3.7) \\
&\underline{\text{out-of-plane, } w\text{:}} \\
&w_3(\pm L, y) = 0, && w_3(x, \pm B) = 0, \\
&\nabla_j w_3(\pm L, y) = 0, && \nabla_j w_3(x, \pm B) = 0, \\
&\qquad w_3(\Gamma) = w_i(\Gamma), && \qquad \nabla_j w_3(\Gamma) = \nabla_j w_i(\Gamma),
\end{aligned}
$$

where the subscript at the displacement field entries ("3" and $i = 1, 2$) refers to the respective part of the plate, $\nabla_j = \left\{ \frac{\partial}{\partial x}, \frac{\partial}{\partial y} \right\}^{\mathrm{T}}$ and Γ describes the boundary of the ellipse, *i.e.*

$$
\Gamma(x,y) = \left(\frac{x}{l}\right)^2 + \left(\frac{y}{b}\right)^2 - 1 = 0. \qquad (4.3.8)
$$

The post-buckling behaviour is modelled with the aid of a Rayleigh–Ritz formulation employing continuous mode-forms in order to approximate the displacement field of the plate. Owing to the description of the boundary of the delamination by Eq. (4.3.8), polynomial shape functions are employed in order to satisfy the geometric boundary and continuity conditions provided in Eq. (4.3.7).[21] Those functions can be expressed in terms of a series which is shown in Eq. (4.3.10)

[20] Plates with an overall length/width to thickness ratio of at least 40 are considered.

[21] In the current description of the geometric model, trigonometric functions do not allow a symbolic integration of the strain energy density as required by the semi-analytical modelling approach.

employing Eq. (4.3.8) and the function defining the boundary of the plate,

$$\Gamma_{\mathrm{P}} = \left(\left(\frac{x}{L}\right)^2 - 1\right)\left(\left(\frac{y}{B}\right)^2 - 1\right) = 0, \tag{4.3.9}$$

thus

part ③:

$$\begin{aligned}
u_3(x,y) &= \varepsilon_0 x + (\Gamma_{\mathrm{P}})\left(\frac{x}{L}\right)\sum_{m=1}^{M}\sum_{n=1}^{N}\left(q_{mn}^{u_3}\left(\frac{x}{L}\right)^{2(m-1)}\left(\frac{y}{B}\right)^{2(n-1)}\right),\\
v_3(x,y) &= (\Gamma_{\mathrm{P}})\left(\frac{y}{B}\right)\sum_{m=1}^{M}\sum_{n=1}^{N}\left(q_{mn}^{v_3}\left(\frac{x}{L}\right)^{2(m-1)}\left(\frac{y}{B}\right)^{2(n-1)}\right),\\
w_3(x,y) &= (\Gamma_{\mathrm{P}})^2\sum_{m=1}^{M}\sum_{n=1}^{N}\left(q_{mn}^{w_3}\left(\frac{x}{L}\right)^{2(m-1)}\left(\frac{y}{B}\right)^{2(n-1)}\right),
\end{aligned}$$

part ⓘ: (4.3.10)

$$\begin{aligned}
u_i(x,y) &= u_3 + (\Gamma)\left(\frac{x}{l}\right)\sum_{m=1}^{M}\sum_{n=1}^{N}\left(q_{mn}^{u_i}\left(\frac{x}{l}\right)^{2(m-1)}\left(\frac{y}{b}\right)^{2(n-1)}\right) + u_i^{\mathrm{rot}},\\
v_i(x,y) &= v_3 + (\Gamma)\left(\frac{y}{b}\right)\sum_{m=1}^{M}\sum_{n=1}^{N}\left(q_{mn}^{v_i}\left(\frac{x}{l}\right)^{2(m-1)}\left(\frac{y}{b}\right)^{2(n-1)}\right) + v_i^{\mathrm{rot}},\\
w_i(x,y) &= w_3 + (\Gamma)^2\sum_{m=1}^{M}\sum_{n=1}^{N}\left(q_{mn}^{w_i}\left(\frac{x}{l}\right)^{2(m-1)}\left(\frac{y}{b}\right)^{2(n-1)}\right),
\end{aligned}$$

with $i = 1, 2$, where u_i^{rot} and v_i^{rot} describe contributions to the in-plane displacements of the sublaminates resulting from the rotation of the interface between the sublaminates and the undelaminated part considering the offset of the neutral planes. Such contributions can be approximated by

$$\begin{aligned}
u_i^{\mathrm{rot}} &= h_i\left(-\left.\frac{\partial w_3}{\partial x}\right|_{\Gamma}\right),\\
v_i^{\mathrm{rot}} &= h_i\left(-\left.\frac{\partial w_3}{\partial y}\right|_{\Gamma}\right) \quad \text{with} \quad h_i = \begin{Bmatrix} -\frac{(1-a)t}{2} \\ \frac{at}{2} \end{Bmatrix},
\end{aligned} \tag{4.3.11}$$

where i indicates the respective sublaminate and the offsets of the neutral planes are denoted by h_i. It should be noted that the following symmetries are employed in the displacement functions (Eq. (4.3.10)),

$$\begin{aligned}
u_i(x,y) &= -u_i(-x,-y), & u_i(x,y) &= -u_i(-x,y) &&= u_i(x,-y),\\
v_i(x,y) &= -v_i(-x,-y), & v_i(x,y) &= -v_i(-x,y) &&= v_i(x,-y),\\
w_i(x,y) &= w_i(-x,-y), & w_i(x,y) &= w_i(-x,y) &&= w_i(x,-y),
\end{aligned} \tag{4.3.12}$$

with $i = 1, 2, 3$. Those symmetries are present for typical laminates, such as unidirectional, cross-ply and quasi-isotropic layups, using the coordinates system shown in Fig. 4.8, whereby the symmetry of the out-of-plane displacement is also associated with studying quadratic plates ($L = B$, *cf.* Fig. 4.8), as it is done in the present chapter.

In Eq. (4.3.10), any chosen M and N satisfies the geometric boundary conditions mandatory for the RAYLEIGH–RITZ formulation. However, with increasing M and N the accuracy of the approximation of the displacement field improves which, on the other hand, requires higher computational cost.

With the displacement field being described by a set of generalized coordinates, the analytical framework developed in the current work can be applied. This is done in the subsequent section presenting the energy formalism.

4.3.3 Energy formalism

As concluded in Section 4.3.1, the VON KÁRMÁN modelling approach is employed considering the non-linear terms in the GREEN–LAGRANGE strain tensor associated with the out-of-plane displacements, *i.e.* the VON KÁRMÁN strains, *cf.* Eqs. (4.3.3) and (4.3.4). Bearing this in mind, subsequently a commonly used notation (*cf.* [46, 76, 96]) is adopted henceforth, such that the VON KÁRMÁN strains are also denoted by ε_{ij} and lower case characters are employed for the coordinate system. Thus, the strain energy density w can be written as

$$w = \frac{1}{2}\bar{Q}_{IJ}\varepsilon_I\varepsilon_J, \quad \text{with} \quad I, J = 1, 2, 6, \tag{4.3.13}$$

in which the plane stress assumption is considered, $\bar{Q}_{IJ}$ is the reduced transformed stiffness matrix (*cf.* Eq. (3.3.7)) and ε_I comprises in-plane contributions (VON KÁRMÁN strains $\{\varepsilon_{(0)}\}$) and strains associated with bending deformations ($z\{\kappa\}$),[22] *i.e.*

$$\left\{\varepsilon\right\} = \left\{\varepsilon_{(0)}\right\} + z\left\{\kappa\right\} = \begin{Bmatrix} \frac{\partial u}{\partial x} + \frac{1}{2}\left(\frac{\partial w}{\partial x}\right)^2 \\ \frac{\partial v}{\partial y} + \frac{1}{2}\left(\frac{\partial w}{\partial y}\right)^2 \\ \frac{\partial u}{\partial y} + \frac{\partial v}{\partial x} + \frac{\partial w}{\partial x}\frac{\partial w}{\partial y} \end{Bmatrix} + z \begin{Bmatrix} -\frac{\partial^2 w}{\partial x^2} \\ -\frac{\partial^2 w}{\partial y^2} \\ -2\frac{\partial^2 w}{\partial x \partial y} \end{Bmatrix}. \tag{4.3.14}$$

Integrating Eq. (4.3.13) over the volume and employing Eq. (4.3.14) and the

[22] In this chapter, the in-plane strains are denoted by $\{\varepsilon_{(0)}\}$ in order to avoid confusion with the applied strain ε_0 used in the model description.

Classical Laminate Theory (*cf.* Section 3.3.2) yields the strain energy,

$$W = \frac{1}{2} \int_y \int_x \left(\varepsilon_I^0 A_{IJ} \varepsilon_J^0 + 2\varepsilon_I^0 B_{IJ} \kappa_J + \kappa_I D_{IJ} \kappa_J \right) \mathrm{d}y \, \mathrm{d}x, \tag{4.3.15}$$

where A_{IJ}, B_{IJ} and D_{IJ} are the in-plane, coupling and bending stiffness matrix respectively. Owing to the subdivision of the plate into three parts, the strain energy of each part is determined with Eq. (4.3.15) and subsequently summed up.

Since a displacement-controlled configuration is studied in this chapter, the strain energy in Eq. (4.3.15) is the governing functional. Thus, by employing the Rayleigh–Ritz method using the displacement field defined in Eq. (4.3.10), a set of non-linear algebraic equations is obtained by applying the variational principle, *i.e.*

$$\delta\Pi = \delta W(q_i) = 0 \Longrightarrow \frac{\partial W}{\partial q_i} = 0, \tag{4.3.16}$$

where all generalized coordinates used in Eq. (4.3.10) are comprised by the set q_i. Eq. (4.3.16) yields the deformation path for the case of stationary delaminations in terms of $q_i(\varepsilon_0)$ since ε_0 is the loading parameter in the current model description.

As in Section 3.4 for the delaminated strut, an imperfection caused by the pre-existing delamination is assumed in the form of an initial out-of-plane deflection with an amplitude of $t/1000$. The energy contributions associated with the imperfection are deducted from the total potential energy as described in Appendix D.

Following the structural stability analysis framework developed in Chapter 2, with the aid of the equilibrium path $q_i(\varepsilon_0)$, the thermodynamic force, thus the energy release rate, is determined next.

Even though a single damage parameter ξ, *i.e.* the delamination area A_{ell},

$$\xi = A_{\mathrm{ell}} = \pi l b, \tag{4.3.17}$$

is present in the current application example, owing to the model description, delamination growth into two directions can be investigated. The force available for producing delamination growth in the width direction (G_{b}) and in the length direction (G_{l}) of the ellipse can be calculated as

$$G_{\mathrm{b}} = -\frac{1}{\pi l} \frac{\partial W}{\partial b} \quad \text{and} \quad G_{\mathrm{l}} = -\frac{1}{\pi b} \frac{\partial W}{\partial l} \tag{4.3.18}$$

respectively.

As for the problem of a delaminated strut, a quasi-brittle fracture behaviour is

considered, thus growth into the length direction occurs, whenever

$$G_{\mathrm{l}} \geq G_{\mathrm{c}}, \tag{4.3.19}$$

and growth into the width direction, whenever

$$G_{\mathrm{b}} \geq G_{\mathrm{c}}. \tag{4.3.20}$$

It should be noted that simultaneous growth into both directions is also possible, whenever for a current state of loading

$$\left.\begin{matrix} G_{\mathrm{l}} \\ G_{\mathrm{b}} \end{matrix}\right\} \geq G_{\mathrm{c}}. \tag{4.3.21}$$

Subsequently, the extended total potential energy principle (*cf.* Section 2.2.2) is applied in order to determine the post-buckling responses beyond the deformation state causing delamination growth. As has been shown in Section 3.4 and by Fig. 4.6, during stable delamination growth the condition

$$G = G_{\mathrm{c}} \tag{4.3.22}$$

holds, which can be rewritten in terms of the current model description, such that

$$G_{\mathrm{b}} = G_{\mathrm{c}} \quad \text{or} \quad G_{\mathrm{l}} = G_{\mathrm{c}}. \tag{4.3.23}$$

Eq. (4.3.23) is the requirement for the existence of an extended total potential energy, thus the total work of deformation being a potential of the generalized forces (*cf.* Section 2.2.1.1).

Since the width and length of the ellipse cannot be explicitly obtained from Eq. (4.3.23), it is rewritten such that

$$G_{\mathrm{b}} - G_{\mathrm{c}} = D_{\mathrm{b}}(q_i, \varepsilon_0, b) = 0 \quad \text{and} \quad G_{\mathrm{l}} - G_{\mathrm{c}} = D_{\mathrm{l}}(q_i, \varepsilon_0, l) = 0, \tag{4.3.24}$$

from where the width and length of the ellipse are implicitly given by the functions D_{b} and D_{l} respectively. It should be noted that the indicated dependencies of D_{b} on the width b and D_{l} on the length l only account for the possible directions of growth and do not delineate two distinct damage parameters.

As described in Section 3.3.4, an explicit form of the width b and the length l of the ellipse is obtained by a TAYLOR series approximation (*cf.* Eq. (3.3.43)) around the damage state (q_i^0, ε_0^0), *i.e.* the deformation state at which delamination growth

is initiated. Thus, the delamination width and length are obtained in terms of

$$b = b(q_i, \varepsilon_0) \quad \text{and} \quad l = l(q_i, \varepsilon_0) \tag{4.3.25}$$

respectively, depending on whether growth in the width or length direction is initiated. In the current application example, the TAYLOR series is truncated after the second order terms.

For growth in the width direction, the extended total potential energy can be derived by inserting Eq. $(4.3.25)_1$ into the strain energy of the plate (Eq. (4.3.15)) and adding the dissipative energy associated with delamination growth,

$$W_{\mathrm{d}} = G_{\mathrm{c}}(A_{\mathrm{ell}} - A^0_{\mathrm{ell}}) \tag{4.3.26}$$

which can be rewritten regarding growth in the width direction, *i.e.*

$$W_{\mathrm{d}} = G_{\mathrm{c}}\pi l(b - b^0), \tag{4.3.27}$$

where A^0_{ell} and b^0 denote the initial delamination area and the initial delamination width respectively. Thus, the extended total potential energy, *i.e.* the total work of deformation, during delamination growth in the width direction reads

$$W_{\mathrm{tot}} = W(q_i, \varepsilon_0, b(q_i, \varepsilon_0)) + W_{\mathrm{d}}(b(q_i, \varepsilon_0)). \tag{4.3.28}$$

For growth in the length direction, Eq. $(4.3.25)_2$ is used instead for replacing the delamination length in Eqs. (4.3.26) and (4.3.28) while keeping the delamination width b constant.

The total work of deformation given by Eq. (4.3.28) (or the respective form for growth in the length direction) is a potential of the generalized forces and the governing functional of the deformation process during delamination growth. Thus, the variational principle,

$$\delta W_{\mathrm{tot}}(q_i) = 0, \tag{4.3.29}$$

is applied yielding the equilibrium path in terms of $q_i(\varepsilon_0)$ starting from the damage state (q_i^0, ε_0^0). It should be stressed that for each loading step the energy release rates for growth in the length and width direction need to be determined in order to trace the growth direction accurately. Furthermore, as described in Section 3.3.4, owing to the TAYLOR series approximation, the respective delamination parameter has to be recalculated once the respective condition of $G = G_{\mathrm{c}}$ is violated.[23]

[23] This strictly refers to a violation due to the approximation of the damage parameter.

With the variational principles in Eqs. (4.3.16) and (4.3.29) an entire loading process starting from an unloaded configuration up to the failure displacement (stability and/or material failure) can be modelled.

Before results for characteristic post-buckling responses of multi-layered composite plates with embedded elliptical delaminations are presented, the adequate choice of the order of the displacement functions shown in Eq. (4.3.10) is addressed next. This is done in order to enable an efficient modelling approach for describing post-buckling responses of such structures. Efficiency is understood as an optimal choice in between accuracy of the approximation and computational cost.

4.3.4 Order of the displacement functions

Regarding an adequate choice of the displacement functions, *i.e.* determining the order of the polynomials provided in Eq. (4.3.10), plates exhibiting the following features are considered:

- quadratic dimensions, *i.e.* $L = B$ (*cf.* Fig.4.8),
- a length/width to thickness ratio of greater than 40,
- elliptical delaminations (including circular delaminations) and
- delamination depth of less than 0.2 (normalized to the total thickness of the plate), *i.e.* shallow delaminations.

All plates investigated in the current chapter are required to comply with the aforementioned criteria. As done by the vast majority of studies, quadratic plates are studied, as discussed in Section 4.2. The length to thickness ratio is taken such that shear effects are small. Elliptical delaminations are studied owing to the experimental proof provided in [11]. Shallow delaminations are investigated which is defined such that $a \leq 0.2$ (*cf.* Fig.4.8).

The displacement functions investigated are evaluated by means of the prediction of the buckling and post-buckling response for the case of a stationary delamination. The displacement functions are determined by performing two steps. First, the order of the polynomials is continuously increased. Second, generalized coordinates remaining negligibly small are omitted. Furthermore, it is well-documented and therefore considered that the in-plane displacements require higher order approximations than the out-of-plane displacement [71, 110, 111].

The outcome of the evaluation is presented in Fig. 4.9 showing a post-buckling response for the case of stationary delamination in terms of normalized compressive applied strain against normalized midpoint deflection. A plate with the dimensions $150\,\text{mm} \times 150\,\text{mm} \times 3.115\,\text{mm}$ and an elliptical delamination of $l = 25\,\text{mm}$ and

$b = 50\,\mathrm{mm}$ is taken as an example. The plate has a unidirectional layup of 35 layers. The material parameters are provided in Table 3.3 (*cf.* Section 3.4). The delamination is in between the 32nd and 33rd layer ($a = 3/35$).

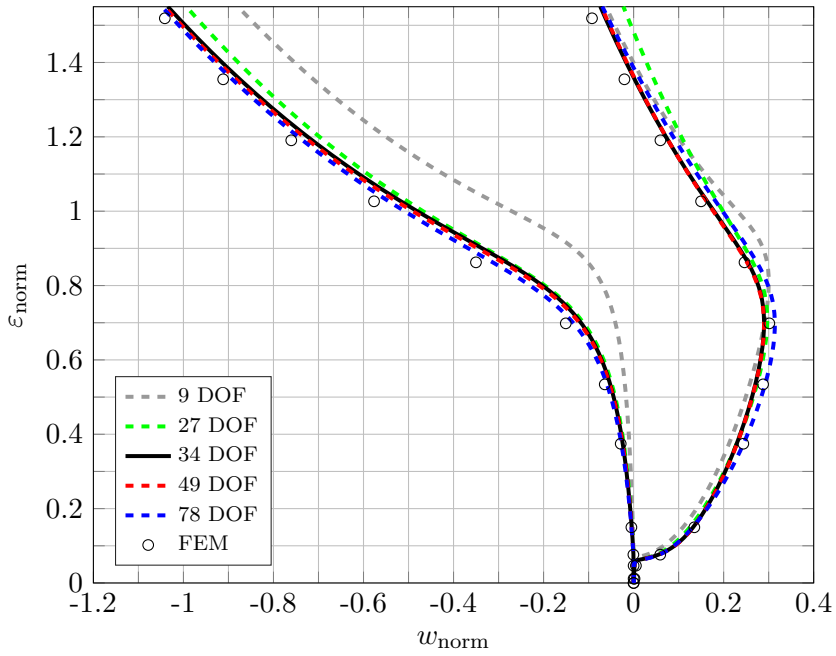

Fig. 4.9: Post-buckling response in terms of applied normalized strain ($\varepsilon_{\mathrm{norm}}$) against normalized midpoint deflections (w_{norm}) for different numbers of degrees of freedom (DOF).

The cases shown in Fig. 4.9 are compared with findings obtained from a finite element simulation using Abaqus and refer to Eq. (4.3.10) as follows:

- nine degrees of freedom (9 DOF, and thus nine generalized coordinates) – first order polynomials for the out-of-plane and in-plane displacements,
- 27 degrees of freedom (27 DOF) – second order polynomials for the out-of-plane and in-plane displacements,
- 34 degrees of freedom (34 DOF) – second order polynomials for the out-of-plane and third order polynomials for the in-plane displacements; omitting vanishingly small coefficients ($|q_i| \leq 10^{-4}$),
- 49 degrees of freedom (49 DOF) – second order polynomials for the out-of-plane and third order polynomials for the in-plane displacements,
- 78 degrees of freedom (78 DOF) – third order polynomials for the out-of-plane and fourth order polynomials for the in-plane displacements.

As can be seen in Fig. 4.9, the case of 9 DOF does not yield adequately accurate results. A significant improvement is documented in between the cases of 9

DOF and 27 DOF. The post-buckling response improves further specifically for normalized compressive strains greater than 1 for the case of 34 DOF. The cases of 34 and 49 DOF are barely distinguishable with the thicker lower sublaminate showing marginally larger out-of-plane deflections (softer response). The case of 78 DOF exhibits an improvement of approximately 2% compared with the case of 34 DOF.

Based on the findings, the case of 34 DOF is chosen to model the post-buckling behaviour of delaminated composite plates. This case covers all buckling phenomena (critical and post-critical responses) adequately and yields quantitative results which are deemed sufficiently, *i.e.* being in a margin of 5% to the reference solution (the finite element simulation). On the other hand, computational cost is significantly lower in comparison with the cases 49 and 78 DOF.

Concluding, an efficient modelling approach being understood as an optimal choice in between accuracy and computational cost is provided by the case of 34 DOF which is adopted henceforth.

4.4 Results

The application of the geometric model (*cf.* Section 4.3.2) and the analytical framework (*cf.* Chapter 2) is demonstrated by studying the post-buckling responses of delaminated plates with a unidirectional ($[0°]_{35}$) and a cross-ply ($[0°/(90°/0)_{17}]$) layup. The same unidirectional plies as in Section 3.4 are used for the laminates, such that the material parameters are provided in Table 3.3.

The dimensions of the plate are taken as $150\,\text{mm}\times150\,\text{mm}\times3.1115\,\text{mm}$ ($2L \times 2B \times t$). A delamination is assigned in between the 32nd and 33rd layer, thus $a = 3/35$ (*cf.* Fig. 4.8). The dimension of the plate as well as the amount of layers follow case studies from the literature (*e.g.* [70]).

The results are compared with findings from finite element simulations using Abaqus. The finite element model consists of two layers possessing the layup of the upper and lower sublaminate, respectively. The layers are built-up by S4R elements. The two layers are bonded with each other in the undelaminated region and disbonded in the region of the delamination. The virtual crack closure technique, as implemented in Abaqus, was employed where growth is allowed to propagate in the plane of the delamination. The mesh is refined around the delamination tip with an element size of $0.5\,\text{mm}\times0.5\,\text{mm}$. An element size of $1.5\,\text{mm}\times1.5\,\text{mm}$ is assigned to the rest of the model. A small imperfection load at the centre of the plate is used to enable the tracing of the post-buckling path.

First, post-buckling responses of the unidirectional laminate are studied. An elliptical delamination with $l_{\text{norm}} = 1/3$ and $b_{\text{norm}} = 2/3$ is investigated where the lengths are normalized against the respective dimension of the plate, *i.e.*: $l_{\text{norm}} = l/L$ and $b_{\text{norm}} = b/B$. The condition of $G_{\text{c}} = G_{\text{c}}^{\text{I}}$ is employed in the analytical model and the finite element simulation.

Fig. 4.10 comprises the structural stability and the material damaging behaviour of the system by delineating the deformation paths in terms of normalized compressive applied strain ($\varepsilon_{\text{norm}}$) *vs.* normalized midpoint deflections (w_{norm}) in Fig. 4.10a and by visualizing the delamination growth contours calculated with the aid of the current model and with the finite element simulation in Fig. 4.10b and Fig. 4.10c respectively.

Characteristic deformation states which are analysed with regards to the delamination growth behaviour are highlighted in Fig. 4.10 by Roman numerals for the current analytical model and by Arabic numerals for the finite element simulation (denoted by FEM in 4.10a).

The applied strain is normalized against the buckling strain of an undelaminated plate which was determined by a linear analysis employing a Rayleigh–Ritz formulation in which only the out-of-plane displacement is considered. The midpoint deflection is normalized with respect to the total thickness of the plate.

Fig. 4.10a shows that, initially, the upper less stiff sublaminate mainly experiences out-of-plane deflection (local response), whereas the lower more stiff sublaminate slightly deflects in the opposite direction. Thus, the delaminated composite plate exhibits an opening-mode buckling response. Once the global buckling response is triggered, the thicker more stiff sublaminate pulls the upper sublaminate into the negative direction. However, as discussed in Section 3.4.3.2, the buckling response remains in the opening-mode.

The post-buckling behaviour determined by the analytical model is in very good agreement with the finite element model. The critical behaviour as well as the initial post-buckling response coincide. In the post-buckling range, small deviations of approximately 4% are present in between the analytical model and the FEM.

The onset of delamination growth is indicated in Fig. 4.10a by Ⓘ (red dot) for the analytical model and by ⓪ and ① (blue circles) for the FEM. Two deformation states, ⓪ and ①, are used for the FEM in order to emphasize the difference in predicting delamination growth compared with the current model description Ⓘ, which is discussed next.

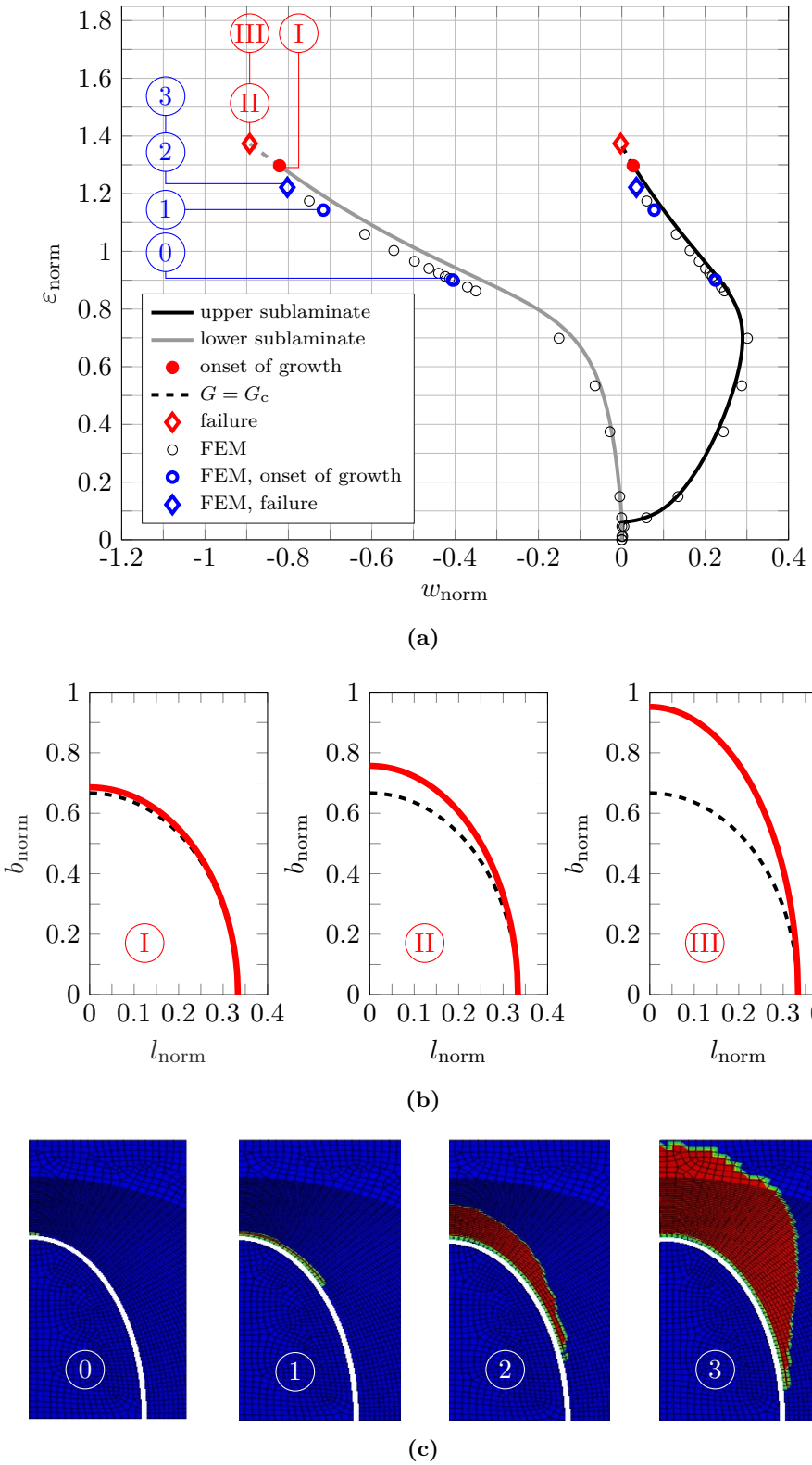

Fig. 4.10: Post-buckling response of a $[0^{\circ}_{35}]$ plate with an elliptical delamination ($l_{\text{norm}} = 1/3$ and $b_{\text{norm}} = 2/3$) at depth $a = 3/35$; **(a)** normalized compressive applied strain ($\varepsilon_{\text{norm}}$) against normalized midpoint deflections (w_{norm}); **(b)** delamination growth contours of the current model (Roman numerals); **(c)** delamination growth contours of the FEM (Arabic numerals).

In the FEM, the initiation of growth is given by disbonding of a single node as shown by ⓪ in Fig. 4.10c, whereas the analytical model predicts growth by an entire disbonding of the boundary (① in Fig. 4.10b). After growth is initiated, during the subsequent post-buckling path, only further disbonding along the boundary occurs in the FEM. Thus, the FEM generates a delamination growth contour which is similar to the one of the current model. Therefore, the second growth contour ① is provided in Fig. 4.10c which serves for the comparison with the analytical model as it constitutes the deformation state at which growth is generated beyond the initial boundary.

Comparisons between the deformation states assigned by Ⓘ and ① in Fig. 4.10a and associated with the growth contours Ⓘ and ① in Figs. 4.10b and 4.10c respectively show good agreement in which the quantitative values for applied strain and midpoint deflection deviate by approximately 12%.

Subsequently, both models predict the same behaviour where growth occurs in the width (b) direction and the post-buckling path remains thoroughly stable. At the deformation states denoted by Ⓘ for the analytical model and by ② for the FEM in Fig. 4.10a, the maximum load bearable by the system is reached. For those deformation states, the growth profiles associated with Ⓘ and ② in Figs. 4.10b and 4.10c respectively almost coincide.

At the deformation state denoted by Ⓘ in Fig. 4.10a, the energy release rate for growth in the length direction of the ellipse reaches the critical energy release rate, thus $G_\mathrm{l} = G_\mathrm{b} = G_\mathrm{c}$. As discussed in Section 4.2.2, if $G_\mathrm{l} = G_\mathrm{b} = G_\mathrm{c}$, unstable damage growth is caused (*cf.* Fig. 4.4). Thus, at Ⓘ sudden failure of the system occurs which is indicated by the red symbol "◇" in Fig. 4.10a. The applied strain at "◇" can therefore be seen as the failure load of the system. As a consequence, the delamination grows instantaneously from Ⓘ to Ⓘⓘ in Fig. 4.10b which visualizes the material failure.[24]

This behaviour is verified by the FEM where failure is indicated by the blue "◇" in Fig. 4.10a which is associated with an instantaneous growth of the delamination from ② to ③ in Fig. 4.10c.

As mentioned before, the findings provided in Fig. 4.10 are associated with the condition that $G_\mathrm{c} = G_\mathrm{c}^\mathrm{I}$ which may be regarded as a conservative measure. However, mode mixture is, in general, relevant for the case of plates with embedded delaminations.

Therefore, the effect of mode mixture is addressed with the aid of another example (Fig. 4.11) in which a delamination of $l_\mathrm{norm} = 0.20$ and $b_\mathrm{norm} = 0.53$ is assigned to the plate with the unidirectional layup. Moreover, this case further clarifies the effect of the description of the delamination by the parameters l and b on predicting the onset of delamination growth.

[24] The solving algorithm is aborted at a delamination size in which l or b exceeds 0.95.

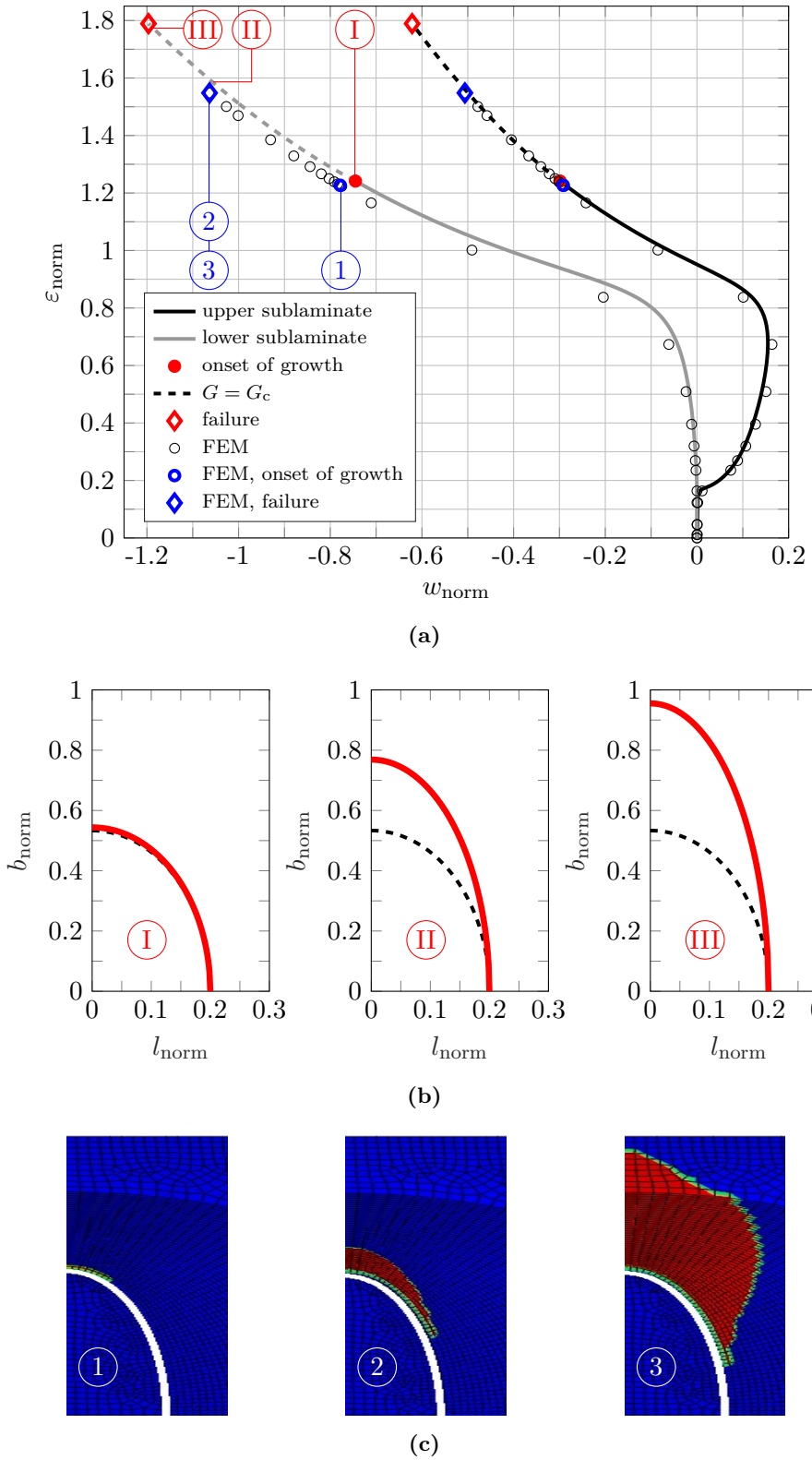

Fig. 4.11: Post-buckling response of a $[0^\circ_{35}]$ plate with an elliptical delamination ($l_{\text{norm}} = 0.20$, $b_{\text{norm}} = 0.53$) at depth $a = 3/35$; **(a)** normalized compressive applied strain ($\varepsilon_{\text{norm}}$) against normalized midpoint deflections (w_{norm}); **(b)** delamination growth contours of the current model (Roman numerals); **(c)** delamination growth contours of the FEM (Arabic numerals).

Fig. 4.11 shows the post-buckling response (Fig. 4.11a) in terms of normalized compressive applied strain ($\varepsilon_{\text{norm}}$) *vs.* normalized midpoint deflections (w_{norm}) as well as the delamination growth contours of the analytical model (Fig. 4.11b) and the finite element simulation (Fig. 4.11c).

The qualitative post-buckling behaviour is similar to the case studied in Fig. 4.10. However, owing to the smaller delamination area—specifically the smaller delamination length—the critical load is increased, the local buckling response is smaller than in Fig. 4.10a and the global buckling response is more dominant. The post-buckling response determined with the aid of the model description is in very good agreement with the finite element simulation ("FEM" in Fig. 4.11a).

The effect of the decreased length of the delamination is clearly visible when studying the deformation state causing delamination growth which is highlighted in Fig. 4.11a by Ⓘ (red dot) and by ① (blue circle) for the analytical model and the FEM respectively. The deformation state causing growth almost coincides for the analytical model and the FEM. The smaller length of the elliptical delamination yields that the onset of delamination growth is associated with a larger disbond along the boundary compared with the case studied in Fig. 4.10. This is visualized by the delamination contours Ⓘ and ① in Figs. 4.11b and 4.11c respectively.

As can be seen in Fig. 4.11a, the onset of growth does not change the stability of the deformation process, thus further loading can be applied during delamination growth.

Regarding mode mixture, in the FEM, the Benzeggagh–Kenane criterion [5], as implemented in Abaqus, is considered.[25] Since the analytical model description does not consider mode mixture, it is assumed, due to the geometry of the delamination, that growth in the length direction is dominated by mode II, thus $G_{\text{c}}^{\text{l}} = G_{\text{c}}^{\text{II}}$, and growth in the width direction by mode I, thus $G_{\text{c}}^{\text{b}} = G_{\text{c}}^{\text{I}}$. This is similar to [7], however, it may only serve as a rough approximation.

The influence of the mode mixture on the growth behaviour as well as the post-buckling response is documented by the growth profiles Ⓘⓘ and Ⓘⓘⓘ as well as ② and ③ in Figs. 4.11b and 4.11c respectively in conjunction with the post-buckling path during growth (Fig. 4.11a). In both models, growth occurs in the width direction. However, the analytical model assumes that growth follows $G_{\text{c}}^{\text{b}} = G_{\text{c}}^{\text{I}}$ along the entire boundary of the delamination. In the FEM, growth is only governed by mode I around the vertex of the delamination $(0, b)$. Outside the vicinity of the vertex $(0, b)$ growth is governed by mode II. Thus, growth proceeds significantly slower in comparison with the analytical model and is more localized around the vertex of the ellipse $(0, b)$. This is visualized by the delamination

[25] The parameters used are: $G_{\text{c}}^{\text{I}} = 0.19\,\text{N/mm}$, $G_{\text{c}}^{\text{II}} = 0.63\,\text{N/mm}$, $G_{\text{c}}^{\text{III}} = 0.63\,\text{N/mm}$, mixture parameter $\eta = 1.75$.

contours associated with (II) and (2) in Figs. 4.11b and 4.11c respectively. At the deformation states indicated with (II) and (2) in Fig. 4.11, the analytical model predicts more than double the magnitude of growth compared with the FEM.

Furthermore, mode mixture and the local description of damage growth affect the qualitative behaviour of delamination growth. As mentioned before, whenever the condition of $G_\mathrm{l} = G_\mathrm{b} = G_\mathrm{c}$ is fulfilled, unstable growth is triggered. This condition refers to a global description of the delamination in terms of the parameters l and b. Thus, in the analytical model the condition for unstable growth reads $G_\mathrm{l} = G_\mathrm{c}^\mathrm{II}$ and $G_\mathrm{b} = G_\mathrm{c}^\mathrm{I}$ which is not fulfilled during the post-buckling response in Fig. 4.11a. In the FEM, the direction of growth as well as the mode partition are evaluated node-wise. As a consequence, unstable growth is caused in the FEM at the blue symbol "◇" causing failure of the system.

Further information can be gained by studying the post-buckling response in terms of normalized compressive force (P_norm) against normalized end-shortening ($\mathcal{E}_\mathrm{norm}$), as shown in Fig. 4.12.

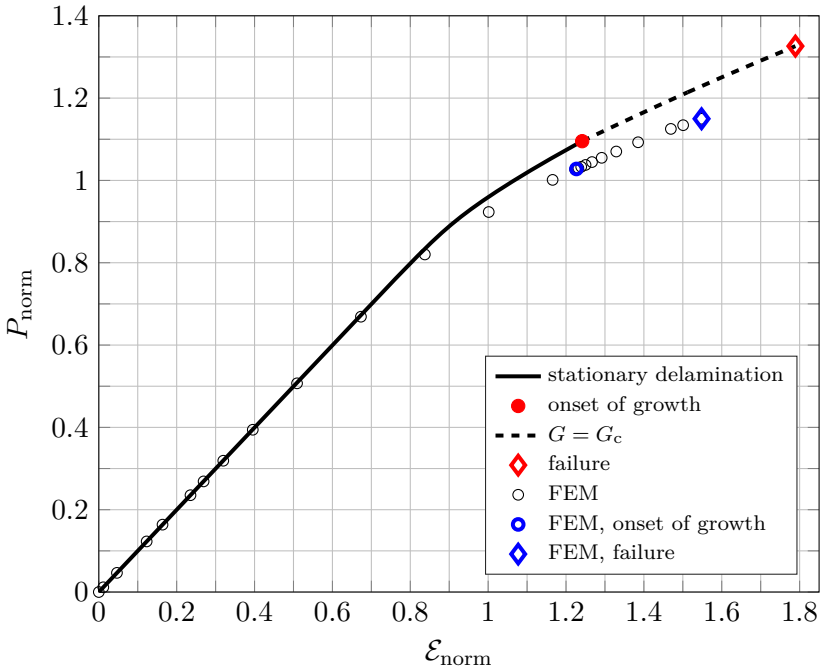

Fig. 4.12: Normalized compressive force (P_norm) against normalized end-shortening ($\mathcal{E}_\mathrm{norm}$) of a $[0^\circ_{35}]$ laminate with an elliptical delamination ($l_\mathrm{norm} = 0.20$, $b_\mathrm{norm} = 0.53$) at the depth $a = 3/35$.

The force associated with the applied strain is calculated by integrating the force resultant n_{xx} at the boundary (L, y) over the width of the plate, *i.e.*

$$P = \int_{-B}^{B} n_{xx}\Big|_{x=L} \,\mathrm{d}y. \tag{4.4.1}$$

The end-shortening is calculated by simple multiplication of the applied strain with the entire length of the plate.

As can be seen in Fig. 4.12, the local buckling response of shallow delaminations barely affects the compressive stiffness of the system. Once global buckling occurs, a change in the compressive stiffness of the system is documented where a large ratio of the compressive stiffness is retained in the post-buckling range. This is a characteristic response for fully clamped plates (*cf.* Section 4.1). Thus, visually, delamination growth is barely detectable from Fig. 4.12. As a consequence, unexpected failure may occur at the deformation state indicated by the symbol "$\diamond$".

Compared with the FEM, the analytical model shows approximately 5% larger forces in the post-buckling regime after the global buckling occurred. The post-buckling stiffness as well as the prediction of the onset of delamination growth are similar for both models. During delamination growth, the differences in the quantitative and qualitative damage growth behaviour due to the mode mixture, as described in Fig. 4.11, causes the FEM to fail by unstable growth at the blue symbol "$\diamond$", whereas further loading can be applied in the analytical model which predicts failure by delamination growth through the entire width of the plate at the red symbol "$\diamond$".

Next, the post-buckling behaviour of a cross-ply laminate ($[0°/(90°/0)_{17}]$) is compared with the response of the unidirectional layup ($[0°_{35}]$). This provides insight into the influence of the stacking sequence on the initiation of delamination growth, *i.e.* the resistance against damage growth, and the subsequent post-buckling behaviour during delamination growth.

Therefore, a delamination with a normalized length (l_{norm}) of 0.2 and a width (b_{norm}) of 0.267 is assigned to the plate, *i.e.* the aspect ratio (b/l) is 4/3. The delamination depth remains unchanged compared with the cases studied for the unidirectional layup ($a = 3/35$). Fig. 4.13 shows the normalized compressive applied strain ($\varepsilon_{\text{norm}}$) against the normalized midpoint deflections (w_{norm}) for each laminate. It should be stressed that, in order to analyse the effect of the stacking sequence on the delamination growth, both responses are normalized against the critical strain for the respective undelaminated plate.

First, Fig. 4.13 shows for the case of stationary delaminations that the unidirectional laminate provides a larger resistance against buckling delineated by a higher critical load, smaller out-of-plane deflections during the local response as well as a "sharper" transition into the global buckling response.

The deformation state causing delamination growth is indicated in Fig. 4.13 by the red (cross-ply) and blue (unidirectional) symbol "$\bullet$". It can be seen that for the cross-ply laminate growth is generated with the onset of the global buckling response. On the other hand, the unidirectional laminate experiences delamination

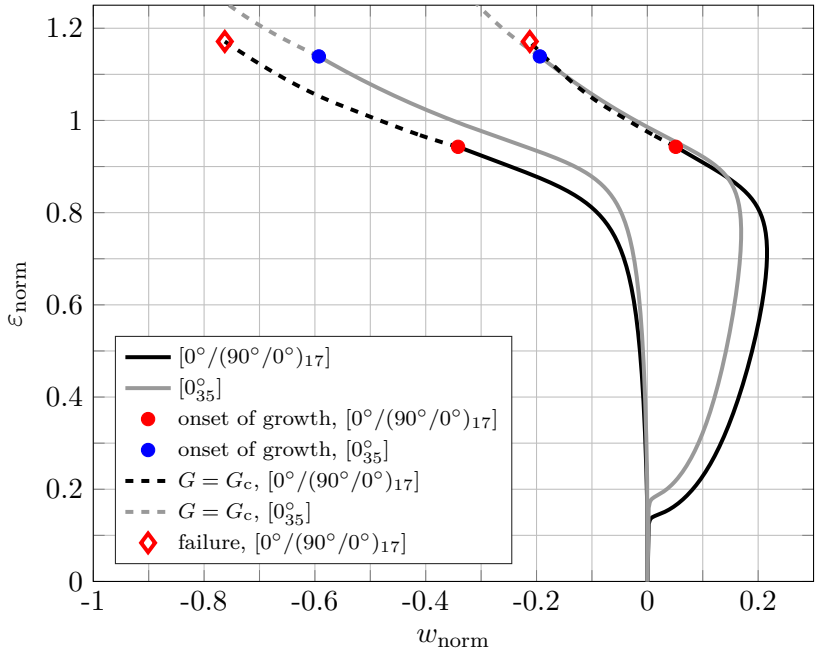

Fig. 4.13: Normalized compressive applied strain ($\varepsilon_{\text{norm}}$) against normalized midpoint deflection (w_{norm}) of a $[0°/(90°/0)_{17}]$ laminate and a $[0°_{35}]$ laminate; elliptical delamination with $l_{\text{norm}} = 0.20$ and $b_{\text{norm}} = 0.267$ at the depth $a = 3/35$.

growth considerably later during global buckling. Thus, for the case considered in Fig. 4.13, the unidirectional laminate exhibits a higher resistance against delamination growth than the cross-ply laminate. This is further underlined by the fact that the cross-ply laminate already fails by a complete separation along the width of the plate, indicated by the red symbol "$\diamond$", shortly after growth is initiated for the unidirectional laminate.

Significantly higher loads beyond the range shown in Fig. 4.13 can be withstood by the unidirectional laminate which is, for illustration purposes, visualized in Fig. 4.14 which shows the post-buckling responses in terms of normalized compressive force (P_{norm}) against normalized end-shortening ($\mathcal{E}_{\text{norm}}$). In order to enable a comparison, the response of the unidirectional laminate is, in contrast with Fig. 4.13, visualized by a dashed green line. Post-buckling paths during delamination growth are provided by dotted lines.

Fig. 4.14 shows that delamination growth for the cross-ply laminate is generated when the system starts to lose its linear behaviour visually, thus at the onset of the global buckling response. During the ensuing post-buckling response with increasing delamination size, an effect of growth on the post-buckling stiffness is barely detectable.

Comparing the compressive force causing growth for both laminates a difference of approximately 15% is documented in Fig. 4.14. Furthermore, whereas the

cross-ply laminate experiences growth at smaller forces than the critical buckling load of an undelaminated plate, the unidirectional layup can be loaded slightly above the critical point without causing delamination growth.

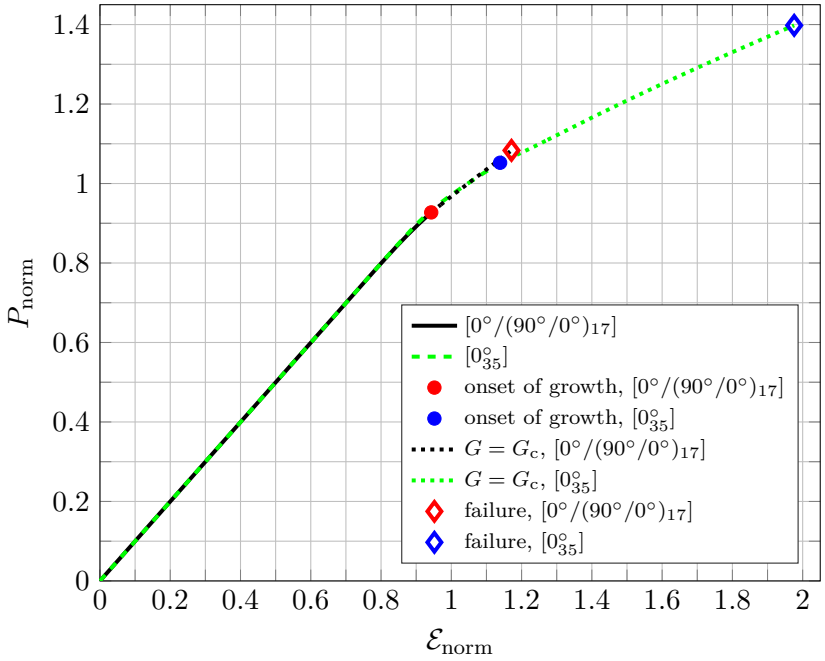

Fig. 4.14: Normalized compressive force (P_{norm}) against normalized end-shortening ($\mathcal{E}_{\text{norm}}$) of a $[0°/(90°/0)_{17}]$ laminate and a $[0°_{35}]$ laminate; elliptical delamination with $l_{\text{norm}} = 0.20$ and $b_{\text{norm}} = 0.267$ at the depth $a = 3/35$.

In addition, Fig. 4.14 visualizes that significantly larger forces are required to cause a complete separation (red and blue symbols "◇") along the width of the unidirectional plate than for the cross-ply laminate. This also underlines the higher resistance against delamination growth of the unidirectional layup for the case studied in Figs. 4.13 and 4.14.

4.5 Concluding remarks

The objective of applying the analytical framework to the problem of multi-layered delaminated composite plates subjected to compressive in-plane loading is accomplished. Thus, it is shown that the analytical framework can be successfully applied to mechanical problems requiring a larger amount of generalized coordinates. Characteristic post-buckling responses of unidirectional and cross-ply laminates are obtained. In the following, conclusions are drawn regarding the semi-analytical modelling approach and the post-buckling responses obtained.

4.5.1 Semi-analytical modelling

With the condition for the existence of an extended total potential energy being fulfilled for stable delamination growth (*cf.* Figs. 3.18, 4.4 and 4.6), the analytical framework for a structural stability analysis considering damage growth (*cf.* Section 2.3) can be applied to the given problem. The analytical framework and the model description presented in Section 4.3 yield that the given problem is solved semi-analytically.

The model description developed in Section 4.3 enables the prediction of the post-buckling behaviour of delaminated multi-layered composite plates by means of 34 generalized coordinates. While this constitutes considerably more generalized coordinates than for the problem of a delaminated strut (*cf.* Chapter 3), the amount of generalized coordinates appears small in comparison with semi-analytical models aiming at the case of stationary delaminations and the behaviour of the energy release rate.[26]

The choice of the displacement functions yielded adequate predictions of the post-buckling behaviour with expected confined deviations. Such deviations associated with the order of the approximation, as determined in the preceded analysis in Section 4.3.4, are considered as expedient in order to determine an efficient model description, *i.e.* requiring the least amount of computational cost while yielding adequate buckling responses.

The description of the damage parameter, *i.e.* the delamination area, in terms of the semi major and semi minor axis of the ellipse appears beneficial regarding the approximation of the displacement field, but causes restrictions with regards to the modelling of delamination growth. Such restrictions can be summarized as:

- delamination growth can be modelled in the width and length direction of the ellipse,
- growth in either direction can only be predicted by a complete disbonding of the boundary and
- mode mixture, which would require an analysis along the boundary, cannot be considered.

Studying elliptical delaminations, the influence of the first two bullets diminishes the smaller the dimensions of the ellipse are as well as with increasing aspect ratios (b/l), as delineated in Section 4.4. Neglecting mode mixture and assuming the conservative measure for delamination growth $G_{\mathrm{c}} = G_{\mathrm{c}}^{\mathrm{I}}$ yields very good agreement of the qualitative and quantitative growth behaviour in comparison with the FEM.

[26] For instance, more than 300 generalized coordinates are employed in [71], and more than 30 in [110] for thin-film buckling only.

Characteristic deformation states causing unstable delamination growth and thus sudden failure are determined. The implementation of a rough approximation of mode mixture such that growth in the width direction is governed by mode I and growth in the length direction by mode II results in the adequate prediction of the growth direction but overestimates growth and omits deformation states causing unstable growth.

The aforementioned issues are strictly associated with the model description and thus independent from the analytical framework. Considering the mandatory restrictions of the model description yields results which capture the post-buckling behaviour and damage growth characteristics adequately.

The current semi-analytical approach enables an efficient modelling of the post-buckling behaviour up to the deformation state causing failure (material and/or stability) which provides important insight into the structural stability of delaminated composite plates.

4.5.2 Post-buckling responses

With the aid of the results provided in Section 4.4, the following conclusions regarding the post-buckling behaviour considering delamination growth can be drawn.

- For the plates investigated (unidirectional and cross-ply laminates with elliptical shallow delaminations), the onset of delamination growth does not alter the stability of the system, thus the deformation process remains stable.
- Delamination growth is triggered with the initiation of global buckling or shortly afterwards.
- Delamination growth, initially, commences in the perpendicular direction of the loading for the cases studied (shallow delaminations).
- During an initial period of delamination growth, further loading may be applied to the system and the post-buckling stiffness barely reduces.
- Unstable delamination growth, thus failure of the system, occurs, whenever the energy release rate for growth in the width direction and in the length direction reach the respective critical energy release rates for a given state of loading.

Regarding the structural stability analysis, considering delamination growth in a buckling analysis is crucial, since failure may occur unexpected once growth reaches a certain magnitude. Up to such a deformation state, growth may be

barely detectable tracing the post-buckling paths such as compressive load against midpoint deflections and compressive force against end-shortening. Such a stability analysis is enabled by the semi-analytical modelling approach presented in this chapter.

The post-buckling responses have been verified by comparison with finite element simulations using ABAQUS. The approximation of the displacement field by means of 34 generalized coordinates yields almost no deviations for the critical and the initial post-critical response compared with the FEM. Deviations of approximately 5% regarding the applied loads during the post-buckling response succeeding global buckling are documented.

The issue of mode mixture and the description of growth by means of the delamination length l and width b (*cf.* Fig. 4.8) is addressed. Both affect the post-buckling responses once growth is considered. The influence of describing the delamination by l and b diminishes with increasing aspect ratios (b/l) and decreasing dimensions of the delamination. Since experimental proof for elliptically shaped delaminations exists (*cf.* [11]), such a description may be considered as expedient assuming that the delamination complies with the aforementioned geometry.

5 General discussion

The current chapter is concerned with a general discussion regarding the capabilities, advantages and restrictions of the analytical framework developed as well as its application to the mechanical problems studied in Chapters 3 and 4. Therefore, it stands to reason to subdivide the chapter into these parts which is subsequently done.

5.1 Analytical framework

The analytical framework enables the modelling of deformation processes, comprising both: structural stability phenomena and damage propagation, by employing only a set of generalized coordinates, *i.e.* by considering the configuration of a mechanical system. This is achieved by separating the deformation process in a conservative and a non-conservative part in which the deformation paths, the stability behaviour as well as the damage growth characteristics are obtained with the aid of variational principles (conservative process, non-conservative process) yielding sets of non-linear algebraic equations.

Solving the respective system of algebraic equations requires minimal computational cost. For solving the set of non-linear algebraic equations numerically, the framework also provides an optimal initial guess, which is the deformation state causing damage growth. Thus, the application of the framework to mechanical problems considered within the current work constitutes highly efficient modelling approaches. They are enabled by employing the key requirement of the framework, *viz.* during the non-conservative part of the deformation process equality holds between the forces available for producing a change in structure (thermodynamics forces, f_k) and the forces required for such a change (g_k).

Whenever the equality $f_k = g_k$ holds, then an extended total potential energy may be derived in which the damage parameters ξ_k, *i.e.* the internal state variables, are expressed in terms of the generalized coordinates q_i and the load parameters λ_m, *i.e.* $\xi_k = \xi_k(q_i, \lambda_m)$. This extended total potential energy constitutes the governing functional of the non-conservative part of the deformation process.

Thus, unlike treating the deformation process as a coupled problem of the displacements and the damage states, the framework resolves the direct dependence

of the damage parameters by employing the aforementioned equality. As a consequence, a variational principle of only the generalized coordinates is sufficient to determine the deformation path during the non-conservative process which is in contrast with other variational principles of fracture (*cf.* [17, 21]) where both the deformation state and the damage state are perturbed.

Since the damage parameters are not treated as independent variables in the variational description, the commonly comprised unilateral constraints within the variational description of fracture (Kuhn–Tucker conditions, *cf.* [17]) are not present in the framework. The incorporation of the Kuhn–Tucker conditions would yield the deformation path associated with energy minimization and compliance with the second law of thermodynamics. The analytical framework yields a solution path on which the deformation state is located where damage growth is initiated. Starting from this deformation state, two loading directions are possible. Only one loading direction complies with the second law of thermodynamics—healing of the structure is not allowed—and hence constitutes the actual deformation path of the system, whereas the other one violates it and is therefore omitted. The choice of the correct loading regime and thus the tracing of the actual deformation path—irrespective whether the deformation state constitutes an energy minimum or maximum—is made *a posteriori* in the solving algorithm. From a strictly mathematical point of view, this may be regarded as a disadvantage. However, considering the advantages of the extended total potential energy principle, the basic thermomechanical reasoning required to choose the adequate deformation path and its straightforward implementation in the solving algorithm, this is regarded as expedient and advantageous.

As an outcome, the analytical framework also exhibits the advantageous characteristics of the discrete coordinate approach employed in the general elastic stability theory of Thompson and Hunt [94], such as

- the (semi-)analytical description of mechanical systems,
- the capability to derive modelling approaches of increasing accuracy and/or distinct deformation phenomena and
- the modelling of continuous systems by employing continuous mode-forms in which the generalized coordinates serve as the respective amplitudes,

without the restriction to conservative deformation processes, such that the objective of the current work is accomplished.

Employing the extended total potential energy also restricts the framework. Deformation processes to be investigated must comply with a potential formulation of the total work of deformation and hence an extended total potential energy.

This is, in general, not always feasible, however, many processes are known (*e.g.* metal-like inelasticity, micro-cracking in ceramics, *cf.* [83]) for which such a potential may be derived. Especially regarding composites, studies in [55, 82] have shown that a potential formulation for damaging processes can be found (*e.g.* for matrix cracking).

Furthermore, the analysis of the energy release rate in Chapter 3 has demonstrated that such a potential formulation for delamination growth in layered composites under in-plane compressive loading holds and thus an extended total potential energy exists. As a consequence, the application of the analytical framework requires, besides the description of the deformation behaviour of the mechanical system by a set of generalized coordinates, the analysis of the respective thermodynamic forces concerning the aforementioned equality $f_k = g_k$.

The implementation of the equality between f_k and g_k and thus the replacement of the damage parameters also dictates the applied loading. In the non-conservative regime, each loading step is associated with a certain growth in the respective damage parameters. Thus, the applied load constitutes the load required to generate a certain increase in the damage parameters without limitations on the extent of growth. Unloading of the system is performed by assuming that all damage parameters remain constant (conservative process), such that the conventional total potential energy principle can be applied.

Whenever during a non-conservative deformation process growth of multiple damage parameters is initiated, the framework assumes that all such parameters continuously undergo growth from one loading step to another. Thus, unloading of single damage parameters after growth is initiated, *i.e.* the parameter transitions from active into inactive, is not considered. However, such behaviour might occur during a loading process with multiple active damage parameters which embodies a current restriction of the framework.

The requirement of $f_k = g_k$ also describes the necessary condition for stable damage growth. Whenever stable damage growth is present, the deformation path can be modelled with the aid of the analytical framework. Unstable damage growth may violate the equality, such that an expression of the damage parameters cannot be obtained. However, as has been demonstrated for a certain case of a delaminated composite strut (*cf.* Fig. 3.23), the deformation behaviour during unstable growth may be adequately predicted by implementing the equality $f_k = g_k$ as well as with the understanding that unstable damage growth is also associated with instability in a displacement-controlled configuration. Therefore, certain deformation processes which are associated with unstable growth may be also traced with the analytical framework.

5.2 Application examples

The application examples: delaminated multi-layered composite struts (Chapter 3) and plates (Chapter 4) under compressive in-plane loading, have shown that the structural stability behaviour of mechanical systems, which comply with the requirement for deriving an extended total potential energy, can be efficiently modelled with the aid of the analytical framework. Qualitatively and quantitatively substantial and conclusive results have been obtained. The verification of the findings has been performed by comparison with finite element simulations.

The analysis of the energy release rate has demonstrated that an extended total potential energy can be derived for the problems studied in Chapters 3 and 4, which allows the application of the analytical framework.

Applying the framework to the problem of a delaminated multi-layered composite strut with a through-the-width delamination enabled the description and analysis of various structural stability phenomena associated with non-growing and growing delaminations, such as

- the behaviour of the buckling loads depending on the delamination size and depth,
- the qualitative buckling responses related with opening-mode and closed-mode as well as local and global responses,
- structural instability for small delamination lengths for stationary delaminations in load-controlled problems,
- stable deformation processes for mid-size and large delamination lengths for stationary delaminations in load- and displacement-controlled problems,
- structural instability once delamination growth is initiated during global buckling in load-controlled problems,
- stable and unstable deformation processes as well as processes exhibiting a transition from stable to unstable and *vice versa* in displacement-controlled problems during delamination growth and
- the relation of unstable delamination growth with structural instability.

In summary, the application of the analytical framework has yielded a comprehensive structural stability analysis of delaminated composite struts which has been accomplished by employing only four generalized coordinates.

Regarding the problem of a delaminated multi-layered composite plate with an embedded delamination, Chapter 4 focuses on characteristic post-buckling

phenomena associated with delamination growth. The key findings from applying the analytical framework can be summarized as

- the onset of delamination growth in the post-buckling range does not change the structural stability of the systems in displacement- and load-controlled configurations,
- the initial delamination growth in the post-buckling range is stable for all cases investigated for displacement- and load-controlled problems,
- unstable delamination growth is caused during the post-buckling response, whenever the delamination intends to grow simultaneously in the width and length direction of the plate and
- unstable delamination growth is associated with structural instability.

The insight obtained emphasizes the importance of including delamination growth in the structural stability analysis. Failure owing to unstable delamination growth or complete separation along a dimension of the plate can occur unexpectedly, since initially stable delamination growth in the post-buckling regime may be barely distinguishable from the post-buckling behaviour if growth was omitted.

It should be noted that the application of the framework is highly sensitive to an adequate description of the mechanical systems. Simplifications made in the model description, of course, affect the results obtained by applying the framework. Both the description of the displacement field and the damage state require a certain accuracy such that present deformation characteristics can be modelled. This has been elucidated in Chapter 4 by studying the problem of a delaminated composite plate. Whereas the description of the displacement field by 34 generalized coordinates captured all buckling and post-buckling phenomena with satisfactory accuracy, the description of the delamination by the semi major and semi minor axis of the ellipse resulted in the prediction of delamination growth along the entire boundary as well as the inability to consider mode mixture along the boundary of the delamination. As a consequence, certain shapes of the ellipse, which would mainly cause local delamination growth, are unfavourable for the current modelling approach. Thus, the semi-analytical modelling approach of the delaminated composite plate yields results of increasing accuracy for delaminations with smaller dimensions in comparison with the length and width of the plate as well as with increasing aspect ratios (width to length).

Findings of both application examples have been compared with results from finite element simulations. Considering the vast difference in degrees of freedom between the semi-analytical models and the finite element simulations, it should be stressed that the comparisons made are eminently good. Critical responses

as well as initial post-buckling paths obtained by the semi-analytical modelling approaches and the finite element simulations coincide in the majority of the cases studied. In the post-buckling regime, deviations in the load parameters of 1 to 5% are documented depending on the dimensions of the structures and the delaminations investigated. In all cases studied, the semi-analytical modelling approach overestimates the response in comparison with the finite element simulation. The prediction of the onset of delamination growth deviates by 1 to 4% for the delaminated strut and 1 to 12% for the delaminated plate. The same qualitative post-buckling behaviour during delamination growth has been obtained for the modelling approach and the finite element simulation. Quantitative deviations in the post-buckling response remain unaffected between the conservative and non-conservative part of the deformation process.

In addition, it should be noted that savings of computational cost are tremendous. The computational time required to solve the application examples scales approximately by the relation minutes to hours comparing the semi-analytical models and the finite element simulations.

6 General conclusions and further work

In the current work, a novel analytical framework for the structural stability analysis of damageable structures has been developed and successfully applied to two characteristic mechanical problems.

The framework employs the description of mechanical systems by means of generalized coordinates. The characteristics of the analytical framework comprise:

- the strict separation of a deformation process in a conservative and non-conservative part,
- the description of the conservative part of the deformation process with the aid of the total potential energy principle,
- the analytical derivation of the damage parameters in terms of the generalized coordinates and the applied loading,
- the derivation of an extended total potential energy which constitutes the governing functional of the non-conservative part of the deformation process and
- a variational principle for the extended total potential energy functional yielding the deformation paths considering damage growth.

The framework enables the semi-analytical modelling of the deformation behaviour of mechanical systems prone to structural instability and material failure which comply with the requirement that during the non-conservative part of a deformation process equality holds in between the thermodynamic forces and the forces required to produce a change in structure.

The analytical framework has been applied to the problems of a delaminated multi-layered composite strut and a delaminated multi-layered composite plate subjected to a compressive in-plane load. By doing so, the problems have been—for the first time—semi-analytically modelled, thus the post-buckling behaviour considering delamination growth has been determined. Verification of the results obtained has been provided by findings from finite element simulations.

The application of the framework to the problems studied has yielded qualitatively and quantitatively substantial and conclusive results which provide insight into the structural stability behaviour of such structures.

The mechanical systems investigated in the current work only illustrate first applications of the framework. Various further mechanical problems may be modelled with the analytical framework. For instance, in relation with composites structures, potential problems to be investigated are:

- the effect of matrix cracking on the structural stability of composite plates with and without delaminations,
- the compressive behaviour of sandwich structures prone to core-interface-delaminations and
- matrix cracking and fibre failure associated with kink banding,

which are also highly relevant application examples for practical purposes. Regarding lightweight structures consisting of ductile materials, inelastic buckling responses associated with plasticity describe another area of possible applications.

With regards to the analytical framework, ensuing research will be directed on resolving the current restriction that for multiple active damage parameters the possible transition of single parameters from active to inactive is not incorporated. Considering this will further enhance the generality and the applicability of the analytical framework.

Concluding, the analytical framework developed in this work enables the modelling of specific mechanical deformation processes in a highly efficient manner.

A Relevant aspects of energy balances, laws of thermodynamics and thermodynamic potentials

The strain energy, the dissipative energy (work associated with structural change) and thus the total work of deformation employed in the analytical framework in Chapter 2, can be derived from the total energy balance of a closed system and the laws of thermodynamics. The subsequent derivation follows [61, 63, 65]. The total energy of a closed system reads

$$E_{\mathrm{tot}} = (U + K) = \int\limits_{V(t)} \left(\rho u + \rho \frac{v_i v_i}{2}\right) \, \mathrm{d}V, \tag{A.1}$$

in which U and K are the internal and kinetic energy respectively. In Eq. (A.1), the velocity field is denoted by v_i, the specific internal energy by u, the density by ρ and the volume by V. For demonstration purposes, the system is considered in its actual configuration (EULERian description). The total energy is a conserved quantity; its temporal change, *i.e.* the balance of the total energy of a closed system, can be written as

$$\begin{aligned} \frac{\mathrm{d}}{\mathrm{d}t} \int\limits_{V(t)} \left(\rho u + \rho \frac{v_i v_i}{2}\right) \, \mathrm{d}V = \\ \oint\limits_{\partial V(t)} (-q_i n_i) \, \mathrm{d}A + \int\limits_{V(t)} r \, \mathrm{d}V + \oint\limits_{\partial V(t)} t_i v_i \, \mathrm{d}A \int\limits_{V(t)} \rho b_i v_i \, \mathrm{d}V, \end{aligned} \tag{A.2}$$

in which the first two integrals on the right hand side (r.h.s.) of Eq. (A.2) are the rate of heat received by the system with q_i being the heat flux, r the volumetric density of the internal heat production and n_i the outward unit normal to ∂V, *i.e.* the boundary of the system. The last two integrals on the r.h.s. in Eq. (A.2) describe the actual power of the external forces with $t_i = n_j \sigma_{ji}$ being the surface tractions (σ_{ij} is the CAUCHY stress tensor) and b_i the body forces.

Next, the temporal change of the entropy of a system is considered which can

be written as,

$$\frac{\mathrm{d}}{\mathrm{d}t}\int\limits_{V(t)} \rho s \,\mathrm{d}V = -\oint\limits_{\partial V(t)} \frac{q_j}{T} n_j \,\mathrm{d}A + \int\limits_{V(t)} \frac{r}{T} \,\mathrm{d}V + \int\limits_{V(t)} \sigma \,\mathrm{d}V. \tag{A.3}$$

in which s is the specific entropy, T is the temperature and σ is the entropy production rate density. The *second law of thermodynamics* states that the entropy production rate is always non-negative [65], thus irreversible, *i.e.*

$$\sigma \geq 0. \tag{A.4}$$

Rewriting Eq. (A.3) using the divergence theorem (also referred to as Gauss theorem), *i.e.*:

$$\oint\limits_{\partial V} (\bullet) n_i \,\mathrm{d}A = \int\limits_{V} \frac{\partial(\bullet)}{\partial x_i} \,\mathrm{d}V, \tag{A.5}$$

where $(\bullet)$ may be a continuously differentiable tensor field of arbitrary order, yields

$$\int\limits_{V(t)} \left(\rho \frac{\mathrm{d}s}{\mathrm{d}t} + \frac{\partial}{\partial x_i}\left(\frac{q_i}{T}\right) - \frac{r}{T}\right) \mathrm{d}V = \int\limits_{V(t)} \sigma \,\mathrm{d}V \geq 0. \tag{A.6}$$

The radiation in Eq. (A.6) can be replaced using the balance of the internal energy in the local form,

$$\rho \frac{\mathrm{d}u}{\mathrm{d}t} = \sigma_{ij} d_{ij} + r - \frac{\partial q_i}{\partial x_i} \tag{A.7}$$

which is deducible from Eq. (A.2) by subtracting the terms associated with the balance of the kinetic energy (*cf.* [65]) yielding

$$\rho \frac{\mathrm{d}s}{\mathrm{d}t} + \frac{\partial}{\partial x_i}\left(\frac{q_i}{T}\right) - \frac{1}{T}\left(\rho \frac{\mathrm{d}u}{\mathrm{d}t} - \sigma_{ij} d_{ij} + \frac{\partial q_i}{\partial x_i}\right) = \sigma \geq 0, \tag{A.8}$$

where d_{ij} is the rate of the deformation tensor which in the case of small deformations is equal to the strain rate tensor $\mathrm{d}\varepsilon_{ij}/\,\mathrm{d}t = \dot{\varepsilon}_{ij}$, which is subsequently employed.

Eq. (A.8) is regarded as the fundamental inequality containing the first and second law of thermodynamics [61].[1] By multiplying Eq. (A.8) with T and ensuing

[1] Eq. (A.8) represents a specific form of the Clausius–Duhem inequality.

rearranging, the fundamental inequality can be expressed as

$$\sigma_{ij}\dot{\varepsilon}_{ij} - \rho\left(\frac{\mathrm{d}u}{\mathrm{d}t} - T\frac{\mathrm{d}s}{\mathrm{d}t}\right) - \frac{q_i}{T}\frac{\partial T}{\partial x_i} = T\sigma \geq 0. \tag{A.9}$$

Furthermore, by introducing the specific HELMHOLTZ free energy,

$$\phi = u - Ts, \tag{A.10}$$

with its derivative with respect to time

$$\frac{\mathrm{d}\phi}{\mathrm{d}t} = \frac{\mathrm{d}u}{\mathrm{d}t} - T\frac{\mathrm{d}s}{\mathrm{d}t} - s\frac{\mathrm{d}T}{\mathrm{d}t}, \tag{A.11}$$

Eq. (A.9) can also be rewritten, such that

$$\sigma_{ij}\dot{\varepsilon}_{ij} - \rho\left(\frac{\mathrm{d}\phi}{\mathrm{d}t} + s\frac{\mathrm{d}T}{\mathrm{d}t}\right) - \frac{q_i}{T}\frac{\partial T}{\partial x_i} = T\sigma \geq 0. \tag{A.12}$$

Eqs. (A.8), (A.9) and (A.12) represent forms of the so-called CLAUSIUS–DUHEM inequality.

Next, the deformation processes studied in the current work are considered. Thus, isothermal processes are investigated and it is assumed that dissipation is entirely associated with a change of the internal state variables (ξ_k) describing the current state of damage. Irreversible deformation associated with plasticity are herein omitted even though such processes may be considered. As a consequence, the specific HELMHOLTZ free energy is a function of the strains (ε_{ij}) and the internal state variables (ξ_k), thus

$$\mathrm{d}\phi = \frac{\partial\phi}{\partial\varepsilon_{ij}}\,\mathrm{d}\varepsilon_{ij} + \frac{\partial\phi}{\partial\xi_k}\,\mathrm{d}\xi_k, \tag{A.13}$$

such that from Eq. (A.12) follows

$$\left(\sigma_{ij} - \rho\frac{\partial\phi}{\partial\varepsilon_{ij}}\right)\dot{\varepsilon}_{ij} - \rho\frac{\partial\phi}{\partial\xi_k}\dot{\xi}_k = T\sigma \geq 0. \tag{A.14}$$

which yields the relationships

$$\rho\frac{\partial\phi}{\partial\varepsilon_{ij}}\bigg|_{\xi_k} = \sigma_{ij} \tag{A.15}$$

and

$$-\rho\frac{\partial\phi}{\partial\xi_k}\bigg|_{\varepsilon_{ij}}\dot{\xi}_k = T\sigma \geq 0. \tag{A.16}$$

Employing the definition of the thermodynamic force densities associated with the internal state variables, *i.e.*

$$\mathcal{F}_k = -\rho \frac{\partial \phi}{\partial \xi_k}, \tag{A.17}$$

Eq. (A.16) can be rewritten as

$$\mathcal{F}_k \dot{\xi}_k = T\sigma = \mathcal{D} \geq 0, \tag{A.18}$$

in which, as commonly done (*cf.* [61, 63]), the existence of a dissipation potential $\mathcal{D}(\xi_k)$ is postulated.

From Eqs. (A.15) and (A.16) follows that the HELMHOLTZ free energy density ($\rho\phi$) is a thermodynamic potential of the stresses and the thermodynamic force densities as well as it constitutes, for the processes considered, the strain energy density w which can be obtained by integration along the actual deformation path from a reference state ("0") to a current state ("1"), *i.e.*

$$w = \int_0^1 \rho \, \mathrm{d}\phi. \tag{A.19}$$

Thus, the density of the total work of deformation is

$$w_\mathrm{t} = w + \int_0^1 \mathcal{F}_k \, \mathrm{d}\xi_k. \tag{A.20}$$

Integration of Eq. (A.20) over the volume yields the total work of deformation of the system.

In the case of independent stresses, the associated thermodynamic potential can be derived with the aid of the LEGENDRE transformation, *i.e.*

$$\begin{aligned}
\rho \, \mathrm{d}\phi &= \sigma_{ij} \, \mathrm{d}\varepsilon_{ij} - \mathcal{F}_k \, \mathrm{d}\xi_k && \Leftrightarrow \\
\rho \, \mathrm{d}\phi &= \mathrm{d}(\sigma_{ij}\varepsilon_{ij}) - \varepsilon_{ij} \, \mathrm{d}\sigma_{ij} - \mathcal{F}_k \, \mathrm{d}\xi_k && \Leftrightarrow \\
\rho \, \mathrm{d}(\phi - \sigma_{ij}\varepsilon_{ij}) &= -\varepsilon_{ij} \, \mathrm{d}\sigma_{ij} - \mathcal{F}_k \, \mathrm{d}\xi_k && \Leftrightarrow \\
\rho \, \mathrm{d}\psi &= -\varepsilon_{ij} \, \mathrm{d}\sigma_{ij} - \mathcal{F}_k \, \mathrm{d}\xi_k,
\end{aligned} \tag{A.21}$$

where $\psi = \psi(\sigma_{ij}, \xi_k)$ is referred to as specific GIBBS free energy, which is, for the processes investigated in the current work, the specific total potential energy of the system.

B Effective in-plane, coupling and bending stiffness

The equations for calculating the effective material parameters used in the modelling approach in Chapter 3 are provided in this appendix. The parameters are obtained by determining the strains ε_{yy} and $2\varepsilon_{xy}$ as well as the curvatures κ_{yy} and κ_{xy} from Eq. (3.3.16) which are subsequently replaced in the equations for the in-plane force resultant n_{xx} and the moment resultant m_{xx}, respectively. Rearranging the equations in the form of Eq. (3.3.17) yields the effective parameters.

The effective in-plane stiffness (A_{eff}), the effective coupling stiffness (B_{eff}) and the effective bending stiffness (D_{eff}) are provided in Eqs. (B.1) to (B.3). It should be noted that Eqs. (B.1) to (B.3) state the general form in which all entries of the in-plane stiffness matrix (A_{IJ}), the coupling stiffness matrix (B_{IJ}) and the bending stiffness matrix (D_{IJ}) are considered while employing the symmetry of the stiffness matrices. The equations may simplify significantly for symmetric layups and certain stacking sequences. For the cross-ply laminate investigated in Chapter 3, the entries A_{16}, A_{26}, D_{16}, D_{26} are zero. Furthermore, in the case of an asymmetric cross-ply laminate (delaminated part of the strut in Chapter 3), all entries of the coupling matrix, except B_{11} and B_{22}, are zero.

$$
\begin{aligned}
A_{\text{eff}} = -\Big(& A_{11} B_{26}^4 - 2 A_{12} B_{16} B_{26}^3 + A_{22} B_{16}^2 B_{26}^2 + A_{11} B_{22}^2 B_{66}^2 + A_{22} B_{12}^2 B_{66}^2 + A_{66} B_{12}^2 B_{26}^2 + A_{66} B_{16}^2 B_{22}^2 + A_{11} A_{26}^2 D_{26}^2 \\
& + A_{16}^2 A_{22} D_{26}^2 + A_{12}^2 A_{66} D_{26}^2 + A_{16}^2 B_{26}^2 D_{22} + A_{26}^2 B_{16}^2 D_{22} + A_{12}^2 B_{66}^2 D_{22} + A_{12}^2 B_{26}^2 D_{66} + A_{16}^2 B_{22}^2 D_{66} + A_{26}^2 B_{12}^2 D_{66} - 2 A_{12} A_{16} A_{26} D_{26}^2 \\
& + 2 A_{16} B_{16} B_{22} B_{26}^2 + 2 A_{26} B_{12} B_{16} B_{26}^2 - 2 A_{26} B_{16}^2 B_{22} B_{26} - 2 A_{12} B_{12} B_{22} B_{66}^2 + 2 A_{12} B_{12} B_{26}^2 B_{66} - 2 A_{16} B_{16} B_{22}^2 B_{66} \\
& - A_{11} A_{22} A_{66} D_{26}^2 - 2 A_{11} B_{22} B_{26}^2 B_{66} - 2 A_{26} B_{12}^2 B_{26} B_{66} + 2 A_{12} A_{16} B_{26}^2 D_{26} - 2 A_{11} A_{26} B_{26}^2 D_{26} - A_{11} A_{22} B_{66}^2 D_{22} \\
& - A_{11} A_{22} B_{26}^2 D_{66} - A_{11} A_{66} B_{26}^2 D_{22} - A_{22} A_{66} B_{16}^2 D_{22} - A_{11} A_{66} B_{22}^2 D_{66} - A_{22} A_{66} B_{12}^2 D_{66} - 2 A_{26}^2 B_{12} B_{16} D_{26} \\
& - 2 A_{16}^2 B_{22} B_{26} D_{26} - 2 A_{12}^2 B_{26} B_{66} D_{26} - A_{11} A_{26}^2 D_{22} D_{66} - A_{16}^2 A_{22} D_{22} D_{66} - A_{12}^2 A_{66} D_{22} D_{66} + 2 A_{12} B_{16} B_{22} B_{26} B_{66} \\
& + 2 A_{16} B_{12} B_{22} B_{26} B_{66} - 2 A_{22} B_{12} B_{16} B_{26} B_{66} + 2 A_{26} B_{12} B_{16} B_{22} B_{66} - 2 A_{66} B_{12} B_{16} B_{26} B_{22} - 2 A_{16} B_{22} B_{26}^2 D_{26} \\
& - 2 A_{16} A_{22} B_{16} B_{26} D_{26} + 2 A_{16} A_{26} B_{12} B_{26} D_{26} + 2 A_{16} A_{26} B_{16} B_{22} D_{26} - 2 A_{16} A_{26} B_{16} B_{26} D_{22} - 2 A_{12} A_{16} B_{22} B_{26} D_{22} \\
& + 2 A_{12} A_{16} B_{22} B_{66} D_{26} - 2 A_{12} A_{16} B_{26} B_{66} D_{22} - 2 A_{12} A_{26} B_{12} B_{26} D_{66} + 2 A_{12} A_{26} B_{12} B_{66} D_{26} - 2 A_{16} A_{22} B_{16} B_{26} D_{66} + 2 A_{12} A_{16} B_{22} B_{26} D_{66} \\
& - 2 A_{12} A_{66} B_{12} B_{26} D_{26} - 2 A_{12} A_{66} B_{16} B_{22} D_{26} + 2 A_{12} A_{66} B_{16} B_{26} D_{22} + 2 A_{16} A_{22} B_{12} B_{26} D_{66} - 2 A_{16} A_{22} B_{12} B_{66} D_{26} \\
& + 2 A_{16} A_{22} B_{16} B_{66} D_{22} - 2 A_{16} A_{26} B_{12} B_{22} D_{66} + 2 A_{22} A_{66} B_{12} B_{16} D_{26} + 2 A_{11} A_{22} B_{26} B_{66} D_{26} + 2 A_{11} A_{22} B_{26} B_{22} D_{66} \\
& - 2 A_{11} A_{26} B_{22} B_{66} D_{26} + 2 A_{11} A_{26} B_{26} B_{66} D_{22} + 2 A_{11} A_{66} B_{22} B_{26} D_{26} + 2 A_{12} A_{66} B_{12} B_{22} D_{66} + 2 A_{12} A_{16} A_{26} D_{22} D_{66} \\
& + A_{11} A_{22} A_{66} D_{22} D_{66} \Big) \Big/ \\
\Big(& A_{22} A_{66} D_{26}^2 - B_{22}^2 B_{66}^2 - A_{26}^2 D_{26}^2 - B_{26}^4 + 2 B_{22} B_{26}^2 B_{66} + 2 A_{26} B_{26}^2 D_{26} + A_{22} B_{66}^2 D_{22} + A_{22} B_{26}^2 D_{66} + A_{66} B_{26}^2 D_{22} \\
& + A_{66} B_{22}^2 D_{66} + A_{26}^2 D_{22} D_{66} - 2 A_{22} B_{26} B_{66} D_{26} - 2 A_{26} B_{22} B_{26} D_{66} + 2 A_{26} B_{22} B_{66} D_{26} - 2 A_{26} B_{26} B_{66} D_{22} \\
& - 2 A_{66} B_{22} B_{26} D_{26} - A_{22} A_{66} D_{22} D_{66} \Big)
\end{aligned}
\tag{B.1}
$$

$$
\begin{aligned}
B_{\text{eff}} = -\Big(& B_{11}B_{26}^4 - 2B_{12}B_{16}\,B_{26}^3 - A_{12}\,B_{26}^3 D_{16} - A_{16}B_{26}^3 D_{12} + B_{16}^2 B_{22}B_{26}^2 + B_{11}B_{22}^2 B_{66}^2 - B_{12}^2 B_{22}\,B_{66}^2 + B_{12}^2 B_{26}^2 B_{66} \\
& - B_{16}^2\,B_{22}^2 B_{66} + A_{26}^2 B_{11} D_{26}^2 - A_{12}B_{26}B_{16}D_{26}^2 + A_{16}A_{22}B_{16}D_{26}^2 - A_{16}A_{26}B_{12}D_{26}^2 + A_{12}A_{66}B_{12}D_{26}^2 - A_{22}A_{66}B_{11}D_{26}^2 \\
& - 2B_{11}B_{22}B_{26}^2 B_{66} + A_{12}B_{16}B_{26}^2 D_{26} + A_{16}B_{12}B_{26}^2 D_{26} + A_{16}B_{16}B_{26}^2 D_{22} + A_{16}B_{22}B_{26}^2 D_{16} + A_{22}B_{16}B_{26}^2 D_{16} + A_{26}B_{12}B_{26}^2 D_{16} \\
& + A_{26}B_{16}B_{26}^2 D_{12} - 2A_{26}B_{11}B_{26}^2 D_{26} - A_{22}B_{16}^2 B_{26}D_{26} + A_{26}B_{16}^2 B_{22}D_{26} - A_{26}B_{16}^2 B_{26}D_{22} + A_{12}B_{12}B_{66}^2 D_{22} - A_{12}B_{22}B_{66}^2 D_{12} \\
& + A_{22}B_{12}B_{66}^2 D_{12} + A_{12}B_{12}B_{26}^2 D_{66} + A_{12}B_{26}^2 B_{66}D_{12} + A_{66}B_{12}B_{26}^2 D_{12} + A_{16}B_{16}B_{22}^2 D_{66} - A_{16}B_{22}^2 B_{66}D_{16} + A_{66}B_{16}B_{22}^2 D_{16} \\
& - A_{22}B_{11}B_{66}^2 D_{22} - A_{66}B_{11}B_{26}^2 D_{66} - A_{22}B_{11}B_{26}^2 D_{22} + A_{22}B_{16}^2 B_{66}D_{22} - A_{26}B_{16}^2 B_{66}D_{26} + A_{26}B_{12}^2 B_{66}D_{26} - A_{66}B_{12}^2 B_{26}D_{26} \\
& - A_{66}B_{11}B_{22}^2 D_{66} + A_{66}B_{12}^2 B_{22}D_{66} - A_{26}^2 B_{12}D_{16}D_{26} - A_{26}^2 B_{16}D_{12}D_{26} + A_{26}^2 B_{16}D_{16}D_{22} + A_{26}^2 B_{12}D_{12}D_{66} - A_{26}^2 B_{11}D_{22}D_{66} \\
& + 2B_{12}B_{16}B_{22}B_{26}B_{66} - 2A_{16}B_{16}B_{22}B_{26}D_{26} + 2A_{26}B_{12}B_{16}B_{26}D_{26} - 2A_{26}B_{16}B_{22}B_{26}D_{16} - 2A_{12}B_{12}B_{26}B_{66}D_{26} - A_{12}B_{16}B_{22}B_{26}D_{66} \\
& + A_{12}B_{16}B_{22}B_{66}D_{26} - A_{12}B_{16}B_{26}B_{66}D_{22} + A_{12}B_{22}B_{26}B_{66}D_{16} - A_{16}B_{12}B_{22}B_{26}D_{66} + A_{16}B_{12}B_{22}B_{66}D_{26} - A_{16}B_{12}B_{26}B_{66}D_{22} \\
& + A_{16}B_{22}B_{26}B_{66}D_{12} + A_{22}B_{12}B_{16}B_{26}D_{66} - A_{22}B_{12}B_{16}B_{66}D_{26} - A_{22}B_{12}B_{26}B_{66}D_{16} - A_{22}B_{16}B_{26}B_{66}D_{12} - A_{26}B_{12}B_{16}B_{22}D_{66} \\
& - A_{26}B_{12}B_{16}B_{66}D_{22} + A_{26}B_{12}B_{22}B_{66}D_{16} - 2A_{26}B_{12}B_{26}B_{66}D_{12} + A_{26}B_{16}B_{22}B_{66}D_{12} - A_{66}B_{12}B_{16}B_{22}D_{26} + A_{66}B_{12}B_{16}B_{26}D_{22} \\
& - A_{66}B_{12}B_{22}B_{26}D_{16} - A_{66}B_{16}B_{22}B_{26}D_{12} + 2A_{22}B_{11}B_{26}B_{66}D_{26} + 2A_{26}B_{11}B_{22}B_{26}D_{66} - 2A_{26}B_{11}B_{22}B_{66}D_{26} + 2A_{26}B_{11}B_{26}B_{66}D_{22} \\
& + 2A_{66}B_{11}B_{22}B_{26}D_{26} + A_{12}A_{26}B_{26}D_{16}D_{26} - A_{16}A_{22}B_{26}D_{16}D_{26} + A_{16}A_{26}B_{22}D_{16}D_{26} + A_{16}A_{26}B_{26}D_{12}D_{26} - A_{16}A_{26}B_{26}D_{16}D_{22} \\
& + A_{12}A_{26}B_{16}D_{22}D_{66} - A_{12}A_{26}B_{26}D_{12}D_{66} + A_{12}A_{26}B_{66}D_{12}D_{26} - A_{12}A_{26}B_{66}D_{16}D_{22} - A_{12}A_{66}B_{22}D_{16}D_{26} - A_{12}A_{66}B_{26}D_{12}D_{26} \\
& + A_{12}A_{66}B_{26}D_{16}D_{22} - A_{16}A_{22}B_{16}D_{22}D_{66} + A_{16}A_{22}B_{26}D_{12}D_{66} - A_{16}A_{22}B_{66}D_{12}D_{26} + A_{16}A_{22}B_{66}D_{16}D_{22} + A_{16}A_{26}B_{12}D_{22}D_{66} \\
& - A_{16}A_{26}B_{22}D_{12}D_{66} + A_{22}A_{66}B_{12}D_{16}D_{26} + A_{22}A_{66}B_{16}D_{12}D_{26} - A_{22}A_{66}B_{16}D_{16}D_{22} - A_{12}A_{66}B_{12}D_{22}D_{66} + A_{12}A_{66}B_{22}D_{12}B_{66} \\
& - A_{22}A_{66}B_{12}D_{12}D_{66} + A_{22}A_{66}B_{11}D_{22}D_{66}\Big) \Big/ \\
& \Big(A_{22}A_{66}D_{26}^2 - B_{22}^2 B_{66}^2 - A_{26}^2 D_{26}^2 - B_{26}^4 + 2B_{22}B_{26}^2 B_{66} + 2A_{26}B_{26}^2 D_{26} + A_{22}B_{66}^2 D_{22} + A_{22}B_{26}^2 D_{66} + A_{66}B_{26}^2 D_{22} + A_{66}B_{22}^2 D_{66} \\
& + A_{26}^2 D_{22} D_{66} - 2A_{22}B_{26}B_{66}D_{26} - 2A_{26}B_{22}B_{26}D_{66} + 2A_{26}B_{22}B_{66}D_{26} - 2A_{26}B_{26}B_{66}D_{22} - 2A_{66}B_{22}B_{26}D_{26} - A_{22}A_{66}D_{22}D_{66}\Big)
\end{aligned}
\tag{B.2}
$$

$$
\begin{aligned}
D_{\mathrm{eff}} = -\Big(& B_{26}^4 D_{11} - 2B_{12}B_{26}^3 D_{16} - 2B_{16}B_{26}^3 D_{12} + A_{22}B_{16}^2 D_{26}^2 + A_{22}B_{26}^2 D_{16}^2 + A_{22}B_{66}^2 D_{12}^2 + A_{66}B_{12}^2 D_{26}^2 + A_{66}B_{22}^2 D_{16}^2 \\
& + A_{66}B_{26}^2 D_{12}^2 + B_{16}^2 B_{26}^2 D_{22} + B_{22}^2 B_{66}^2 D_{11} + B_{12}^2 B_{66}^2 D_{22} + B_{12}^2 B_{26}^2 D_{66} + B_{16}^2 B_{22}^2 D_{66} + A_{26}^2 D_{11} D_{26}^2 + A_{26}^2 D_{16}^2 D_{22} \\
& + A_{26}^2 D_{12}^2 D_{66} - 2A_{26}B_{12}B_{16}D_{26}^2 - 2A_{26}B_{22}B_{26}D_{16}^2 - 2A_{26}B_{26}B_{66}D_{12}^2 + 2B_{12}B_{16}B_{26}^2 D_{26} + 2B_{16}B_{22}B_{26}^2 D_{16} - 2B_{16}^2 B_{22}B_{26}D_{26} \\
& - 2B_{12}B_{22}B_{66}^2 D_{12} + 2B_{12}B_{26}^2 B_{66} D_{12} - 2B_{16}B_{22}^2 B_{66} D_{16} - A_{22}A_{66}D_{11}D_{26}^2 - 2B_{22}B_{26}^2 B_{66} D_{11} - A_{22}A_{66}D_{16}^2 D_{22} - 2B_{12}^2 B_{26}B_{66}D_{26} \\
& - A_{22}A_{66}D_{12}^2 D_{66} + 2A_{26}B_{26}^2 D_{12} D_{16} - 2A_{26}B_{26}^2 D_{11} D_{26} - A_{22}B_{66}^2 D_{11} D_{22} - A_{22}B_{26}^2 D_{11} D_{66} - A_{66}B_{26}^2 D_{11} D_{22} - A_{22}B_{16}^2 D_{22} D_{66} \\
& - A_{66}B_{22}^2 D_{11} D_{66} - A_{66}B_{12}^2 D_{22} D_{66} - 2A_{26}^2 D_{12} D_{16} D_{26} - A_{26}^2 D_{11} D_{22} D_{66} - 2B_{12}B_{16}B_{22}B_{26}D_{66} + 2B_{12}B_{16}B_{22}B_{66}D_{26} \\
& - 2B_{12}B_{16}B_{26}B_{66}D_{22} + 2B_{12}B_{22}B_{26}B_{66}D_{16} + 2B_{16}B_{22}B_{26}B_{66}D_{12} - 2A_{22}B_{16}B_{26}D_{16}D_{26} + 2A_{26}B_{12}B_{26}D_{16}D_{26} + 2A_{26}B_{16}B_{22}D_{16}D_{26} \\
& + 2A_{26}B_{16}B_{26}D_{12}D_{26} - 2A_{26}B_{16}B_{26}D_{16}D_{22} + 2A_{22}B_{16}B_{26}D_{12}D_{66} - 2A_{22}B_{16}B_{66}D_{12}D_{26} + 2A_{22}B_{16}B_{66}D_{16}D_{22} - 2A_{22}B_{26}B_{66}D_{12}D_{16} \\
& + 2A_{26}B_{12}B_{16}D_{22}D_{66} - 2A_{26}B_{12}B_{26}D_{12}D_{66} + 2A_{26}B_{12}B_{66}D_{12}D_{26} - 2A_{26}B_{12}B_{66}D_{16}D_{22} - 2A_{26}B_{16}B_{22}D_{12}D_{66} + 2A_{26}B_{22}B_{66}D_{12}D_{16} \\
& - 2A_{66}B_{12}B_{22}D_{16}D_{26} - 2A_{66}B_{12}B_{26}D_{12}D_{26} + 2A_{66}B_{12}B_{26}D_{16}D_{22} - 2A_{66}B_{22}B_{26}D_{12}D_{16} + 2A_{22}B_{26}B_{66}D_{11}D_{26} + 2A_{26}B_{22}B_{26}D_{11}D_{66} \\
& - 2A_{26}B_{22}B_{66}D_{11}D_{26} + 2A_{26}B_{26}B_{66}D_{11}D_{22} + 2A_{66}B_{22}B_{26}D_{11}D_{26} + 2A_{66}B_{12}B_{22}D_{12}D_{66} + 2A_{22}A_{66}D_{12}D_{16}D_{26} \\
& + A_{22}A_{66}D_{11}D_{22}D_{66}\Big) \Big/ \\
\Big(& A_{22}A_{66}D_{26}^2 - B_{22}^2 B_{66}^2 - A_{26}^2 D_{26}^2 - B_{26}^4 + 2B_{22}B_{26}^2 B_{66} + 2A_{26}B_{26}^2 D_{26} + A_{22}B_{66}^2 D_{22} + A_{22}B_{26}^2 D_{66} + A_{66}B_{26}^2 D_{22} \\
& + A_{66}B_{22}^2 D_{66} + A_{26}^2 D_{22} D_{66} - 2A_{22}B_{26}B_{66}D_{26} - 2A_{26}B_{22}B_{26}D_{66} + 2A_{26}B_{22}B_{66}D_{26} - 2A_{26}B_{26}B_{66}D_{22} - 2A_{66}B_{22}B_{26}D_{26} \\
& - A_{22}A_{66}D_{22}D_{66}\Big)
\end{aligned}
\tag{B.3}
$$

C Strain energy of a thin multi-layered composite plate

The strain energy density w of a structure obeying a linear elastic material behaviour reads

$$w = \int_{\tilde{\varepsilon}_{ij}=0}^{\tilde{\varepsilon}_{ij}=\varepsilon_{ij}} \sigma_{ij}(\tilde{\varepsilon}_{ij})\,\mathrm{d}\tilde{\varepsilon}_{ij} = \frac{1}{2} C_{ijkl}\varepsilon_{ij}\varepsilon_{kl}, \tag{C.1}$$

where C_{ijkl} is the fourth order stiffness tensor, ε_{ij} is the infinitesimal strain tensor and σ_{ij} is the CAUCHY stress tensor.

Regarding thin multi-layered composite plates, with the assumption of plane stress as well as VOIGT's notation, Eq. (C.1) can be rewritten as

$$w = \frac{1}{2}\varepsilon_I \bar{Q}_{IJ}\varepsilon_J, \tag{C.2}$$

in which $I, J = 1, 2, 6$ and $\bar{Q}_{IJ}$ is the transformed reduced stiffness matrix (*cf.* Eqs. (3.3.5) and (3.3.7)). Next, as done in the CLASSICAL LAMINATE THEORY [76], the strains ε_I are subdivided in a part associated with the in-plane force resultants (ε_I^0) and a part associated with the moment resultants (ε_I^κ), thus:

$$\varepsilon_I = \begin{Bmatrix} \varepsilon_{xx} \\ \varepsilon_{yy} \\ 2\varepsilon_{xy} \end{Bmatrix} = \varepsilon_I^0 + \varepsilon_I^\kappa = \begin{Bmatrix} \varepsilon_{xx}^0 \\ \varepsilon_{yy}^0 \\ 2\varepsilon_{xy}^0 \end{Bmatrix} + z \begin{Bmatrix} \kappa_{xx} \\ \kappa_{yy} \\ \kappa_{xy} \end{Bmatrix}, \tag{C.3}$$

where $\{\kappa\}$ are the curvatures of the neutral plane of the plate and z is the distance of the respective layers from the neutral plane.

Inserting Eq. (C.3) in Eq. (C.2) yields

$$w = \frac{1}{2}\left(\varepsilon_I^0 \bar{Q}_{IJ}\varepsilon_J^0 + 2z\varepsilon_I^0 \bar{Q}_{IJ}\kappa_J + z^2 \kappa_I \bar{Q}_{IJ}\kappa_J\right). \tag{C.4}$$

The strain energy of the plate is obtained by integrating Eq. (C.4) over the volume,

i.e.

$$W = \frac{1}{2} \int_x \int_y \int_z \left(\varepsilon_I^0 \bar{Q}_{IJ} \varepsilon_J^0 + 2z \varepsilon_I^0 \bar{Q}_{IJ} \kappa_J + z^2 \kappa_I \bar{Q}_{IJ} \kappa_J \right) \mathrm{d}z \, \mathrm{d}y \, \mathrm{d}x. \tag{C.5}$$

Employing the definitions of the in-plane stiffness matrix A_{IJ} (*cf.* Eq. (3.3.8)), the coupling stiffness matrix B_{IJ} (*cf.* Eq. (3.3.9)) and the bending stiffness matrix D_{IJ} (*cf.* Eq. (3.3.10)) yields

$$W = \frac{1}{2} \int_x \int_y \left(\varepsilon_I^0 A_{IJ} \varepsilon_J^0 + 2 \varepsilon_I^0 B_{IJ} \kappa_J + \kappa_I D_{IJ} \kappa_J \right) \mathrm{d}y \, \mathrm{d}x, \tag{C.6}$$

which constitutes the strain energy of a thin multi-layered composite plate employing the Classical Laminate Theory.

D Geometric imperfection

As mentioned in Chapters 3 and 4, an initial geometric imperfection in the form of an out-of-plane displacement w^* is considered in the modelling approaches. The imperfection is assumed to be caused by the presence of the delamination and is verified by the experimental studies in [23, 68, 69, 70]. An illustration of such a geometric imperfection is provided in Fig. D.1 showing the delaminated region of a plate. The magnitude of the amplitude of the imperfection q^* is taken as $t/1000$ in Chapters 3 and 4 which results in a measure of the order 10^{-3} mm. The parameter t is the total thickness of the plate.

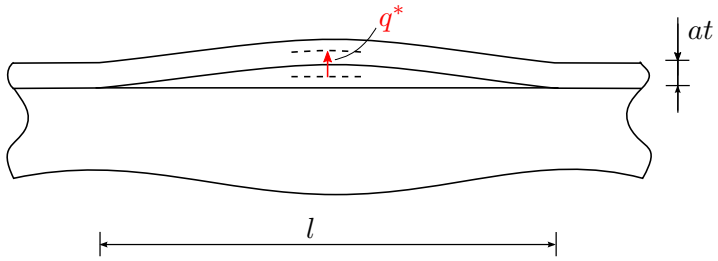

Fig. D.1: Sketch of a segment of a plated structure (delaminated region) with an initial geometric imperfection q^*; at describes the thickness of the delaminated region.

For instance, the out-of-plane displacement associated with the imperfection for the problem of a delaminated composite plate can be modelled as

$$w^*(x,y) = q^* \left[\left(\frac{x}{l}\right)^2 + \left(\frac{y}{b}\right)^2 - 1 \right]^2 \tag{D.1}$$

where l and b describe the semi major and semi minor axis of an elliptical delamination respectively (*cf.* Fig. 4.8).

The geometric imperfection does not contribute to the work of deformation. Thus, the deformations associated with the geometric imperfection, *i.e.* the strains,

$$\begin{Bmatrix} \varepsilon^*_{xx} \\ \varepsilon^*_{yy} \\ 2\varepsilon^*_{xy} \end{Bmatrix} = \begin{Bmatrix} \frac{1}{2}\left(\frac{\partial w^*}{\partial x}\right)^2 \\ \frac{1}{2}\left(\frac{\partial w^*}{\partial y}\right)^2 \\ \frac{\partial w^*}{\partial x}\frac{\partial w^*}{\partial y} \end{Bmatrix}, \tag{D.2}$$

and the curvatures,

$$\begin{Bmatrix} \kappa^*_{xx} \\ \kappa^*_{yy} \\ \kappa^*_{xy} \end{Bmatrix} = \begin{Bmatrix} -\frac{\partial^2 w^*}{\partial x^2} \\ -\frac{\partial^2 w^*}{\partial y^2} \\ -2\frac{\partial^2 w^*}{\partial x \partial y} \end{Bmatrix}, \tag{D.3}$$

have to be subtracted from the strains and curvatures in the energy formulation yielding

$$\{\varepsilon\} = \begin{Bmatrix} \varepsilon_{xx} \\ \varepsilon_{yy} \\ 2\varepsilon_{xy} \end{Bmatrix} = \begin{Bmatrix} \frac{\partial u}{\partial x} + \frac{1}{2}\left(\frac{\partial w}{\partial x}\right)^2 - \frac{1}{2}\left(\frac{\partial w^*}{\partial x}\right)^2 \\ \frac{\partial v}{\partial y} + \frac{1}{2}\left(\frac{\partial w}{\partial y}\right)^2 - \frac{1}{2}\left(\frac{\partial w^*}{\partial y}\right)^2 \\ \frac{\partial u}{\partial y} + \frac{\partial v}{\partial x} + \frac{\partial w}{\partial x}\frac{\partial w}{\partial y} - \frac{\partial w^*}{\partial x}\frac{\partial w^*}{\partial y} \end{Bmatrix} \tag{D.4}$$

and

$$\{\kappa\} = \begin{Bmatrix} \kappa_{xx} \\ \kappa_{yy} \\ \kappa_{xy} \end{Bmatrix} = \begin{Bmatrix} -\frac{\partial^2 w}{\partial x^2} + \frac{\partial^2 w^*}{\partial x^2} \\ -\frac{\partial^2 w}{\partial y^2} + \frac{\partial^2 w^*}{\partial y^2} \\ -2\frac{\partial^2 w}{\partial x \partial y} + 2\frac{\partial^2 w^*}{\partial x \partial y} \end{Bmatrix}. \tag{D.5}$$

Eqs. (D.4) and (D.5) are the strains $\{\varepsilon\}$ and curvatures $\{\kappa\}$ associated with the displacement field $u_i = \{u(x,y), v(x,y), w(x,y)\}^{\mathrm{T}}$ of the delaminated part of the plate (*cf.* Section 4.3.2) considering the initial geometric imperfection. It should be noted that the amplitude of the imperfection q^* is also the initial value of the respective generalized coordinate describing the amplitude of the delaminated region.

References

[1] P. Bajurko and P. Czarnocki. Numerical and experimental investigations of embedded delamination growth caused by compressive loading. *J Theor App Mech-Pol*, 52(2):301–312, 2014.

[2] E. J. Barbero and J. N. Reddy. Modeling of delamination in composite laminates using a layer-wise plate theory. *Int J Solids Struct*, 28(3):373–388, 1991.

[3] R. C. Batra and J. Xiao. Analysis of post-buckling and delamination in laminated composite st. venant–kirchhoff beams using czm and layer-wise tsndt. *Compos Struct*, 105:363–384, 2013.

[4] Z. P. Bažant and L. Cedolin. *Stability of Structures: elastic, inelastic, fracture and damage theories*. World Scientific, 2010.

[5] M. L. Benzeggagh and M. Kenane. Measurement of mixed-mode delamination fracture toughness of unidirectional glassepoxy composites with mixed-mode bending apparatus. *Compos Sci Tech*, 56:439–449, 2013.

[6] R. Butler, A. T. Rhead, W. Liu, and N. Kontis. Post-buckled propagation model for compressive fatigue of impact damaged laminates. *Int J Solids Struct*, 45:4349–4361, 2008.

[7] R. Butler, A. T. Rhead, W. Liu, and N. Kontis. Compressive strength of delaminated aerospace composites. *Phil Trans R Soc Lond A*, 370:1759–1779, 2012.

[8] F. Capello and D. Tumino. Numerical analysis of composite plates with multiple delaminations subjected to uniaxial buckling load. *Compos Sci Tech*, 66:264–272, 2006.

[9] H. Chai and C. D. Babcock. Two-dimensional modelling of compressive failure in delaminated laminates. *J Compos Mater*, 19:67–98, 1985.

[10] H. Chai, C. D. Babcock, and W. G. Knauss. One dimensional modelling of failure in laminated plates by delamination buckling. *Int J Solids Struct*, 17(11):1069–1083, 1981.

[11] H. Chai, W. G. Knauss, and C. D. Babcock. Observation of damage growth in compressively loaded laminates. *Exp Mech*, 23(3):329–337, 1983.

[12] A. Chattopkdhyay and H. Gu. New higher order plate theory in modeling delamination buckling of composite latihihates. *AIAA Journal*, 32(8):1709–1716, 1994.

[13] H.-P. Chen. Shear deformation theory for compressive delamination buckling and growth. *AIAA Journal*, 29(5):813–819, 1991.

[14] R. M. Christensen. *Mechanics of composite materials*. Dover Publications, 2005.

[15] B. D. Davidson. Delamination buckling: Theory and experiment. *J Compos Mater*, 25:1351–1378, 1991.

[16] B. D. Davidson, H. Hurang, and R. A. Schapery. An analytical crack-tip element for layered elastic structures. *J Appl Mech-T ASME*, 62:294–305, 1995.

[17] G. Del Piero. A variational approach to fracture and other inealstic phenomena. *J Elast*, 112(1):3–77, 2013.

[18] E. J. Doedel and B. E. Oldeman. Auto-07p: Continuation and bifurcation software for ordinary differential equations, 2012. User's Manual.

[19] P. R. Everall and G. W. Hunt. Arnold tongue predictions of secondary buckling in thin elastic plates. *J Mech Phys Solids*, 47:2187–2206, 1999.

[20] P. R. Everall and G. W. Hunt. Mode jumping in the buckling of struts and plates: a comparative study. *Int J Non-Linear Mech*, 35:1067–1079, 2000.

[21] G. A. Francfort and J.-J. Marigo. Revisiting brittle fracture as an energy minimization problem. *J Mech Phys Solids*, 46(8):1319–1342, 1998.

[22] A. A. Griffith. The phenomena of rupture and flow in solids. *Phil Trans R Soc Lond A*, 221:163–198, 1921.

[23] H. Gu and A. Chattopkdhyay. An experimental investigation of delamination buckling and postbuckling of composite laminates. *Compos Sci Tech*, 59:903–910, 1999.

[24] R. Hill. A general theory of uniqueness and stability in elastic-plastic solids. *J Mech Phys Solids*, 6:236–246, 1958.

[25] R. Hill. Uniqueness criteria and extremum principles in self-adjoint problems of continuum mechanics. *J Mech Phys Solids*, 10:185–194, 1962.

[26] H. Hosseini-Toudeshky, S. Hosseini, and B. Mohammadi. Buckling and delamination growth analysis of composite laminates containing embedded delaminations. *Appl Compos Mater*, 17:95–109, 2010.

[27] H. Hosseini-Toudeshky, S. Hosseini, and B. Mohammadi. Delamination buckling growth in laminated composites using layerwise-interface element. *Compos Struct*, 92:1846–1856, 2010.

[28] H. Huang and G. A. Kardomateas. Buckling of orthotropic beam-plates with multiple central delaminations. *Int J Solids Struct*, 35(13):1355–1362, 1998.

[29] G. W. Hunt and B. A. Burgan. Hidden asymmetries in the Shanley model. *J Mech Phys Solids*, 33(1):83–94, 1985.

[30] G. W. Hunt, B. Hu, R. Butler, D. P. Almond, and J. E. Wright. Nonlinear modeling of delaminated struts. *AIAA Journal*, 42(11):2364–2372, 2004.

[31] G. W. Hunt, M. A. Peletier, and M. A. Wadee. The Maxwell stability criterion in pseudo-energy models of kink banding. *J Struct Geol*, 22:669–681, 2000.

[32] G. W. Hunt and M. A. Wadee. Localization and mode interaction in sandwich structures. *Proc R Soc Lond A*, 454:1197–1216, 1998.

[33] K. Huseyin. *Nonlinear theory of elastic stability.* Noordhoff International Publishing, 1975.

[34] J. W. Hutchinson, M. Y. He, and A. G. Evans. The influence of imperfections on the nucleation and propagation of buckling driven delaminations. *J Mech Phys Solids*, 48:709–734, 2000.

[35] J. W. Hutchinson and Z. Suo. Mixed mode cracking in layered materials. *Adv Appl Mech*, 29:63–191, 1992.

[36] S.-F. Hwang and C.-P. Mao. Failure of delaminated carbon/epoxy composite plates under compression. *J Compos Mater*, 35(18):1634–1653, 2001.

[37] The Math Works, Inc. MATLAB. *High-performance numeric computation and visualization software.* The Math Works Inc., 2015.

[38] G. A. Kardomateas. Buckling and postbuckling of delaminated composites under compressive loads including transverse shear effects. *AIAA Journal*, 26(3):337–343, 1988.

[39] G. A. Kardomateas. The initial post-buckling and growth behaviour of internal delaminations in composite plates. *J Appl Mech*, 60:903–910, 1993.

[40] B. L. Karihaloo and H. Stang. Buckling-driven delamination growth in composite laminates: Guidelines for assessing the threat posed by interlaminar matrix delamination. *Compos B*, 39:386–395, 2008.

[41] C. Kassapoglou. Buckling, post-buckling and failure of elliptical delaminations in laminates under compression. *Compos Struct*, 9:139–159, 1988.

[42] M. Kharazi and H. R. Ovesy. Postbuckling behavior of composite plates with through-the-width delaminations. *Thin Wall Struct*, 46:939–946, 2008.

[43] M. Kharazi, H. R. Ovesy, and M. A. Mooneghi. Buckling analysis of delaminated composite plates using a novel layerwise theory. *Thin Wall Struct*, 74:246–254, 2014.

[44] J.-H. Kim. Postbuckling analysis of composite laminates with a delamination. *Comput Struct*, 62(6):975–983, 1997.

[45] J. Klug, X. X. Wu, and C. T. Sun. Efficient modeling of postbuckling delamination growth in composite laminates using plate elements. *AIAA Journal*, 34(1):178–184, 1996.

[46] W. T. Koiter and M. Pignataro. *A general theory for the interaction between local and overall buckling of stiffened panels.* Tech. Rept. WTHD 83, Delft University of Technology, The Netherlands., 1976.

[47] A. Köllner, R. Jungnickel, and C. Völlmecke. Delamination growth in buckled composite struts. *Int J Fract*, 202(2):261–269, 2016.

[48] A. Köllner and C. Völlmecke. An analytical framework to extend the general structural stability analysis by considering certain inelastic effects—theory and application to delaminated composites. *Compos Struct*, 170:261–270, 2017.

[49] A. Köllner and C. Völlmecke. Buckling and postbuckling behaviour of delaminated composite struts. *Int J Comput Meth Eng Sci Mech*, 18(1):25–33, 2017.

[50] R. Krueger. Virtual crack closure technique: History, approach, and applications. *Appl Mech Rev*, 57(2):109–143, 2004.

[51] R. Krueger. A summary of benchmark examples to assess the performance of quasi-static delamination propagation prediction capabilities in finite element codes. *J Compos Mater*, 49(26):3297–3316, 2015.

[52] R. Krüger, S. Rinderknecht, C. Hänsel, and M. König. Computational structural analysis and testing: An approach to understand delamination growth. *Key Eng Mater*, 120-121:181–202, 1996.

[53] W.-M. Kyoung and C.-G. Kim. Delamination buckling and growth of composite laminated plates with transverse shear deformations. *J Compos Mater*, 29(15):2047–2068, 1995.

[54] J. La Salle and S. Lefschetz. *Stability by Liapunov's Direct Method with Applications*. Academic Press, 1961.

[55] M. J. Lamborn and R. A. Schapery. An investigation of the existence of a work potential for fiber-reinforced plastic. *J Compos Mater*, 27(4):352–382, 1993.

[56] P.-L. Larsson. On delamination buckling and growth in circular and annular orthotropic plates. *Int J Solids Struct*, 27(1):15–28, 1991.

[57] J. Lee, Z. B. Gürdal, and O. H. Griffin. Layer-wise approach for the bifurcation problem in laminated composites with delaminations. *AIAA Journal*, 31(2):331–338, 1993.

[58] J. Lee, Z. B. Gürdal, and O. H. Griffin. Postbuckling of laminated composites with delaminations. *AIAA Journal*, 33(10):1963–1970, 1995.

[59] S.-Y. Lee and D.-Y. Park. Buckling analysis of laminated composite plates containing delaminations using the enhanced assumed strain solid element. *Int J Solids Struct*, 44:8006–8027, 2007.

[60] H. Leipholz. *Stability theory: An Introduction to the Stability of Dynamic Systems and Rigid Bodies*. Springer, 1987.

[61] J. Lemaitre and J.-L. Chaboche. *Mechanics of solid materials*. Cambridge university press, 1994.

[62] P. F. Liu, S. J. Hou, J. K. Chu, X. Y. Hu, C. L. Zhou, J. L. Liu, J. Y. Zheng, A. Zhao, and L. Yan. Finite element analysis of postbuckling and delamination of composite laminates using virtual crack closure technique. *Compos Struct*, 93:1549–1560, 2011.

[63] G. A. Maugin. *The thermomechanics of nonlinear irreversible behaviors.* World Scientific, 1999.

[64] B. Mohammadi and F. Shahabi. On computational modeling of postbuckling behavior of composite laminates containing single and multiple through-the-width delaminations using interface elements with cohesive law. *Eng Fract Mech*, 152:88–104, 2016.

[65] W. H. Müller. *An expedition to continuum theory.* Springer, 2014.

[66] W. H. Müller and F. Ferber. *Technische Mechanik für Ingenieure.* Fachbuchverl. Leipzig im Carl-Hanser-Verlag, 2008.

[67] B. P. Naganarayana and S. N. Atluri. Strength reduction and delamination growth in thin and thick composite plates under compressive loading. *Comput Mech*, 16:170–189, 1995.

[68] K.-F. Nilsson, L. E. Asp, J. E. Alpman, and L. Nystedt. A theoretical and experimental investigation of buckling induced delamination growth. *J Mech Phys Solids*, 41(4):749–782, 1993.

[69] K.-F. Nilsson, L. E. Asp, J. E. Alpman, and L. Nystedt. Delamination buckling and growth for delaminations at different depths in a slender composite panel. *Int J Solids Struct*, 38:3039–3071, 2001.

[70] K.-F. Nilsson, L. E. Asp, and A. Sjögren. On transition of delamination growth behaviour for compression loaded composite panels. *Int J Solids Struct*, 38:8407–8440, 2001.

[71] H. R. Ovesy and M. Kharazi. Compressional stability behavior of composite plates with through-the-width and embedded delaminations by using first order shear deformation theory. *Comput Struct*, 89:1829–1839, 2011.

[72] H. R. Ovesy and M. Kharazi. Stability analysis of composite plates with through-the-width delamination. *J Eng Mech ASCE*, 137(2):87–100, 2011.

[73] S. O. Peck and G. S. Springer. The behavior of delaminations in composite plates-analytical and experimental results. *J Compos Mater*, 25:907–929, 1991.

[74] H. Petryk. A consistent energy approach to defining stability of plastic deformation processes. In *Stability in the Mechanics of Continua, Proc. IUTAM Symp. Nümbrecht,* Ed. Schröder, F.H., pages 262–272, 1981.

[75] H. Petryk. The energy criteria of instability in time-independent inelastic solids. *Arch Mech*, 43(4):519–545, 1991.

[76] J. N. Reddy. *Mechanics of laminated composite plates and shells: theory and analysis*. CRC press, 2004.

[77] A. T. Rhead and R. Butler. Compressive static strength model for impact damaged laminates. *Compos Sci Tech*, 69:2301–2307, 2009.

[78] A. Riccio and E. Pietropaoli. Modeling damage propagation in composite plates with embedded delamination under compressive load. *J Compos Mater*, 42:1309–1335, 2008.

[79] J. R. Rice. A path independent integral and the approximate analysis of strain concentration by notches and cracks. *J Appl Mech*, 35:379–386, 1968.

[80] J. R. Rice. Inelastic constitutive relations for solids: an internal-variable theory and its application to metal plasticity. *J Mech Phys Solids*, 19:433–455, 1971.

[81] S. Rinderknecht and B. Kröplin. A computational method for the analysis of delaminatiom growth in composite plates. *Comput Struct*, 64(1-4):359–373, 1997.

[82] R. A. Schapery. Deformation and fracture characterization of inelastic composite materials using potentials. *Polym Eng Sci*, 27(1):63–76, 1987.

[83] R. A. Schapery. A theory of mechanical behavior of elastic media with growing damage other changes in structure. *J Mech Phys Solids*, 38(2):215–253, 1990.

[84] R. A. Schapery and B. D. Davidson. prediction of energy release rate for mixed-mode delamination using classical plate theory. *Appl Mech Rev*, 43(5):281–287, 1990.

[85] H. Schürmann. *Konstruieren mit Faser-Kunststoff-Verbunden*. Springer, 2005.

[86] M. J. Sewell. The static perturbation technique in buckling problems. *J Mech Phys Solids*, 13:247–265, 1965.

[87] I. Sheinman, G. A. Kardomateas, and A. A. Pelegri. Delamination growth during pre- and post-buckling phases of delaminated composite laminates. *Int J Solids Struct*, 35(1-2):19–31, 1998.

[88] I. Sheinman and M. Soffer. Delamination growth during pre- and post-buckling phases of delaminated composite laminates. *Int J Solids Struct*, 27(5):639–646, 1991.

[89] G. J. Simitses and S Sallam. Delamination buckling and growth of flat composite structural elements. Technical report, AFOSR-TR. 85-1067, Georgia Institute of Technology, 1984.

[90] G. J. Simitses, S. Sallam, and W. L. Yin. Effect of delamination of axially loaded homogeneous laminated plates. *AIAA Journal*, 23(9):1437–1444, 1985.

[91] ASTM Standard. Standard test method for compressive residual strength properties of damaged polymer matrix composite plates. *ASTM D7137/D7137M. West Conshohocken, PA: American Society for Testing and Materials*, 2007.

[92] X. Sun and L. Tong. Progressive failure analysis of laminated plates with delamination. *J Reinf Plast Compos*, 20(16):1370–1389, 2001.

[93] Abaqus. *Version 6.14.* Providence RI, USA: Dassault Systèmes, 2014.

[94] J. M. T. Thompson and G. W. Hunt. *A general theory of elastic stability.* John Wiley & Sons, 1973.

[95] J. M. T. Thompson and G. W. Hunt. *Elastic instability phenomena.* John Wiley & Sons, 1984.

[96] S. P. Timoshenko and J. M. Gere. *Theory of Elastic Stability.* McGraw-Hill, 1961.

[97] Toho Tenax Europe GmbH. *Delivery programme and characteristics for Tenax® UTS filament yarn*, 04 2009.

[98] C. Völlmecke. *Nonlinear buckling of delaminated panels.* PhD thesis, Imperial College of Science, Technology & Medicine, London, 2010.

[99] M. A. Wadee. Localized buckling in sandwich struts with pre-existing delaminations and geometrical imperfections. *J Mech Phys Solids*, 50:1767–1787, 2002.

[100] M. A. Wadee and R. Edmunds. Kink band propagation in layered structures. *J Mech Phys Solids*, 53:2017–2035, 2005.

[101] M. A. Wadee, G. W. Hunt, and M. A. Peletier. Kink band instability in layered structures. *J Mech Phys Solids*, 52:1071–1091, 2004.

[102] M. A. Wadee and C. Völlmecke. Semi-analytical modelling of buckling driven delamination in uniaxially compressed damaged plates. *IMA J Appl Math*, 76:120–145, 2011.

[103] M. A. Wadee, C. Völlmecke, J. F. Haley, and S. Yiatros. Geometric modelling of kink banding in laminated structures. *Phil Trans R Soc A*, 370:1827–1849, 2012.

[104] S. Wang and Y. Zhang. Buckling, post-buckling and delamination propagation in debonded composite laminates Part 2: Numerical applications. *Compos Struct*, 88:131–146, 2009.

[105] S. Wang and Y. Zhang. Post-local buckling-driven delamination in bilayer composite beams. *Compos Struct*, 113:1058–1066, 2015.

[106] Y. C. Wee and C. G. Boay. Analytical and numerical studies on the buckling of delaminated composite beams. *Compos Struct*, 80:307–319, 2007.

[107] J. D. Whitcomb. Finite element analysis of instability related delamination growth. *J Compos Mater*, 15:403–426, 1981.

[108] J. D. Whitcomb. Three-dimensional analysis of a postbuckled embedded delamination. *J Compos Mater*, 23:862–889, 1989.

[109] W.-L. Yin. The effects of laminated structure on delamination buckling and growth. *J Compos Mater*, 22:502–517, 1988.

[110] W.-L. Yin and K. C. Jane. Refined buckling and postbuckling analysis of two-dimensional delamination—I. Analysis and validation. *Int J Solids Struct*, 29(5):591–610, 1992.

[111] W.-L. Yin and K. C. Jane. Refined buckling and postbuckling analysis of two-dimensional delamination—II. Results for anisotropic laminates and conclusion. *Int J Solids Struct*, 29(5):611–639, 1992.

[112] Y. Zhang and S. Wang. Buckling, post-buckling and delamination propagation in debonded composite laminates Part 1: Theoretical development. *Compos Struct*, 88:121–130, 2009.

[113] C. Zschernack, M. A. Wadee, and C. Völlmecke. Nonlinear buckling of fibre-reinforced unit cells of lattice materials. *Compos Struct*, 136:217–228, 2016.